Design of a DNA-Encoded Human Papilloma Virus-Like Particle Displaying a Vascular Endothelial Growth Factor Antagonistic Peptide for Characterization in Mammalian Cells

by

Deborah Pushparajah

A thesis

presented to the University of Waterloo

in fulfillment of the

thesis requirement for the degree of

Master of Science

in

Pharmacy

Waterloo Ontario, Canada, 2022

Author’s Declaration

I hereby declare that I am the sole author of this thesis. This is a true copy of this thesis, including any required final revisions, as accepted by my examiners. I understand that my thesis may be made electronically available to the public.

Abstract

Cancer immunotherapy has evolved as an effective platform for the treatment of a variety of cancer types by enhancing and/or modulating the functionality of the immune system to target cancer cells and consequently mitigate tumour growth. Within the last decade, self-assembled viral-derived protein complexes, known as virus-like particles (VLPs), have been extensively studied for their application toward cancer immunotherapy. These structural viral-mimicking particles possess the capability to engender potent immune responses, and in doing so, combat the immunosuppressive tumour microenvironment. VLP-based vaccines have been commercialized, however, VLPs encoded as a genetic sequence, such as a DNA-VLP strategy, for delivery and subsequent *in vivo* formation, has not been licensed to date. This would enable transcription and translation of the introduced genetic sequence into viral structural proteins, assembly of the expressed proteins to form VLPs, and successive immune response stimulation, characterizing this type of treatment modality as both an immunotherapeutic and gene therapeutic. Delivery of VLPs encoded as a genetic sequence, opposed to conventional VLP delivery, enables viral structural protein expression and assembly into VLPs directly within cancer and immune cells, promoting enhanced cell-mediated immune responses, which can contribute to a greater extent towards tumour eradication.

Here, we are seeking to apply this concept toward the design of a DNA-VLP gene cassette to produce human papillomavirus (HPV) 16 VLPs as a gene therapy-based cancer immunotherapeutic. The DNA-VLP gene cassettes were designed to encode the major capsid protein of HPV16, known as L1, along with an inserted peptide. This peptide, known as VGB, is characterized as an anti-angiogenic molecule that has previously demonstrated active reduction of

cancer cell proliferation and tumour growth. Transfection of the designed DNA-VLP gene cassettes was conducted within mammalian cells, which successfully encoded the HPV16 L1 protein, in addition to possible *in vitro* assembly of VGB-displaying HPV16 L1 VLPs. This was validated via western blot analysis, enzyme-linked immunosorbent assay experimentation, and visualization using transmission electron microscopy. Potential display of the VGB peptide within surface exposed regions of the VLPs was observed by increased binding towards VGB's targeted receptor, VEGFR. The prospective for cell lysis contributed by the accumulation of VLPs within mammalian cells was not validated, as decreased cell growth and viability subsequent to transfection were not observed. Overall, the characterization of VGB-displaying HPV16 L1 VLPs encoded within the designed DNA-VLP gene cassettes, promotes further investigation to employ this as a potential gene therapy-based cancer immunotherapeutic for future clinical applications.

Acknowledgements

Firstly, I would like to thank Dr. Roderick Slavcev and Dr. Marc Aucoin for their continual support and for providing me with this amazing learning experience. I am so thankful for their guidance these past two years which has allowed me to grow both professionally and academically. I would also like to thank the members of my advisory committee, Dr. Emmanuel Ho and Dr. Valerie Ward, for their support. For the financial funding of this research, I would like to thank the School of Pharmacy of the University of Waterloo and the Process Engineering of Emerging Nano-Medicines Research Program.

The work in this thesis would not be possible without the help of so many individuals whom I would like to specifically thank: Tania Rodríguez Ramos for her training for the western blot and ELISA experiments; the Dixon lab for allowing me to use their lab space and resources whenever needed; Mishi Groh for training me for the use of the transmission electron microscope; Madhuja Chakraborty and Dr. Faranak Mavandadnejad for their help with the flow cytometer; Dr. Christiane Noguiera and Scott Boegel for their cell culture training; Andrew Ng for his help with the purification process of this work; the Nekkar lab for their supply of the TEM grids; Rahul Chowdary Karuturi for his help with the preparation of the samples for TEM; and Dr. Shirley Wong and Jesse St. Jean who provided me with many helpful insights that enhanced my project and experiments.

There are a few people who not only helped me on an academic level, but also on a personal level these past few years. I am so thankful to Merium Fernando and Dr. Salma Jiminez, who trained me throughout my first lab experiences as an undergrad. Their mentorship and close friendship as an undergrad, which has also continued throughout my graduate studies, gave me the confidence

and determination to pursue studies in research. I am also so grateful to Rohini Prakash, for always helping me at any time with so many things in the lab and for becoming one of my closest friends that provided me with immense support throughout the ups and downs of my academic and personal journey.

I would like to thank the whole Slavcev lab (Merium Fernando, Jesse St. Jean, Dr. Shirley Wong, Dr. Salma Jiminez, Heba Alattas, Rohini Prakash, Andrew Ng, Harikka Nagireddy, Nicholas Cheng, and Jiayang Li) for their friendships, laughs, and memorable times together. It has been so fun and such a pleasure to work with you all. I also appreciate the whole Aucoin Lab (Madhuja Chakraborty, Jacqueline Powichrowski, Scott Boegel, Dr. Christiane Noguiera, Lisa Nielson, Aaron Yip, Sara Haghayegh Khorasani, and Dr. Faranak Mavandadnejad), for their wonderful time in the lab.

My greatest appreciation and love goes to my family, to whom I am so grateful for. To my parents, who always believe in me and for their unconditional support and encouragement in every single aspect of my life. To my brothers, for always being there for me and for being my best friends. To my grandma (Ammammah), who always believed in my potential. To all my friends and family who have been such a blessing throughout my life. Most importantly, I am grateful to my Lord and Saviour, Jesus Christ, for providing me with this amazing opportunity to learn and for His continual faithfulness (Jeremiah 29:11).

Dedication

This thesis is dedicated to my parents, Mohan and Anne Pushparajah, for their unconditional love and support.

Table of Contents

List of Tables

List of Figures

List of Abbreviations

aa	amino acid
Ab	antibody
Amp	ampicillin
AmpR	ampicillin resistance
AAV	adeno-associated virus
APC	antigen presenting cell
APS	ammonium persulfate
ATCC	American Type Culture Collection
ATP	adenine triphosphate
biAb	bispecific antibody
BCMA	B-cell maturation antigen
bp	base pair
CAR	chimeric antigen receptor
CMV	cytomegalovirus
CPMV	cowpea mosaic virus
CTL	cytotoxic T-lymphocyte
CTLA	cytotoxic T-lymphocyte associated protein
DC	dendritic cell
DMEM	Dulbecco's modified eagle medium
DNA	deoxyribonucleic acid
D-PBS	Dulbecco's phosphate buffered saline
EGF	epidermal growth factor
EGFR	epidermal growth factor receptor
ELISA	enzyme-linked immunosorbent assay
FDA	Food and Drug Administration
FBS	fetal bovine serum
GF	growth factor
gfp	green fluorescent protein

HBV	hepatitis B virus
HEK	human embryonic kidney
HIV	human immunodeficiency virus
HPV	human papillomavirus
HRP	horseradish peroxidase
IFN	interferon
Ig	immunoglobulin
IL	interleukin
kb	kilobases
kDa	kilodaltons
LB	Luria broth
mAb	monoclonal antibody
MHC	major histocompatibility complex
NEB	New England Biolabs
NK	natural killer
ORF	open reading frame
ori	origin of replication
PASP	pathogen associated structural pattern
PBS	phosphate-buffered saline
PBS-T	phosphate-buffered saline/tween
PD	programmed cell death protein
PIGF	placental growth factor
polyA	polyadenylation
PNK	polynucleotide kinase
PRR	pattern recognition receptor
PTA	phosphotungstic acid
RE	restriction enzyme
rpm	revolutions per minute
RTK	receptor tyrosine kinase
SDS-PAGE	sodium dodecyl sulfate-polyacrylamide gel electrophoresis

SEM	standard error of the mean
SHIV	simian-human immunodeficiency virus
SS	super sequence
SV	simian virus
TBS	tris-buffered saline
TBS-T	tris-buffered saline/tween
TEM	transmission electron microscopy
TEMED	tetramethylethylenediamine
Th	T helper
TIL	tumour infiltrating lymphocytes
TLR	toll-like receptor
TMB	Tetramethylbenzidine
TME	tumour microenvironment
TNF	tumour necrosis factor
Treg	T regulatory
V	volts
VEGF	vascular endothelial growth factor
VEGFR	vascular endothelial growth factor receptor
VLP	virus-like particle

1. Introduction

1.0 Perspective

In Canada, cancer is the leading cause of death (Figure 1; Canadian Cancer Statistics, 2019) imparting negative social and emotional implications on society and an increased economic burden on the healthcare system (D. R. Brenner et al., 2022). Conventional cancer therapeutic modalities employed today include chemotherapy, radiotherapy, and surgery. These therapeutic strategies have demonstrated limited successful outcomes in the past, and present some predominant challenges due to 1) the development of drug resistance; 2) negative effects towards non-cancerous cells; and 3) challenges related to drug tumour penetration (Chakraborty & Rahman, 2012; Chidambaram et al., 2011; H. Wang et al., 2016). Therefore, it is imperative that more effective methods of cancer treatment are developed and comprehensively tested (Pucci et al., 2019).

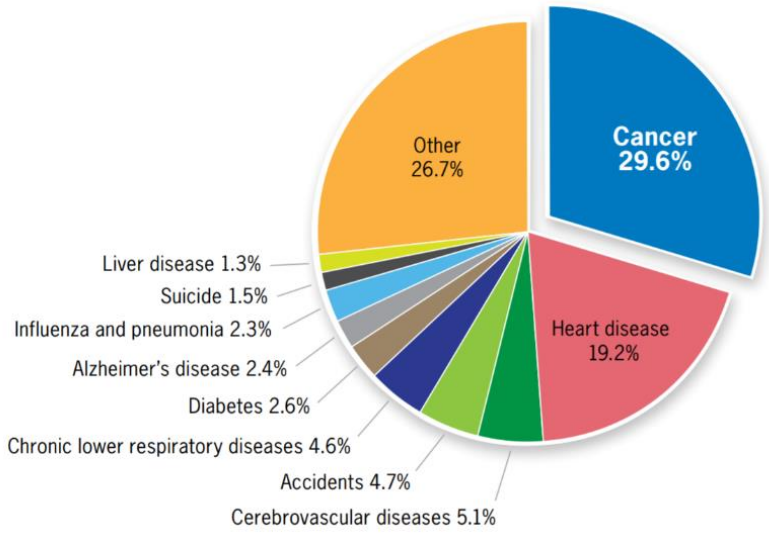

Figure 1. Death percentages in Canada attributed to cancer and other causes. The percentage of deaths caused by cancer makes up the highest proportion of deaths in Canada (~ 30%) (Taken from Canadian Cancer Statistics, 2019).

Several treatment modalities have been investigated to overcome the aforementioned limitations of conventional cancer therapy by exploiting the inherent ability of the human body's immune system to attack foreign entities, and in particular, viruses (Hemminki et al., 2020). This includes the use of oncolytic viruses, which possess the ability to promote the onset of strong immune responses while simultaneously lysing cancer cells. However, these particles constitute the category of replicative viruses, which limits their safety profile and applicability in clinical settings (Buijs et al., 2015; Vähä-Koskela et al., 2007). Potential risks associated with this type of treatment include non-selective viral replication, reversion to a wild-type viral state, and administration toxicity (Buijs et al., 2015; Goldufsky et al., 2013; Hemminki et al., 2020).

In contrast, virus-like particles (VLPs), which have been extensively studied over the last few decades as a form of immunotherapy against cancer, do not contain viral genomes, rendering them unable to produce viral progeny and therefore, represent a safer alternative to replicative viral treatment (Caldeira et al., 2020; Grgacic & Anderson, 2006; Mohsen et al., 2020). VLPs mimic the structural formation of a representative authentic virus, enabling them to stimulate powerful immune responses (Mohsen & Bachmann, 2022; Ong et al., 2017). Direct application of VLP vaccines for the preventative treatment of hepatitis B virus (HBV) and human papillomavirus (HPV) have been commercialized (Zepeda-Cervantes et al., 2020). Studies have shown the assembly of VLPs within cells when delivered as a gene or a combination of genes encoding the structural proteins required for VLP formation, (Leder et al., 2001; Rayner et al., 2021; Szécsi et al., 2009; Young et al., 2004), however, this type of vaccine has not been licensed to date (Tariq et al., 2022; Uddin et al., 2019). Furthermore, VLPs can be engineered to display specific peptides/proteins on their surface (Rohovie et al., 2017). However, not all VLPs are created

equally; nor are all able to display proteins/peptides (Frietze et al., 2016). Therefore, a major milestone in moving this project forward is the selection of a suitable virus for VLP formation.

This project aims to design a gene cassette encoding a human papillomavirus (HPV) 16 L1 gene for the expression and formation of HPV16 L1 VLPs in mammalian cells. Furthermore, we will attempt to display a peptide of interest on the surface of the VLPs to enhance the anti-cancer properties of this anticipated treatment. Successful formation of HPV16 L1 VLPs displaying the peptide of interest will support the evaluation of the designed DNA-VLP gene cassettes contained within a mammalian expression plasmid, as a potential gene-based immunotherapeutic vaccine.

1.1 Cancer immunotherapy

Cancer immunotherapy is a form of cancer treatment that artificially stimulates the immune system to constructively fight cancer and inhibit tumour progression (Esfahani et al., 2020). Many cancer immunotherapies predominantly induce T-cell adaptive immune responses to fight cancer, however, both adaptive and innate immune responses are fundamental components of anti-tumour immunity and work in concert to promote this process (Moynihan & Irvine, 2017). This section will briefly outline and visualize a simplified overview of key anti-cancer immune responses (Figure 2), in addition to immune responses within the tumour microenvironment (TME) that are downregulated due to the advancement of immune evasion strategies (Tang et al., 2016). Understanding these facets of anti-cancer immunity is essential for the development of successful cancer immunotherapeutics which can encompass antibody (Ab) therapy, immune checkpoint inhibitor therapy, and adoptive T-cell transfer, including chimeric antigen receptor (CAR) T-cell therapy, which in recent years, has proved to be highly efficacious (Koury et al., 2018; M. Liu & Guo, 2018; Tang et al., 2016).

1.1.1 Important anti-cancer immune responses

The adaptive immune response (aka acquired immune response) progressively activates over time and is predominantly characterized by immune responses instigated by antigen presentation via major histocompatibility complex (MHC) I and II molecules towards T- and B-cells (Bonilla & Oettgen, 2010). T-cells play an integral role in anti-cancer immunity. There are two major types of T-cells: $CD8^+$ cytotoxic T-cells and $CD4^+$ T-helper (Th) cells (Waldman et al., 2020). $CD8^+$ cytotoxic T-cells are most effective at directly killing cancer cells and destroying tumours (Martínez-Lostao et al., 2015). In this process, dendritic cells (DCs), which are antigen-presenting cells (APCs), present MHC class I molecules displaying foreign antigens to $CD8^+$ T-cells to induce the production of effector $CD8^+$ T-cells, known as cytotoxic T lymphocytes (CTLs) (Farhood et al., 2019; Gotwals et al., 2017). CTLs then invade the TME and impart their effect by directly killing cancer cells and promoting apoptosis (Maher & Davies, 2004). To promote apoptosis, CTLs induce the production of pores within cell membranes via the use of a protein known as perforin, promoting the importation of proteins, including granzyme B, for cellular destruction (Voskoboinik et al., 2015; Weigelin et al., 2021). Additionally, the infiltration of high densities of CTLs within tumours has been shown to be associated with the killing of cancer cells by the activation of cytotoxic cytokines, including interferon-γ (IFN-γ) and tumour necrosis factor (TNF) (Tosolini et al., 2011; Weigelin et al., 2021). $CD4^+$ Th cells interact with MHC class II molecules displaying foreign antigens, inducing the secretion of the aforementioned cytotoxic cytokines, including a variety of interleukin (IL) factors (2, 4, 5, 13, etc), which consequently reinforces the stimulation of $CD8^+$ cytotoxic T-cell activity (Farhood et al., 2019; García-Foncillas et al., 2019; Kershaw et al., 2013). Th cells also recruit B-cells which promote their differentiation into plasma cells, memory B cells, and the secretion of Abs which can lead to Ab-dependent cellular

cytotoxicity and complement-dependent cytotoxicity (Janeway, 2001; Spurrell & Lockley, 2014). Subsets of Th cells impart their anti-tumour effects differentially within tumours (H.-J. Kim & Cantor, 2014). TNF-α and IFN-γ cytokines specifically produced from Th1 cells have been shown to induce cancer cell death, in addition to the activation of macrophages, which will be outlined in more detail in the following paragraph (Hsu et al., 2010; H. L. Lee et al., 2019). Other subsets of Th cells have been shown to promote both anti- and pro-tumour responses (H.-J. Kim & Cantor, 2014). This includes Th2 cells and Th17 cells, among others. Th2 cells primarily impart their anti-cancer effects by the production of IL-4, in addition to the recruitment of innate immune cells toward tumours (Ellyard et al., 2007; Modesti et al., 1993; Nishimura et al., 1999). Th17 cells have been shown to induce the recruitment of DCs, which subsequently instigates the onset of anti-tumour CTL responses (R. Wang et al., 2018).

The innate immune response is an immediate reaction to the introduction of foreign entities into the body. This type of immune response also exemplifies a critical role in the development of anti-tumour immunity (Munhoz & Postow, 2016). In general, the innate immune response complements the adaptive immune response and can aid in the enhancement of $CD8^+$ T-cell immune responses (Y. Liu & Zeng, 2012). Natural killer (NK) cells are important innate immune cells that respond to stress ligands emitted by tumours and can kill cancer cells via the release of cytotoxic granules. This can lead to the release of cytokines including IFN-γ, which constitutes a variety of anti-tumour properties (Lanier, 2008; Moynihan & Irvine, 2017; Qin et al., 2003; S.-R. Woo et al., 2015). Stimulation of macrophages can also assist in the eradication of tumours via Ab-dependent cellular phagocytosis or through the secretion of nitric oxide species (Klug et al., 2013; M. Singh et al., 2014; Weiskopf & Weissman, 2015). Tumour-infiltrating neutrophils reinforce T-cell responses and proliferation in a positive-feedback loop, highlighting its anti-

tumour potential (Eruslanov et al., 2014; Musiani et al., 1996). Eosinophils enhance anti-tumour immunity via the release of granzyme B, an effective pro-apoptotic protein, in addition to the recruitment of T-cells towards the TME (Carretero et al., 2015; Moynihan & Irvine, 2017). Overall, these innate immune cells work together to engender strong immune signals within tumours, signifying their fundamental role in the development of anti-cancer immunity and cancer cell lysis (Labani-Motlagh et al., 2020).

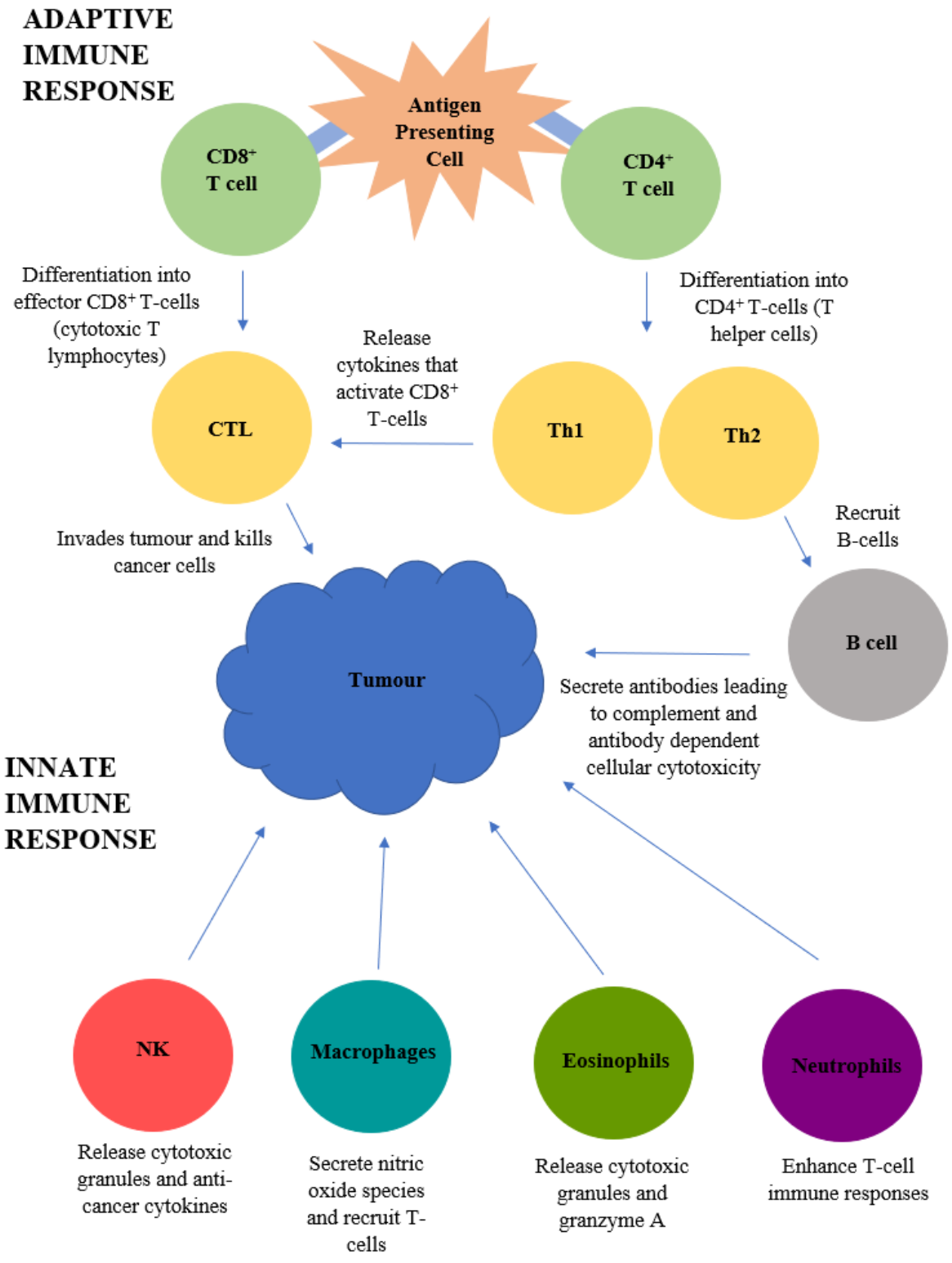

Figure 2. Anti-cancer immune responses. The activation of $CD8^+$ and $CD4^+$ T-cells via antigen presentation from MHC I and II molecules into effector cells promotes tumour eradication. The recruitment of innate immune cells promotes the adaptive immune response and cancer cell lysis.

1.1.2 TME immune suppression

The TME is characterized as a highly heterogenous and dynamic entity composed of a combination of proliferating malignant cells, non-malignant cells, extracellular matrix proteins, infiltrating immune cells, vasculature, and associated tissues (Chowell et al., 2018; Labani-Motlagh et al., 2020). Tumours progressively evolve over the course of their growth and can acquire the ability to evade the immune system, hence permitting tumour survival and excessive growth over time (Chowell et al., 2018; Gonzalez et al., 2018; Tran et al., 2016). Their ability to evade the immune system is notably influenced by molecular mechanisms and interactions within the TME (Balkwill et al., 2012; Whiteside, 2008). Within the TME, anti-cancer immune responses imparted by NK cells, $CD8^+$ T-cells, $CD4^+$ T-cells, DCs, etc., are counteracted primarily by T-regulatory (Treg) cells. These cells are a subset of $CD4^+$ T-cells that markedly suppress the immune response to maintain immune homeostasis (J.-H. Kim et al., 2020). They can inhibit $CD8^+$ T-cell, IFN-γ secreting T-cell, and NK cell immune responses by the production of IL-10 and transforming growth factor β (TGF-β) (Jarnicki et al., 2006). They can additionally inhibit DC function by the expression of cytotoxic T-lymphocyte associated protein 4 (CTLA-4) on Treg cells (Chen, Du, et al., 2017). Overall, the effects of Treg cells intercept the recognition of tumours by the immune system and NK-cell mediated immune surveillance, accordingly prohibiting tumour eradication (Balkwill et al., 2012; Labani-Motlagh et al., 2020).

Tumours also employ other molecular mechanisms to evade the immune system. This can involve the upregulation of immune system checkpoints on Treg cells within the TME, which are characterized as molecules involved in mitigating immune responses as a means to avoid the onset of autoimmunity (Pardoll, 2012). Upregulation of immune checkpoint receptors, which are recognized by immune checkpoints, further inhibits immune response stimulation against tumours

(Schadendorf et al., 2017; Wherry & Kurachi, 2015). Immunosuppressive leukocytes can also be recruited to the TME, combatting the effectiveness of some anti-tumour immune responses (Ferrone & Dranoff, 2010). Some cancer cells also lose MHC I antigen presentation machinery, rendering these cells unable to effectively present antigens to $CD8^+$ T-cells for their activation (Campoli & Ferrone, 2008). Overall, one of the major hurdles facing the efficacy of cancer immunotherapy is characterized by the immunosuppressive TME. Therefore, it is critical that cancer immunotherapeutics overcome immune evasion strategies contributing to the evolvement of the immunosuppressive TME in order to successfully eradicate and treat tumours (Sun et al., 2020).

1.1.3 Immuno-oncology therapies

This section outlines the different types of immuno-oncology treatments that have been studied in clinical trials and approved for medicinal use. The predominant forms of immune-oncology treatments include monoclonal Abs (mAb), checkpoint inhibitors, and T-cell based therapies. A table briefly summarizing the information reported in this section is presented in the table below.

Table 1. Overview of immuno-oncology therapies

Type of Treatment	Name of Treatment	Primary use	How it works	Reference
mAbs Against Growth Factors	-Cetuximab -Pantimumab	-metastatic colorectal cancer and head and neck cancer (Cetuximab) -colorectal cancer (Pantimumab)	-blocks the binding of ligands to EGFR	Garcia-Foncillas et al., 2019
	-Ramucirumab -Bevacizumab	-gastric cancer (Ramicirumab) -metastatic colorectal cancer (Bevacizumab)	-blocks the binding of ligands to VEGFR	Javle et al., 2014

Checkpoint Inhibitor	-Ipilimumab	-melanoma	-blocks the binding of CTLA-4 to its ligand, enabling T-cell activation	Wolchok et al., 2013
	-Pembrolizumab -Dostarlimab	-melanoma (Pembrolizumab) -endometrial cancer (Dostarlimab)	-blocks the binding of PD-1 to its ligand, enabling T-cell activation	Deeks et al., 2016
T-Cell Transfer	-Tisagenlecleucel -Acisabtagene ciloleucel	-B-cell acute lymphoblastic leukemia	-T-cells that recognize and bind to CD19, enabling T-cell activation	Halford et al., 2021;
	-Idecabtagene vicleucel	-multiple myeloma	-T-cells that recognize and bind to BCMA, enabling T-cell activation	Munshi et al., 2021

Ab: antibody; BCMA: B-cell maturation antigen; CTLA: cytotoxic T-lymphocyte associated antigen; CD: cluster of differentiation; EGFR: epidermal growth factor receptor; mAb: monoclonal antibody; PD: programmed cell death protein; VEGFR: vascular endothelial growth factor receptor

1.1.3.1 Targeted Ab treatments

Monoclonal antibodies (mAbs) are effective at inhibiting cancer cell growth by recognition and neutralization of Ab-specific antigens. Monoclonal Ab immunotherapy is a well-established, highly specific treatment that has been applied toward several cancer types and constitutes a major portion of standard cancer treatments (García-Foncillas et al., 2019). A more advanced form of Ab treatment is the use of bispecific Abs (biAbs), which are directed towards two targets as opposed to one, by merging the variable domains of the mAbs of interest into a single structure (Thakur & Lum, 2010). The dual-specificity of biAbs can be imparted by the configuration of one construct that binds to tumour antigens presented directly on tumour cells, and another construct that targets receptors on immune effector cells (Fendly et al., 1990; Grosse-Hovest et al., 2003; Thakur & Lum, 2010).

This category of cancer treatment has been designed to target a wide assortment of molecules including tumour antigens, oncogenic signalling molecules, and growth factors (GFs)/growth factor receptors (GFRs) (Zahavi & Weiner, 2020). GFRs are a collection of surface proteins that are involved in an array of fundamental cellular functions including cell growth, survival, and angiogenesis (Harris, 1991; Tiash & Chowdhury, 2015). The overexpression of some of these GFRs in different cancer types promotes dysregulation of cellular signalling, driving cells to multiply and grow at accelerated rates and evade apoptosis (Witsch et al., 2010). Considering many cancer types are exemplified by the overexpression of these types of receptors, there are currently several clinically approved mAbs that specifically target GFs, GFRs and their associated signalling molecules (Yamaoka et al., 2018).

Epidermal growth factor receptor (EGFR) is a cell surface receptor that is over-expressed in cancer cells and is significantly involved in the growth and survival of epithelial tumours when bound to its corresponding ligand, epidermal growth factor (EGF) (Zaczek et al., 2005). Clinically approved mAb drugs targeted against EGFR include cetuximab and panitumumab, which target the extracellular domain of this receptor and can be used alongside chemotherapy treatments (García-Foncillas et al., 2019). Vascular endothelial growth factor receptor (VEGFR) is also a cell surface receptor that binds to vascular endothelial growth factor (VEGF), and is overexpressed in cancer cells and primarily involved in the formation of blood vessels (termed angiogenesis), a process that is pivotal for tumour formation (Duffy et al., 2013). Overall, VEGFR plays a critical role in both the evolution and conservation of tumours (Duffy et al., 2013). Ramucirumab was recently approved in 2014 for the treatment of gastric cancer. It consists of a humanized immunoglobulin (Ig) G1 mAb that effectively targets VEGFR to inhibit its activation. In doing so, this obstructs the upregulation of downstream signalling pathways that further advance angiogenesis (Javle et al.,

2014). Supplementary studies outlining other effective anti-angiogenic therapeutics that target VEGF and VEGFR will be outlined in Section 1.2.

1.1.3.2 Checkpoint inhibitors

As previously described, tumours can evade the immune system via dysregulation of immune checkpoints, fabricating an immunosuppressive TME (Schadendorf et al., 2017). Checkpoint inhibitors constitute a class of anti-cancer drugs that also generally takes the form of mAbs which specifically block the receptors that immune checkpoints recognize for their activation. This prevents inhibitory signalling toward T-cells, thereby enabling T-cell activation and T-cell-mediated immune responses (Koury et al., 2018). T-cell activation then promotes the production of effector cells that enhance the immunogenicity of tumour antigens, consequently promoting the recognition of tumours by the immune system and mitigating the tumour immunosuppressive environment (Chmielewski et al., 2013; S. Singh et al., 2020). Several Food and Drug Administration (FDA) approved mAb checkpoint inhibitors are currently on the market, including Ipilimumab and Pembrolizumab, for the treatment of melanoma (S. Singh et al., 2020). These drugs target CLTA-4 and PD-1, respectively, which are integral immune checkpoint receptors that efficiently downregulate immune responses (Deeks, 2016; Lipson & Drake, 2011; Wolchok et al., 2013). Recently, a PD-1 checkpoint inhibitor drug, known as dostarlimab, was used for a clinical trial for the treatment of rectal cancer and demonstrated successful cancer remission for all patients in the trial. However, it is worth noting that the trial only consisted of 12 patients and further confirmatory testing is required (Cercek et al., 2022). This drug was previously approved for the treatment of endometrial cancer (Oaknin et al., 2022), however, considering the results obtained from the aforementioned study (Cercek et al., 2022), its indication is now being expanded for the treatment of rectal cancer. All patients participating in this recent trial had a condition known as

mismatch repair deficiency (Cercek et al., 2022). Individuals with this condition cannot repair errors introduced into the chromosome during DNA replication by methylation-based recognition, rendering frequent mutations during cell divisions (Olave & Graham, 2022). In the past, mismatch repair-deficient colorectal cancer patients have been shown to be responsive to PD-1 checkpoint inhibitors (André et al., 2020). Accordingly, this type of treatment was applied in the aforementioned recent clinical trial for the treatment of rectal cancer (Cercek et al., 2022). Based on the studies indicated above, the versatility of this platform is highly attractive making it a popular form of cancer treatment (Fan et al., 2021). However, systemic administration of immune checkpoint-blocking Abs can be limited by low response rates (Fan et al., 2021). A recent study investigated the use of an enhanced tumour-targeted delivery system for this Ab treatment by fusing the immune checkpoint inhibitor with a tumour-homing ligand, promoting augmented tumour-specific inhibitory effects (Fan et al., 2021).

1.1.3.3 Adoptive T-Cell transfer

Adoptive T-cell transfer treatments encompass the infusion of different cell types into the body, including tumour-infiltrating lymphocytes (TILs) and chimeric antigen receptor (CAR) T-cells (J. C. Yang & Rosenberg, 2016). IL-2 is a cytokine signalling molecule that is known to promote T-cell growth and is commonly employed with these types of treatment for *in vitro* cell expansion (Rosenberg, 2014). TILs possess the ability to invade tumours and have been shown to induce IFN-γ secretion and exert tumour-killing activity (Jiang et al., 2015; Markel et al., 2009). Infusion of these cells in melanoma patients has conferred successful outcomes, with response rates of 50% and greater (S. Lee & Margolin, 2012; Rosenberg et al., 2011). CAR T-cells are genetically engineered cells expressing artificial receptors that promote T-cell activation (Almåsbak et al., 2016). These cells consist of an extracellular single-chain variable fragment derived from an Ab,

a transmembrane domain, and an intracellular CD3ζ domain for T-cell recognition and subsequent activation (Koury et al., 2018). Tisagenlecleucel is a CAR T-cell treatment that was approved by the FDA in 2017 for the treatment of relapsed/refractory B-cell acute lymphoblastic leukemia (Y. Liu et al., 2017). These engineered T-cells are able to specifically recognize the CD19 transmembrane glycoprotein expressed on healthy and malignant B-cells, promoting T-cell activation and the induction of anti-tumour responses (Halford et al., 2021). Another CAR T-cell treatment known as, Axicabtagene ciloleucel, is similarly a CD19-directed treatment and was investigated as a second-line therapy for large B-cell lymphoma. The administration of this drug demonstrated enhanced response and survival rates compared to a standard care treatment (chemotherapy followed by stem-cell transplantation) (Locke et al., 2022). Indecabtagene vicelucel T-cells expressing a receptor for BCMA (B-cell maturation antigen), a member of the tumour necrosis factor superfamily, is another CAR T-cell treatment that has been investigated (Munshi et al., 2021). Studies have shown that BCMA is expressed on the surface of malignant plasma cells in individuals with multiple myeloma and is markedly involved in maintaining cell survival (Carpenter et al., 2013; Roex et al., 2020; Timmers et al., 2019). The application of this treatment in a Phase 2 study demonstrated the induction of strong anti-tumour immunity (Munshi et al., 2021). The efficacy of this treatment promoted its FDA approval in 2021 for the treatment of multiple myeloma (Sharma et al., 2022). The recent breakthroughs of this therapy instigated its approval for the aforementioned cancer types, although, there are still some concerns limiting its widespread application. This includes the induction of some severe toxicities, in addition to its inability to fully overcome the negative repercussions imparted by the evolvement of the immunosuppressive TME (Sterner & Sterner, 2021).

1.2 Cancer and GFRs

Cancer is caused by mutations that promote two distinctive types of responses: activation of oncogene expression or deactivation of tumour suppressor genes. The successive accumulation of these genetic alterations consequently leads to uncontrolled cell growth and eventually tumour formation (Sarkar et al., 2013). Some oncogenes encode for GFRs, which as aforementioned, are overexpressed in many cancer types and promote cancer cell growth at extensive rates (Witsch et al., 2010).

Many GFRs are categorized within a subclass of kinase proteins, known as receptor tyrosine kinases (RTKs). These receptors contain four characteristic structural components including an extracellular ligand binding domain, juxta membrane domain, tyrosine kinase domain and carboxyl-terminal tail (Du & Lovly, 2018). On the surface of cells, RTKs receive information from their surroundings in the form of GFs, which are glycoprotein polypeptides that specifically bind to RTKs (Witsch et al., 2010). GFs bind to the extracellular domain of RTKs, subsequently inducing dimerization of the receptor which leads to autophosphorylation and activation of kinase activity. This triggers the recruitment and binding of downstream signalling proteins that institute the stimulation of cellular signalling pathways for the onset of essential biological functions (Pawson, 2002; Yamaoka et al., 2018). Anti-cancer drugs impart their effects against GFRs through a variety of mechanisms, including mAb neutralization (as aforementioned), inhibition of protein kinases, and cellular signalling protein antagonism (Tiash & Chowdhury, 2015).

This section will outline an integral RTK, known as VEGFR, which binds to VEGF (Duffy et al., 2013). VEGF and VEGFR overexpression characterizes many cancer types, including lung, colon and breast cancers (Costache et al., 2015; Giatromanolaki et al., 2007; S. Guo et al., 2010). Anti-

cancer treatments targeting VEGF/VEGFRs will also be discussed, including the use of VEGF anti-angiogenic isoforms and peptides.

1.2.1 VEGFR

VEGFR is an RTK that binds to VEGF and is expressed on many types of healthy cells, in addition to tumour cells (Duffy et al., 2013). Once receptor-bound, downstream signalling pathways are initiated that promote angiogenesis (Morabito et al., 2006). Angiogenesis, the process of blood vessel formation, is crucial for the development of tumours as they require high demands of oxygen and nutrient levels for continual growth, in addition to the output of metabolites and waste products - a system extensively mediated by the vascular network (Nishida et al., 2006). Accordingly, most solid tumours show upregulated VEGF/VEGFR expression to compensate for their aberrantly rapid metabolic processes (Brown et al., 1993; Hicklin & Ellis, 2005; Ohta et al., 1996). In normal healthy tissues, the vascular network is highly organized and characterized by evenly distributed and hierarchically ordered blood vessels. However, within cancerous tissue, the vascular network is severely disorganized and exemplified by vessels that are twisted, hyper-branched, and prone to leakage, creating areas that are exposed to nutrients and oxygen at significantly diverse levels (De Bock et al., 2011; Khawar et al., 2015; Maione & Giraudo, 2015). Overall, the imbalance of pro-angiogenic and anti-angiogenic molecules and dysregulation of VEGFR-signaling drives tumour angiogenesis, conferring disordered vascular network formation within tumours (Folkman, 2002).

The GFs that constitute the VEGF family include, VEGF-A, VEGF-B, VEGF-C, VEGF-D and placental growth factor (PIGF), that bind to one or more of three VEGFR subtypes (VEGFR-1, VEGFR-2 and VEGFR-3) (Takahashi, 2011). VEGF belongs to the platelet-derived growth factor supergene family characterized by eight conserved cystines and functions as a homodimer structure (Shibuya, 2011). VEGF-A is highly conserved and plays the most predominant role in

angiogenesis within its family, imparting its function by binding to either VEGFR-1 or VEGFR-2 (Gong et al., 2004; Holmes & Zachary, 2005). VEGFR-1 and VEGFR-2 are both highly involved in the regulation of angiogenesis, in addition to endothelial cell migration and vascular permeability (Fong et al., 1995; Hiratsuka et al., 2001; Morabito et al., 2006), while VEGFR-3 is primarily implicated in the formation of lymphatic vessels (aka lymphangiogenesis) upon binding to VEGF-C and D (Alitalo & Carmeliet, 2002). PIGF binds to VEGFR-1 and has been shown to be involved in the stimulation of pathological angiogenesis promoted by VEGF-A (De Falco et al., 2002; Ferrara et al., 2003).

1.2.2 VEGFR in cancer therapy

The discovery of the critical role of VEGF/VEGFR for the growth and perpetuation of tumours has led to the extensive development of anti-cancer drugs that target this receptor-ligand pair and its signaling pathways (Kieran et al., 2012). These drugs counteract angiogenesis through a variety of mechanisms, thereby constraining the supply of nutrients and oxygen delivery that is required for tumour formation (Zirlik & Duyster, 2018). A well-known clinically approved anti-cancer drug, Bevacizumab, is a VEGF humanized mAb that effectively inhibits VEGF-A, and consequently it's binding towards VEGFR (Des Guetz et al., 2006; Foekens et al., 2001; Seto et al., 2006). Ramucirumab is another well-known anti-cancer mAb that specifically targets VEGFR-2, as previously mentioned (Javle et al., 2014). Another category of drugs, known as tyrosine kinase inhibitors, similarly targets VEGFR by blocking its adenosine triphosphate (ATP) binding site (Gotink & Verheul, 2010). Under normal conditions, the phosphorylation of the tyrosine kinase domain within RTKs occurs using ATP for subsequent activation and stimulation of intracellular signaling pathways. However, tyrosine kinase inhibitors block this site, preventing autophosphorylation and leading to the inhibition of RTK activation (Gotink & Verheul, 2010).

Another well-known drug, Aflibercept, is a decoy VEGFR that binds to VEGF-A, VEGF-B and PIGF at elevated levels, but is structurally unable to induce the signalling required for angiogenesis to persist. This drug contains portions of the extracellular domains of two VEGFRs, VEGFR-1 and VEGFR-2, that are fused to the constant region of IgG1 (Holash et al., 2002). This chimeric fusion enables high-affinity binding towards the aforementioned VEGF ligands compared to other commercially available Abs (de Lima Farah et al., 2018).

1.2.3 VEGF anti-angiogenic isoforms and peptides

Anti-angiogenic isoforms and peptides have been investigated for their application towards preventing angiogenesis within tumours via VEGFR targeting (Rosca et al., 2011). These synthetic and native molecules can be advantageous, attributed to their low levels of associated toxicity and heightened specificity towards targeted receptors (Nakamura & Matsumoto, 2005; Saladin et al., 2009). An anti-angiogenic isoform, known as $VEGF_{165b}$, is a differentially spliced variant of VEGF-A that is composed of 165 amino acids (aa) (Woolard et al., 2004). $VEGF_{165b}$ is expressed in normal cells, however, it was initially demonstrated by Bates et al. (2002) to be significantly downregulated in renal tumours, suggesting its involvement in anti-angiogenesis (Bates et al., 2002). Differential splicing of exon 8 of VEGF-A governs its pro-angiogenic and anti-angiogenic states (Dehghanian et al., 2014). In its pro-angiogenic form ($VEGF_{165a}$), exon 8 is made up of 18 bases which encode for 6 aa residues, CDKPRR. However, in its anti-angiogenic form ($VEGF_{165b}$), exon 8 encodes for SLTRKD, comprising of increased neutrally charged aa residues (Harper & Bates, 2008; Woolard et al., 2004). Conformational alterations of this isoform structure renders it unable to bind to neuropilin-1, a co-receptor of VEGFR-2 (Parker et al., 2012; Peach et al., 2018). While it still holds the capacity to bind to VEGFR-2, its binding induces less efficient autophosphorylation, thereby preventing stimulation of VEGFR-2 downstream signaling

pathways (Harper & Bates, 2008; Kawamura et al., 2008; Woolard et al., 2004). Woolard et al., (2004) demonstrated that the $VEGF_{165b}$ isoform inhibits angiogenesis in rabbit cornea and mesentery, in addition to reducing tumour growth, compared to $VEGF_{165}$ expressing tumours.

A synthetically designed peptide, known as VGB, has also been shown to confer anti-angiogenic properties as an antagonist against VEGF-A and VEGF-B. This peptide is composed of 14 aa residues from the VEGF-A ligand and contains three binding sites specific for VEGFR-2 and two binding sites specific for VEGFR-1. The peptide structure was previously predicted *de novo* and is illustrated in Figure 3 (Sadremomtaz, Kobarfard, et al., 2018). Opposed to the targeting of one receptor, this peptide is able to target both VEGFR-1 and VEGFR-2 (Sadremomtaz, Kobarfard, et al., 2018; Sadremomtaz, Mansouri, et al., 2018), conferring enhanced efficacy and limiting the development of resistance (Gille et al., 2007). The binding of this peptide towards VEGFR-1 and VEGFR-2 has been shown to suppress the phosphorylation of VEGF/VEGFR signaling molecules, including P13K/ AKT and MAPK/ERK 1/2, which consequently limits the activation of downstream signaling pathways required for the formation of blood vessels (Sadremomtaz, Kobarfard, et al., 2018). ERK1/2 and AKT signalling pathways are involved in diverse cellular processes including cell proliferation, migration, and vascular permeability (Koch & Claesson-Welsh, 2012; Pettersson et al., 2000). Administration of VGB inhibited VEGF-induced proliferation and migration within human umbilical vein endothelial cells, 4T1 mammary carcinoma tumour cells, and U87 glioblastoma cells. Additionally, treatment with VGB promoted the impediment of metastatic mediators including epithelial-cadherin and nuclear factor-kB. It also inhibited tumour growth within a mammary carcinoma murine model by ~80% (Sadremomtaz, Kobarfard, et al., 2018; Sadremomtaz, Mansouri, et al., 2018). A similar,

but alternative peptide, known as VGB4, works in a comparable manner to VGB, as shown in Figure 5, although it is slightly longer in length (23 aa residues) (Farzaneh Behelgardi et al., 2020).

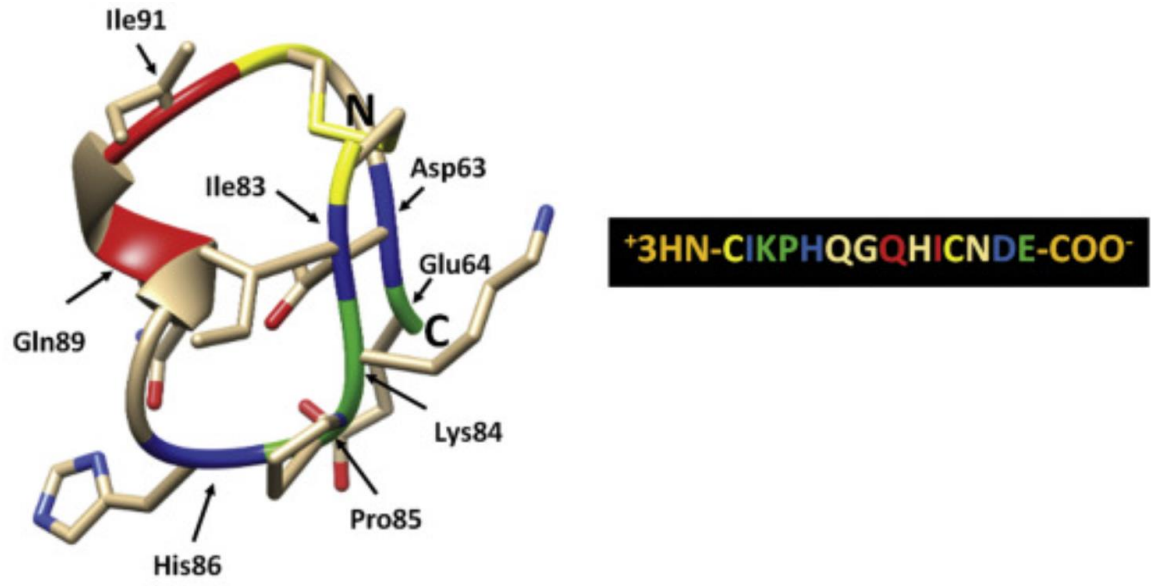

Figure 3. Structural representation of the VGB peptide. The colours indicated on the structure represent the amino acids indicated in letters on the lefthand side of the image (Taken from Sadremomtez, Kobarfard, et al., 2018).

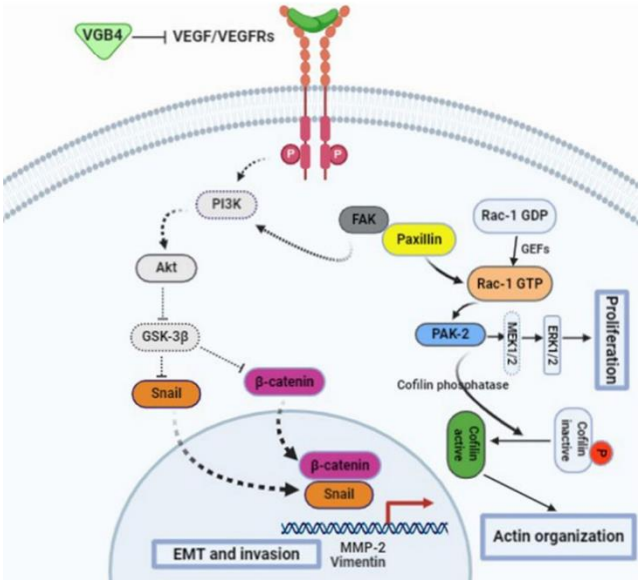

Figure 4. VEGF/VEGFR pathways that are inhibited by VGB4 binding towards VEGFR. VGB4 acts as an antagonist towards VEGF ligands preventing P13K/AKT and MAPK/ERK1/2 signalling pathways from occurring (Taken from Farenzah Behelgardi et al., 2020).

1.3 Gene therapy for cancer

Gene-therapy is a broad-based term that encompasses the use of genetic material (DNA and/or RNA) for expression within cells to aid in the curing of a disease of interest (Scheller & Krebsbach, 2009). One of the most prominent determining factors that characterizes the efficacy of gene therapy-based treatments is the choice of gene-delivery vehicle, which enables the gene/genes of interest to bypass the cell membrane and subsequently transfer into the nucleus for transcription, followed by translation in the cytoplasm of the cell (Begum et al., 2019). To deliver genes into cells, an array of vectors have been employed including non-viral vectors, characterized by their increased safety profile but lower gene-delivery efficiency, and viral vectors, characterized by their decreased safety profile but higher gene-delivery efficiency (Gardlík et al., 2005).

Particularly, for cancerous diseases, the transcription and translation of specified genes can alter tumour cells by a variety of mechanisms, including increasing the expression of apoptotic and tumour suppressor genes and decreasing the expression of oncogenes (Cross & Burmester, 2006; DAS et al., 2015). Furthermore, gene therapy can also be used for the expression of genes that enhance the immunogenicity of tumours to promote immune cell recognition (DAS et al., 2015), which is the fundamental basis of the cancer immunotherapy platform approach designed and investigated in this study. Cancer immunotherapy constitutes a large portion of cancer gene therapy by the exploitation of genes to express molecules within cells that redirect the immune system toward tumours for their eradication (Cross & Burmester, 2006). In general, there are three predominant ways gene therapy can be administrated, specifically in regard to cancer immunotherapy applications (Figure 5; Cross & Burmester, 2006). First, cancer cells can be directly isolated from patients, injected with immunostimulant genes, harvested, and subsequently lysed to release their cellular contents for the generation of vaccines (Cross & Burmester, 2006;

Kowalczyk et al., 2003). Second, immunostimulant genes can also be directly injected into the tumour for subsequent uptake and expression within cancerous cells *in vivo* (Cross & Burmester, 2006; Nawrocki et al., 2001). This gene therapy administration approach is anticipated for the future application of the DNA-VLP gene cassettes investigated in this study. Third, immune cells isolated from patients can be altered by injection of immunostimulant genes, which can then be incorporated into tumours for consequent immune system activation (Cross & Burmester, 2006; Kikuchi, 2006).

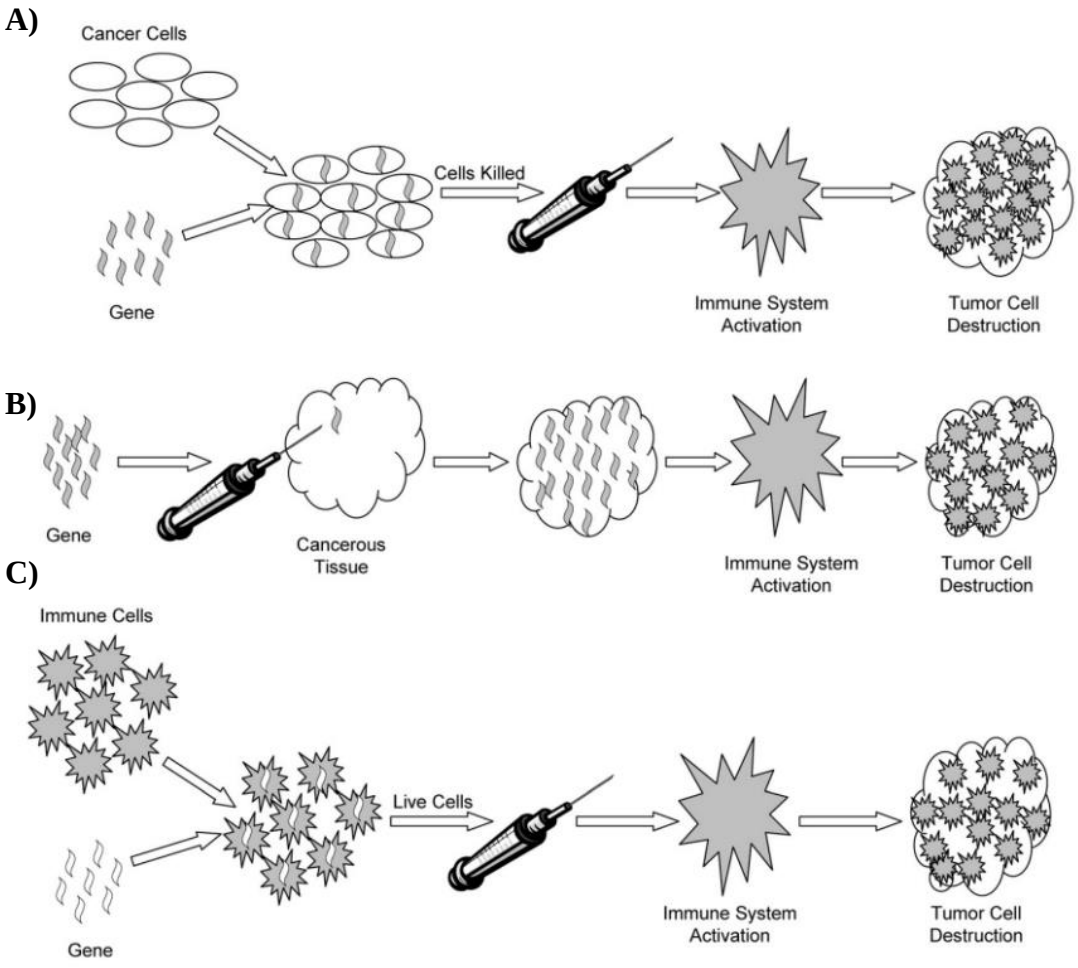

Figure 5. Gene therapy-based cancer immunotherapy application. Methods of gene administration for cancer immunotherapy includes **A)** addition of immunostimulant genes to patients' cancer cells for subsequent lysis and incorporation into a vaccine; **B)** direct administration of immunostimulant genes to tumours; **C)** addition of immunostimulant genes to immune cells for subsequent administration to tumours (Taken from Cross & Burmester, 2006).

1.4 VLP Immunotherapy

VLPs are rapidly emerging as an effective platform for cancer immunotherapy (Mohsen et al., 2020; Tornesello et al., 2022). VLPs are constructed using essential viral structural proteins that self-assemble into non-enveloped or enveloped hollow particles resembling the virus from which they were derived from (Grgacic & Anderson, 2006). Non-enveloped VLPs are composed solely of a native virus' structural proteins enabling a simpler characterization process, while enveloped VLPs contain an additional lipid membrane (envelope) around its structure that is formed via budding from the host membrane, thereby incorporating some of the host's cellular proteins into its structure (Dai et al., 2018). This additional envelope layer imparts a more complex VLP composition contributed by uncertainty in regards to the integrated host membrane components, rendering enveloped VLPs more challenging to characterize (Dai et al., 2018; Naskalska & Pyrć, 2015). In general, the production of VLPs within both eukaryotic and prokaryotic cell types including yeast, plant, bacteria, insect, and mammalian cells, highlights the versatility of production for this platform (Tornesello et al., 2022).

The application of viruses for the treatment of cancer is advantageous as infection and immune response stimulation can impart inhibitory effects toward tumours, promoting decreased survival and progression (Hemminki et al., 2020; Pyeon et al., 2020). Oncolytic viruses have been developed as a potential means of treating cancer by stimulating potent immune responses, in addition to directly killing cancer cells (Buijs et al., 2015). However, compared to oncolytic viruses, VLPs confer increased safety considering they do not contain a viral genome, preventing them from inducing adverse effects that are normally associated with native viral infection and replication (Donaldson et al., 2018). Some characteristic features of VLPs render the use of these particles as an ideal platform for cancer immunotherapy. Firstly, considering VLPs mimic the

structural order of an authentic virus, they are able to engender an effective immune response which can help overcome the immunosuppressive TME (Mohsen et al., 2020; Ong et al., 2017). Secondly, different antigens and peptides of interest can be displayed on the surface of VLPs via genetic or chemical fusion. This can promote the stimulation of more broad immune responses against the peptide/antigen of interest, enable VLP targeting of specific receptors, and induce specific anti-tumour immune responses (Lin et al., 2014; Shirbaghaee & Bolhassani, 2016). Thirdly, considering some non-enveloped viruses exit the cell via cell lysis or bursting from cells (Bird & Kirkegaard, 2015; Zepeda-Cervantes et al., 2020), this may provide VLPs with the capacity to impart oncolytic effects. Within insect cell expression systems, some VLPs have been shown to leave the cell via cell lysis or budding (Arevalo et al., 2016; Zepeda-Cervantes et al., 2020). This section will expand upon anti-cancer immune responses that are instigated by VLPs and how this relates to overcoming the immunosuppressed TME, in addition to outlining the use of preventative and therapeutic VLP vaccines against different types of diseases and more specifically, cancer.

1.4.1 VLP immune response induction

VLPs are capable of simultaneously stimulating both arms of the immune system, encompassing the innate and adaptive immune response, in addition to presenting self-adjuvant effects. The size and surface conformation of VLPs enable efficient recognition and recruitment of innate immune cells (Mohsen et al., 2017). VLPs are able to induce a more enhanced innate immune response given their repetitive structural organization and conformational epitopes compared to single protein/polypeptide treatments (Jegerlehner et al., 2002; Roldão et al., 2010). Administration of VLPs in mice has been shown to induce the infiltration of innate immune cells including macrophages, neutrophils, and DCs (K.-H. Kim et al., 2018; Raghunandan, 2011). The recruitment

of innate immune cells towards the TME can assist in cancer cell killing, in addition to the induction of anti-tumour adaptive immune responses, which ideally can help to overcome the immunosuppressive TME (Labani-Motlagh et al., 2020; Mohsen et al., 2020; Ong et al., 2017). Pathogen-associated structural patterns (PASPs) on VLPs can be directly detected by pattern recognition receptors (PRRs), including toll-like receptor (TLR)-2 and 4 on the surface of DCs (Boehme & Compton, 2004; Compton et al., 2003; Zepeda-Cervantes et al., 2020). This interaction can promote the maturation of DCs which advances the adaptive immune response (Dzopalic et al., 2012; Schiller & Lowy, 2012). Additionally, recognition of VLPs by DCs can also lead to the production of pro-inflammatory cytokines which consequently increases the recruitment of APCs (Fiebiger et al., 2001; Nooraei et al., 2021).

VLPs have virally encoded Th cell-recognized epitopes which, via MHC II on professional APCs, are presented to $CD4^+$ Th cells leading to their activation. This activation subsequently enhances the stimulation of B-cells, T-cells, and macrophages (Chackerian et al., 2008; Yadav et al., 2019). VLPs can also be taken up by $CD8^+$ DCs which are highly effective at cross-presenting peptides on MHC class I molecules (Mohsen et al., 2020). Presentation of VLP epitopes towards $CD8^+$ T-cells induces their activation and killing of cancer cells (Crisci et al., 2012; Zepeda-Cervantes et al., 2020). Additionally, strong B-cell responses and secretion of Abs in response to VLP administration have been detected via the cross-linking of specific receptors on B-cells (Jegerlehner et al., 2002; Roldão et al., 2010). In general, VLPs are capable of inducing a similar level of humoral immunity as the virus from which they are derived (Mohsen et al., 2017). IgM or IgG Ab binding towards VLP surface proteins has been shown to activate the complement cascade, which can lead to tumour cell killing (Caldeira et al., 2020; Roumenina et al., 2019). Overall, the induction of these types of immune responses against VLPs has the capacity to overcome the

tumour immunosuppressive microenvironment and effectively minimize cancer cell growth (Ong et al., 2017).

1.4.2 VLP vaccines

VLP-based vaccines can categorized as both prophylactic (aka preventative) and therapeutic in nature (Mohsen et al., 2020; Ong et al., 2017; Tornesello et al., 2022). Prophylactic-based vaccines work to build a competent immune force towards a specific virus prior to infection to prevent the onset of infection and/or severe symptoms of infection (Sela & Hilleman, 2004). The first commercially available VLP vaccine was against the hepatitis B virus (HBV) using its surface antigen produced in yeast cells (McAleer et al., 1984). This vaccine demonstrated 95% effectiveness in preventing HBV infection (Buonaguro et al., 2011). Currently, there are three HPV VLP vaccines that are commercially available against HPV-induced cervical cancer which are known as, Gardasil-9, Cervarix, and Gardasil-4 (Buonaguro et al., 2011; Yadav et al., 2019). The VLPs for HPV are formed by the expression of HPVs major capsid protein, L1, as reviewed by Yadav et al. (2019). The successful outcomes of these vaccines instigated the development and study of new VLP preventative-based vaccines including those targeted against influenza. Individuals immunized with an insect cell-derived H1N1 influenza VLP vaccine demonstrated persistent Ab production that was detected up to 24 months post-vaccination (Valero-Pacheco et al., 2016). The commercially available VLP-based vaccine against Malaria, known as Mosquirix, consists of the circumsporozoite protein of *Plasmodium falciparum*, the parasite that causes malaria, fused to the HBV surface antigen (Kingston et al., 2019; Mohsen et al., 2017; Tariq et al., 2022). A Phase III study showed the induction of expressive levels of Abs and $CD4^+$ T-cells against the circumsporozoite protein (RTS,S Clinical Trials Partnership et al., 2012). Several other preventative VLP vaccines have been studied to protect against infection including those against

norovirus, chikungunya virus, and human immunodeficiency virus (HIV) (Mohsen et al., 2017, 2020; Tariq et al., 2022). VLP-based applications have recently been expanded towards non-infectious diseases including Alzheimer's. Bacteriophage-based VLPs were designed to display the amyloid-β peptide which specifically aggregates in individuals with Alzheimer's, and demonstrated the effective induction of amyloid-β-specific T-cell responses and prolonged Ab titers (Farlow et al., 2015).

1.4.3 VLPs in cancer therapy

Several VLPs have been investigated for their application towards a variety of cancers including melanoma, breast cancer, pancreatic cancer, cervical cancer, and hepatocellular carcinoma (Caldeira et al., 2020; Mohsen et al., 2020; Tornesello et al., 2022). These types of VLP-based vaccines are therapeutic in nature and confer active immunotherapy by redirecting the host's immune response against tumours (Tornesello et al., 2022). Therapeutic-based vaccines are administered to diseased individuals as a means to simultaneously treat and eradicate the targeted disease, and thus, makes up a large portion of cancer immunotherapeutic vaccines that have been studied (C. Guo et al., 2013). Polyomavirus, Qβ bacteriophage, and cowpea mosaic virus (CPMV) VLPs have been evaluated for the treatment of melanoma (Mohsen et al., 2020). A clinical trial of a Qβ bacteriophage VLP vaccine was conducted and demonstrated the induction of significant tumour-specific $CD8^+$ T-cell responses (Goldinger et al., 2012; Schwarz et al., 2005). Moreover, high levels of IFN-γ secreting $CD8^+$ T-cells were observed, indicative of effector CTL formation (Speiser et al., 2010). CPMV VLPs, which were administered via inhalation into a lung metastatic B16F10 melanoma murine model, demonstrated the activation and inflation of neutrophils in the lungs, in addition to decreased tumour burden (Lizotte et al., 2016; Mohsen et al., 2019). MS2 and AP205 bacteriophages have been investigated for the treatment of breast cancer. MS2 VLPs have

been shown to induce a substantial increase of lung infiltrating NK cells and $CD8^+$ T-cells (Bolli et al., 2017; Rolih et al., 2020). AP205 VLPs displaying the Her2 GFR was applied as a type of vaccine-based mAb therapy and stimulated potent anti-Her2 autoantibody responses, in addition to inhibiting tumour growth in wild-type mice with mammary carcinoma cells expressing Her2 (Palladini et al., 2018). Simian human immunodeficiency virus (SHIV) VLPs have been studied for the treatment of pancreatic cancer with incorporated human mesothelin, a protein that is highly involved in tumour adhesion and dissemination (Rump et al., 2004; S. Zhang et al., 2013). Vaccination of this VLP inhibited the progression of orthopedic pancreatic tumours in mice and increased CTL activity, while also decreasing immunosuppressive Treg cells (Li et al., 2008; S. Zhang et al., 2013). Studies employing HPV VLPs displaying the E7 protein for the treatment of cervical intraepithelial neoplasia, also demonstrated effective CTL responses against the L1 protein and the E7 protein, in addition to the induction of high Ab titers (Jentschke et al., 2020; Kaufmann et al., 2007).

Table 2. Overview of therapeutic VLPs studied for cancer therapy

Virus-Like Particle	Primary Cancer Application	Stage of Approval	VLP Design	Reference
Bacteriophage Qβ	-melanoma	-Phase I and II	-loaded with TLR ligands (RNA or CpG motifs)	(Goldinger et al., 2012; Schwarz et al., 2005)
Bacteriophage MS2	-breast cancer	-Preclinical	-inserted with the sixth and third extracellular domain of human xCT protein (protein over expressed in breast cancer cells)	(Bolli et al., 2017; Rolih et al., 2020)
Acinetobacter Phage	-breast cancer	-Preclinical	-covalently displaying the Her2 protein	(Palladini et al., 2018)
CPMV	-melanoma	-Preclinical	-inserted with a tetanus toxoid epitope and displaying the LCMV-	(Lizotte et al., 2016; Mohsen et al., 2019)

			gp33 peptide (as an additional Th cell epitope)	
SHIV	-pancreatic cancer	-Preclinical	-incorporated human mesothelin (involved in tumour adhesion and dissemination) into SHIV VLPs	(Rump et al., 2004; S. Zhang et al., 2013)
SIV	-pancreatic cancer	-Preclinical	-incorporated Trop2 (glycoprotein overexpressed in pancreatic cancer) into the surface of SIV VLPs	(Cubas et al., 2011)
HPV	-cervical intraepithelial neoplasia	-Phase I	-incorporated the E7 protein into the C-terminal of the L1 capsid protein	(Jentschke et al., 2020; Kaufmann et al., 2007)

CPMV: cowpea mosaic virus; gp: glycoprotein; HPV: human papilloma virus; LCMV: lymphocytic choriomeningitis; RNA: ribonucleic acid; SIV: simian immunodeficiency virus; SHIV: simian human immunodeficiency virus; Th: T helper; VLP: virus-like particle; TLR: toll-like receptor.

1.5 HPV

HPV is a non-enveloped virus that contains a double-stranded DNA genome and infects cutaneous and mucosal epithelial cells. Its infection leads to warts, juvenile respiratory papillomatosis, epithelial lesions, and cancer (Burd & Dean, 2016). Cervical cancer is the most common HPV-related disease (Okunade, 2020). There are over 100 HPV types that have been identified to date, however, only 19 of these are categorized as high-risk types. Specifically, HPV16 and 18 contribute to the highest number of HPV-related cancers worldwide (Tumban, 2019).

The genome of HPV encodes early and late genes (Figure 6). The early genes (E1, E2, E4, E5, E6, and E7) are primarily involved in genome replication and transcription-related processes, and the late genes (L1 and L2) encode capsid proteins which make up the structural composition of the virus (Ferreira et al., 2020; J. W. Wang & Roden, 2013). Expression of the L1 gene post-infection, which encodes for the major capsid protein, leads to the arrangement of this protein into 72

pentamers that assemble within the nucleus into T = 7 icosahedral capsids (Figure 7) containing 360 copies of the L1 protein (Zhao et al., 2014). The L2 protein, also known as the minor capsid protein, is located at the vertices of L1 pentamers and assists in the encapsulation of the viral genome (Holmgren et al., 2005; J. W. Wang & Roden, 2013). Once the viral genome is encapsulated, the subsequent release of newly formed viral particles occurs by disruption of the cytoskeleton and the rupture of infected cells within the upper layers of the epithelium (Doorbar et al., 1991; Humans, 2007; Pinidis et al., 2016).

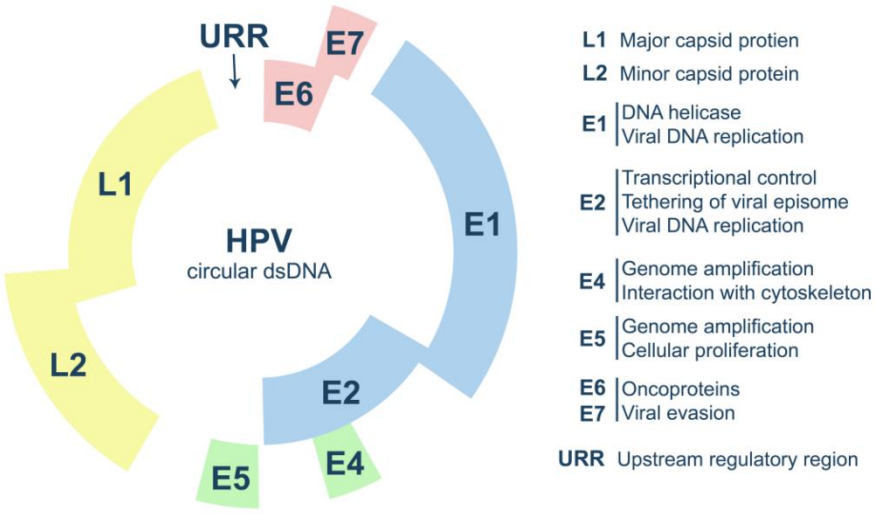

Figure 6. HPV genome. Outline of the major viral proteins encoded within the double-stranded DNA genome of HPV. The functions of each of the proteins encoded by the HPV genome are indicated on the right side of the image (Taken from Ferreira et al., 2020).

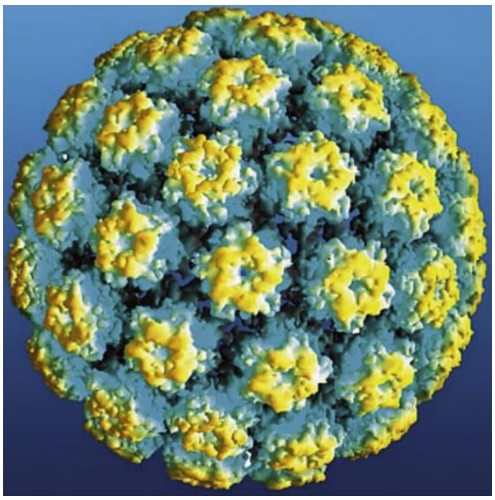

Figure 7. HPV 16 capsid structure. Atomic structure of the HPV16 capsid formed from L1 pentamers (Taken from Zhao et al., 2014).

1.5.1 HPV VLPs

Assembly of L1 into VLPs was first reported for bovine papillomavirus type 1 in 1992, followed by studies demonstrating the self-assembly of HPV VLPs using L1 or the co-expression of L1 and L2 (Hagensee et al., 1993; Kirnbauer et al., 1992; Schiller & Lowy, 2012). The VLP vaccines currently licensed for HPV protect against HPV16 and 18, in addition to a few other HPV types (Tumban, 2019). As aforementioned, these vaccines are known as Gardasil-9, Cervarix, and Gardasil-4, which are produced from the L1 major capsid protein within yeast and insect cells, as reviewed by Yadav et al. (2019). Human codon optimization of the L1 protein of HPV16 and HPV11 for expression in mammalian cells and administration in mice was previously conducted to test the use of VLPs delivered as a DNA vaccine for *in vitro* and *in vivo* assembly (Leder et al., 2001; Mossadegh et al., 2004; Sakauchi et al., 2021).

The highly ordered and repetitive assembly of L1 proteins that form icosahedral HPV VLPs, confers the induction of potent innate immune responses (Lenz et al., 2005; Stanley et al., 2012). This was demonstrated in patients after HPV VLP administration via the activation of DCs which produced significant levels of type 1 IFN-α (Lenz et al., 2005). IFN-α has the ability to induce

macrophage and NK cell cytotoxicity, in addition to enhancing T-cell survival and promoting humoral immunity (Belardelli & Gresser, 1996). HPV VLPs are also able to induce the cytotoxic activity of IL-15 DCs against HPV-positive cervical cancer cells (Van den Bergh et al., 2014). Additionally, stimulation of pro-inflammatory cytokines including IL-1β and TNF-α have been observed upon HPV VLP administration (Van den Bergh et al., 2014), which are cytokines involved in enhancing Th1-mediated immunity against cancer (Haabeth et al., 2015).

Studies show strong and durable Ab production in response to HPV VLP vaccine administration (Nicoli et al., 2020; Stanley et al., 2012). This response could be attributed to the stimulation of long-lived plasma cells which produce antigen-specific Abs at a continual rate (Amanna & Slifka, 2010; Schiller & Lowy, 2012). Results of clinical trials of HPV VLP vaccines also demonstrate virtually 100% seroconversion (Stanley et al., 2012; Villa et al., 2006).

Cell-mediated immune responses have also been detected following HPV VLP vaccine administration including the activation of $CD4^+$ T-cells into effector T-cells, which in turn stimulates the maturation of B cells, as well as cytotoxic $CD8^+$ T-cells (Toh et al., 2015). In a Phase II trial, the induction of notable levels of both $CD8^+$ and $CD4^+$ proliferating T-cells were observed (Pinto et al., 2003). A previous study evaluated $CD4^+$ and $CD8^+$ T lymphocyte responses by stimulation of peripheral blood lymphocytes of cervical cancer patients with L1 VLP-loaded DCs. Strong type 1 L1-specific $CD4^+$ and $CD8^+$ T-cell responses were observed and the production of L1 VLP specific $CD8^+$ T lymphocytes effectively induced the lysis of autologous tumour cells (Bellone et al., 2009).

1.5.2 HPV L1 protein and VLP specific Abs

The production of HPV16 L1 protein and VLPs can be validated by the specific binding of L1 and L1 VLP-specific Abs. Camvir-1 is a well-known Ab that binds to HPV16 L1 proteins by

recognition of a specific linear epitope of the L1 protein (between aa 204 to 210) (Carter et al., 2003). A linear epitope is a region of a protein that is of primary structure and can be recognized by an Ab as a sequence of aa residues for a protein of interest (Deng et al., 2018). Since Camvir-1 recognizes a sequence of aa residues within the L1 protein, it can be used to detect for L1 proteins using western blot analysis (Carter et al., 2003). During the conduction of this technique, proteins are denatured and fractionated on a polyacrylamide gel during sodium dodecyl-sulfate polyacrylamide gel electrophoresis (SDS-PAGE) and immobilized onto a membrane (Mahmood & Yang, 2012). Transferred L1 proteins can be detected by binding towards Camvir-1 and visualized by the production of a coloured band for direct size comparison with protein molecular weight markers (Carter et al., 2003). On the other hand, conformationally dependent Abs bind to larger regions of proteins that form three-dimensional structures. Therefore, it is essential that the protein's native conformation remains intact in order for these Abs to recognize the specific region of interest (Deng et al., 2018). As such, these Abs are not appropriate for L1 protein or L1 VLP detection subsequent to SDS-PAGE and western blot analysis, attributed to protein denaturation and destabilization during the conduction of these steps (Forsström et al., 2015). However, these Abs can be used for other types of experimental analysis to detect for conformational epitopes of the HPV L1 protein and VLPs, which will be described in later sections.

There are a variety of conformationally dependent Abs against the HPV16 L1 protein including H16.V5, H16.E70, and H16.9A, all of which have neutralizing capabilities (Christensen et al., 1996; Combita et al., 2002; Roden et al., 1997; Varsani et al., 2003, 2006; White et al., 1999). A previous study generated a specific Ab, known as H16.U4, against HPV16 L1 VLPs, which can be used to identify for VLP production (Carter et al., 2003; Christensen et al., 1996). This Ab is also characterized as a conformationally dependent Ab, but with a weak neutralizing capability,

and binds to aa residues between 422 to 445 of the C-terminal arm of the L1 protein, in between formed capsomers (Carter et al., 2003; Guan et al., 2015). Within a formed VLP, there are 360 available binding sites for the H16.U4 Ab to recognize, however, the H16.U4 fragment antigen-binding (Fab) only bound to the icosahedral five-fold vortex of the formed capsid structure. This suggests that H16.U4 Ab binding is selective towards HPV16 L1 capsid formation and recognizes a specific conformational region of formed capsomeres (Guan et al., 2015). Guan et al., (2015) indicated that this Ab could potentially be used in the future to identify different stages of maturation of the HPV capsid by identifying for various conformational states that occur during this process.

1.5.3 HPV VLP detection and visualization

HPV VLPs have been visualized in previous studies using transmission electron microscopy (TEM) (Leder et al., 2001; Mossadegh et al., 2004; Patel et al., 2009; Sanchooli et al., 2020; Zahin et al., 2016), as displayed in Figure 8. TEM is one of the most common methods to visualize VLPs, however, during sample preparation there is a possibility for VLP deformation and destabilization to occur (Nooraei et al., 2021). To visualize for VLPs, the samples are stained using heavy metal salts; the most common include uranyl acetate, osmium tetroxide, and phosphotungstic acid (PTA) (González-Domínguez et al., 2020). The presence of heavy metals increases the density around the sample. This enables an image to be generated via differential electron scattering between the VLPs as an electron beam is directed toward the sample (Gulati et al., 2019). Previous studies have visualized the conformation of HPV16 VLPs within mammalian cells and other cell types using TEM, confirming their size to be within the range of 35 to 50 nm (Leder et al., 2001; Sanchooli et al., 2020; Zahin et al., 2016). It has been shown that at 72 hours (h) post-transfection with the L1 capsid sequence, VLPs are contained within the nucleus of mammalian cells (Leder et al., 2001).

Cryo-TEM is a form of TEM that minimizes the disturbance of formed VLPs by imaging the sample in a frozen hydrated state, allowing visualization of the sample as it exists in solution (Stewart, 2017). A study conducted by Guan et al., (2015) performed cryo-TEM after complexing the VLP with the H16.U4 Ab Fab. Using this, 3D reconstructions of the particle (Figure 9) were generated, and densities of the H16.U4 Ab were visualized around the capsomeres of formed VLPs at each five-fold vortex.

As outlined in the previous section, several Abs can be used to identify L1 protein formation, in addition to L1 VLPs. The enzyme-linked immunosorbent assay (ELISA) is a method that has been used to detect for the presence of HPV16 VLPs. If binding between the VLP and its corresponding Ab occurs, a chemical reaction can be induced for direct visualization of this binding (Alhajj & Farhana, 2022). Previous studies demonstrated that chimeric HPV16 L1 VLPs containing peptides inserted into different regions of the L1 protein bound towards linear and conformationally dependent Abs, including the VLP-specific H16.U4 Ab (Carter et al., 2003; Sanchooli et al., 2020; Varsani et al., 2003). This was conducted by performing an indirect ELISA by the coating of plates with chimeric HPV16 L1 VLPs and subsequently incubating with primary Ab. Later, a secondary Ab (directed towards the primary Ab) conjugated to a specific enzyme was added and an enzymatic reaction was induced by substrate addition to visualize for the presence of colour change, indicative of primary Ab binding towards the VLPs (Carter et al., 2003; Sanchooli et al., 2020; Varsani et al., 2003).

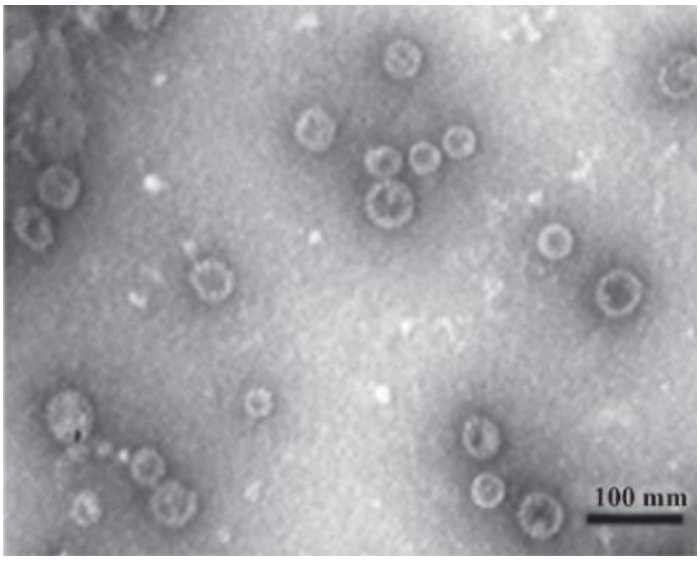

Figure 8. Transmission electron microscopy visualization of HPV16 L1 VLPs. The VLPs were negatively stained and visualized under a 100 V operating voltage (Taken from Patel et al., 2009). Based on the size marker indicated in the bottom right-hand corner (in nanometers (nm)), the VLPs were estimated to be approximately 35 - 50 nm in size.

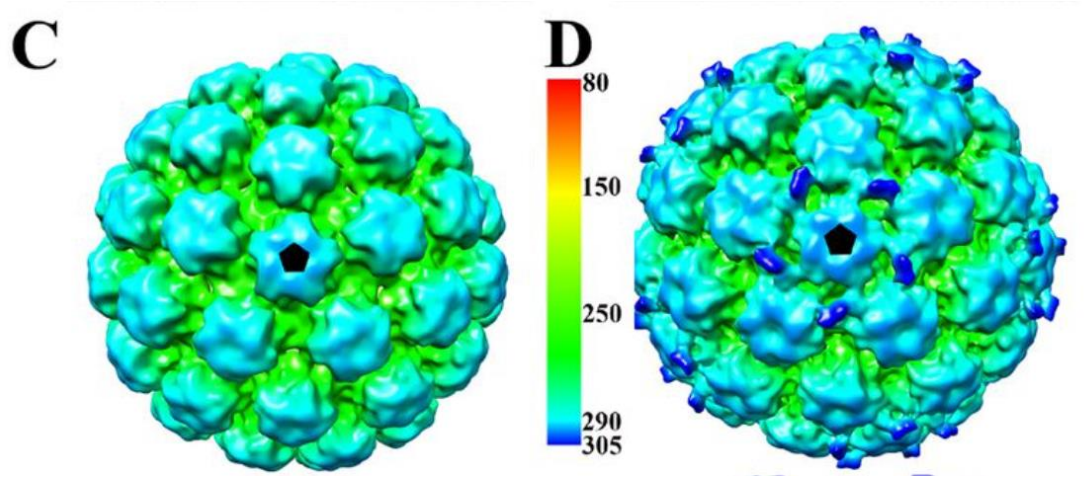

Figure 9. Model of HPV VLPs complexed with the H16.U4 antibody. Taken from Guan et al., (2015).

1.5.4 HPV VLP purification

Small-scale purification of the L1 protein has been predominantly conducted by ultracentrifugation using sucrose cushion or cesium chloride density gradients and size exclusion chromatography (Zahin et al., 2016). Considering VLPs are larger than most contamination particulates, VLPs are commonly purified in the same manner, however, in general, an additional step is required to

remove any remaining contaminants (H. J. Kim et al., 2010; Park et al., 2008; Schädlich, Senger, Kirschning et al., 2009). In general, density gradient centrifugation is a very common method to isolate biomolecules. It separates molecules based on their density within a specific solvent subsequent to sedimentation at high speeds of centrifugation. More dense molecules will sediment near the bottom of the gradient, whereas less dense molecules will float or sediment near the top of the gradient (*Density Gradient Ultracentrifugation*, JoVe, 2022). For the large-scale purification of L1, employing density gradients is not ideal, as this method is extremely time-consuming, costly, and not readily scalable, rendering chromatographic methods more suitable for industrial applications (Zahin et al., 2016). However, for the purposes of this study, generating large-scale quantities of HPV16 L1 VLPs was not necessary. Previous studies have shown that ultracentrifugation using a 45% sucrose cushion gradient and a cesium chloride gradient demonstrated adequate purification of the L1 protein (Park et al., 2008; Sapp et al., 1998; M.-K. Woo et al., 2008; Zahin et al., 2016). Additionally, studies have also used ammonium sulfate precipitation prior to chromatographic or density gradient purification to remove initial contaminants within cell lysate samples, enhancing protein recovery and purity (H. J. Kim et al., 2010; Zahin et al., 2016). Density gradients used for the purification of the L1 protein have also been generated using iodixanol subsequent to sucrose density application (Buck et al., 2005; Rao et al., 2011). The primary benefits of iodixanol includes the fact that it is non-ionic and non-toxic. Additionally, this solution is less viscous and particles can be purified under iso-osmotic conditions which can assist in the preservation of viral particles (Gias et al., 2008; Hermens et al., 1999). Moreover, the use of cesium chloride gradients for purification requires long centrifugation times and its removal after purification, which is not necessary when employing iodixanol gradients (Hermens et al., 1999).

1.5.5 HPV VLP peptide display

Peptide display on the surface of HPV L1 VLPs have been studied for the purpose of enhancing and broadening the immune response across various HPV types (Yadav et al., 2019). Peptide display can also be employed to target VLPs toward specific receptors (Brunel et al., 2010; Kaltgrad et al., 2008). Most studies exhibit an effective display of peptides inserted within the DE loop region, the H4 helix region, and between the H4 helix region and βJ sheet (Table 3), which is visualized structurally in Figure 10. To validate for VLP formation with peptide insertions, studies assessed the binding of L1-specific conformationally dependent Abs including H16.V5, H16.E70, and H16.U4 towards peptide displaying HPV VLPs. Peptides inserted within the DE loop of the L1 protein consistently demonstrated the formation of VLPs, however, VLPs with peptides inserted into the H4 helix region and between the H4 helix region and βJ sheet, showed less consistent VLP formation (Huber et al., 2017; Varsani et al., 2003). Peptides inserted into the latter two regions occasionally formed capsomeres and aggregate formation (Boxus et al., 2016; McGrath et al., 2013; Pineo et al., 2013). However, H16.V5 and H16.E70 Abs showed limited binding to VLPs with peptides inserted into the DE loop (Huber et al., 2017; Varsani et al., 2003). This could be due to an altered Tyr-153-Ser-282 interaction that is critical for the binding of these L1-specific conformationally dependent Abs (Varsani et al., 2003). VLPs with peptides introduced in the H4 helix region and between the H4 helix region and βJ sheet generally showed binding toward most conformationally dependent Abs specific for the L1 protein. Peptides displayed in these regions also demonstrated effective induction and binding towards their corresponding Abs, suggesting successful display of peptides on the surface of the HPV VLPs (Chabeda et al., 2019; Varsani et al., 2003). Other regions including the CD loop, EF loop, and FG loop of the L1 protein generally did not show VLP formation (Table 3). Peptides inserted in the C-terminal region of L1

demonstrated VLP formation, however, in some studies low/no binding of display peptide Abs were detected, indicative of probable ineffective peptide display (Jochmus et al., 1999; W. J. Liu et al., 2000; Schäfer et al., 1999).

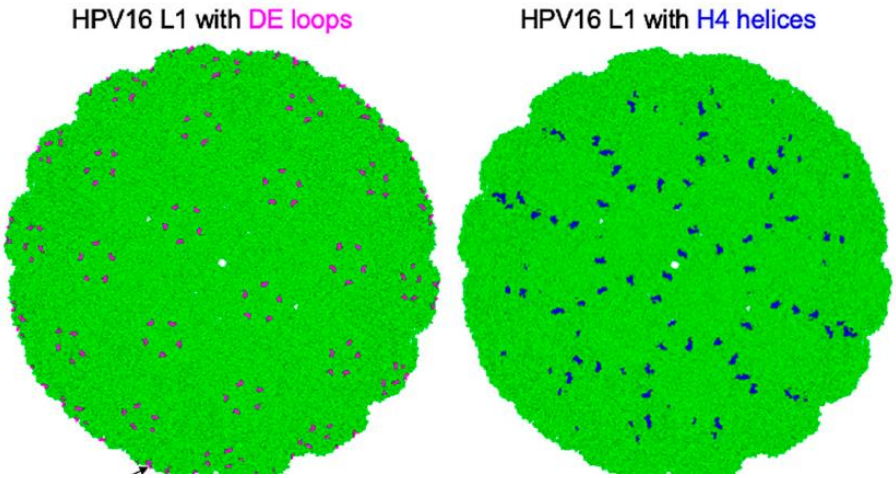

Figure 10. HPV VLP structures containing peptide insertions within surface-exposed regions of the L1 protein. The green areas represent the VLP structural formation of L1 pentamers. The pink areas indicate the location of peptide display within the DE loop region of the L1 protein. The blue areas indicate the location of peptide display within the H4 helix region of the L1 protein. (Taken from Yadav et al., 2019).

Table 3. Overview of HPV VLP peptide display studies

Display Peptide Insertion Region	VLP Formation	Immunogenicity
C-terminal truncated	-Yes (Jochmus et al., 1999; Müller et al., 1997; Schäfer et al., 1999)	-confirmed binding of conformationally dependent L1 neutralizing Abs (Jochmus et al., 1999; W. J. Liu et al., 2000; Müller et al., 1997) -no/low binding of display peptide Abs (W. J. Liu et al., 2000; Müller et al., 1997) -good anti-L1 immune responses in mice (Jochmus et al., 1999; W. J. Liu et al., 2000)
DE Loop	-Yes (Chabeda et al., 2019; Chen, Liu, et al., 2017; Huber et al., 2017;	-weak/no binding of some conformationally dependent L1 neutralizing Abs (Chabeda et al.,

	Schellenbacher et al., 2009; Varsani et al., 2003)	2019; Huber et al., 2017; Varsani et al., 2003) - good level of binding of display peptide Abs (Chen, Liu, et al., 2017; Huber et al., 2017; Schellenbacher et al., 2009, 2019; Varsani et al., 2003) -good anti-L1 and display peptide responses in mice (Chen, Liu, et al., 2017; Schellenbacher et al., 2009)
H4 Helix	-Yes (Matić et al., 2011; McGrath et al., 2013; Pineo et al., 2013) - some capsomere and aggregate formation and some non-consistent VLP formation -No (Varsani et al., 2003)	- confirmed binding of conformationally dependent L1 neutralizing Abs (Matić et al., 2011; McGrath et al., 2013; Pineo et al., 2013; Varsani et al., 2003) - good level of binding of display peptide Abs (Matić et al., 2011; McGrath et al., 2013; Pineo et al., 2013; Varsani et al., 2003) -good anti-L1 and display peptide responses in mice (McGrath et al., 2013; Pineo et al., 2013)
Region Between H4 Helix and βJ Sheet	-Yes (Boxus et al., 2016; Chen et al., 2018; Kondo et al., 2008; Matić et al., 2011; Varsani et al., 2003) - some capsomere and aggregate formation and some non-consistent VLP formation -No (Chabeda et al., 2019)	-confirmed binding of conformationally dependent L1 neutralizing Abs (Chabeda et al., 2019; Chen et al., 2018; Kondo et al., 2008; Varsani et al., 2003) -strong binding of display peptide mAbs (Chen et al., 2018; Kondo et al., 2008; Matić et al., 2011; Varsani et al., 2003)
EF Loop	-No (Varsani et al., 2003)	-
CD Loop	-No (Varsani et al., 2003)	-
FG Loop	-Yes (Slupetzky et al., 2001)	-weak binding of some conformationally dependent L1 neutralizing Abs (Slupetzky et al., 2001)

Ab: antibody; VLP: virus-like particle

2. Rationale, Hypothesis & Objectives

2.1 Rationale

The ineffectiveness of traditional cancer therapeutics is characterized by key limitations including low specificity, limited tumour penetration, and drug resistance development. Unfortunately, this has led to cancer recurrence and insufficient eradication of tumours (Chakraborty & Rahman, 2012; Chidambaram et al., 2011; H. Wang et al., 2016). Many anti-cancer drugs available seek to target cancer cell growth and proliferation, and more specifically, blood vessel formation, as these vessels are extensively involved in the maintenance and survival of tumours (Du & Lovly, 2018). In general, cancer immunotherapy platforms show high specificity, long-term effectiveness, extensive adaptability, limited side effects, and enhanced immune system functionality, counteracting the aforementioned drawbacks of conventional cancer therapies (S. Tan et al., 2020). The use of VLPs as a form of cancer immunotherapy has shown immense potential in previous studies and demonstrates the ability to stimulate effective immune responses against tumours to overcome the immunosuppressive TME, while simultaneously conferring increased safety compared to the use of replicative viral treatment (Mohsen et al., 2020; Ong et al., 2017; Zepeda-Cervantes et al., 2020). Furthermore, display of specific peptides/proteins on the surface of VLPs can be engineered, promoting the induction of tumour-specific immune responses and/or targeted binding towards specific receptors (Rohovie et al., 2017). It is for these reasons that the VLP platform was selected for this study.

VLP vaccines have been previously licensed for preventative applications, however, genetic vaccination of VLP structural proteins encoded as a DNA sequence for *in vivo* formation, has not been licensed to date (Brisse et al., 2020; Mohsen & Bachmann, 2022). In doing so, this would merge two leading treatment modalities within the cancer therapeutic field – gene therapy and

immunotherapy (Rangel-Sosa et al., 2017). In this envisaged strategy, a gene, or combination of genes, would be applied to patients to encode for VLP structural proteins, characterizing the gene therapeutic facet of the intended treatment. Upon protein formation, *in vivo* assembly into VLPs would enhance the immunogenicity of tumours to promote immune cell recognition, characterizing the immunotherapeutic facet of the intended treatment (DAS et al., 2015; Rangel-Sosa et al., 2017.). The administration of VLPs as a genetic sequence, such as a DNA-VLP strategy, for expression and assembly within cells, offers many benefits in comparison to conventional VLP administration. In terms of production, genetic vaccines are relatively easy to manufacture as they are less costly, convey simpler purification processes, and confer increased stability (Leitner et al., 1999). In terms of functionality, gene-based vaccines are characterized by the synthesis of proteins within cancer cells, in addition to directly within APCs, facilitating presentation by MHC molecules and effective priming of T-cell responses, in addition to humoral immune response induction (M. A. Liu & Ulmer, 2000; Wolff et al., 1990; B. Yang et al., 2015). Overall, this is the fundamental basis for the selection of the gene-based cancer immunotherapy platform approach designed and investigated in this study.

For this project, we sought to design a DNA-encoded HPV16 L1 VLP displaying an anti-angiogenic peptide (VGB), for formation, assembly, and characterization within mammalian cells. DNA-VLP gene cassettes encoding the L1 major capsid sequence of HPV16 fused to the VGB peptide sequence within a mammalian expression plasmid, was designed for *in vitro* VLP assembly to assess its potential use as a DNA immunotherapeutic vaccine. HPV was chosen as the VLP of study for several reasons including its ease of characterization and production, potent immunostimulant properties, and peptide fusion tolerance (Appendix C; Table 8). VGB was chosen as the peptide of display as it simultaneously targets two VEGFR receptors (VEGFR-1 and

VEGFR-2) and has been shown to limit tumour formation attributed to its robust anti-angiogenic effects (Behelgardi, 2018; Farzaneh Behelgardi et al., 2020). Upon formation of VLPs within cells, their release and translocation towards VEGFR-1 and VEGFR-2, targeted by VGB, would ideally inhibit VEGF signalling required for the stimulation of angiogenesis, consequently limiting tumour formation. Evidently, this should also enable the targeted recruitment of immune cells toward the tumour vasculature to further augment the inhibition of cancer cell growth. This design highlights the dual applicability of this investigated gene and immunotherapy-based treatment, as both an immunostimulant and antagonistic, receptor-targeted VLP.

2.2 Hypothesis

The designed DNA-VLP gene cassettes will generate viable VGB-displaying HPV16 L1 VLPs *in vitro* in mammalian cells that will accumulate and lyse the host cells for their release into the extracellular environment to target VEGFR.

2.3 Objectives

The main objective of this project is to design the DNA-VLP gene cassettes to characterize the *in vitro* assembly and release of HPV16 L1 VLPs displaying VGB within mammalian cells. Specific objectives are:

1. Identify and select the most suitable VLP for characterization in this study that addresses the main concerns of 1) ease of characterization/production; 2) immunogenicity; and 3) peptide fusion tolerance.
2. Design the DNA-VLP gene cassettes encoding the HPV16 L1 capsid fused to the VGB peptide.
3. Characterize the *in vitro* assembly of VGB-displaying HPV16 L1 VLPs via transfection of mammalian cells.

4. Characterize the accumulation and release of HPV16 L1 VLPs from mammalian cells.
5. Demonstrate that VGB-displaying HPV16 L1 VLPs preferentially bind to VEGFR.

3. Materials and Methods

3.1 Selection of HPV as the VLP of study

Using the PubMed search engine, review articles (Caldeira et al., 2020; Mohsen et al., 2020; Mohsen & Bachmann, 2022; Ong et al., 2017; Tornesello et al., 2022) were selected to evaluate the applicability of different viruses for VLP characterization, and their ability to be operationalized for therapeutic vaccine applications. Key search terms included 'VLP therapeutics', 'VLP vaccines', 'VLP cancer applications', and 'VLP immunogenicity'. Based on the reviewed studies, previously investigated viruses were selected to assess their application for VLP formation. With the feasibility and cancer-therapeutic directed clinical application in mind for this study, specified characteristics were evaluated in terms of ease of characterization/production, peptide fusion tolerance, and immunogenicity. Each of the evaluated VLPs was assigned a score based on their level of relevance towards these features, to select the most suitable VLP for characterization in this study.

3.2 HPV16 L1 VLP sequences and plasmids

The sections below outline the DNA-VLP sequences and plasmids designed and employed for the conduction of the experiments outlined in the remaining sections.

3.2.1 HPV16 L1 VLP sequences

The HPV16 L1 nucleotide sequence was codon optimized for *Homo sapiens* using the codon usage database from GenBank (https://www.kazusa.or.jp/codon/) from the HPV16 L1 protein sequence (accession no. CAC51367.1), which is 1518 nucleotide bases in length. This sequence was generated in a standard pUC57 vector by GenScript (New Jersey, USA) along with the addition of a PmeI restriction enzyme (RE) site (5'GTTTAAC3') at the end of the L1 sequence and a NotI RE site (5'GCGGCCGC3') at the beginning of the L1 sequence, as visualized (Figure 11). The

addition of the RE sites was conducted for the purposes of RE cloning into a mammalian expression plasmid for VLP production, which will be outlined in later sections.

For VLP peptide display, a VEGF antagonist, known as VGB (Sadremomtaz, Kobarfard, et al., 2018; Sadremomtaz, Mansouri, et al., 2018), was inserted into the L1 sequence. This 14 aa peptide ($_2$HN-CIKPHQGQHICNDE-COOH) (Sadremomtaz, Kobarfard, et al., 2018; Sadremomtaz, Mansouri, et al., 2018), introduced in Section 1.2.3, was inserted within the DE loop (between aa 136 and 137) and the H4 helix region (between aa 430 and 433) of the HPV16 L1 sequence. The peptide was flanked with GGC linker nucleotides at each end to ideally limit the disruption of L1 capsid protein conformation and peptide display by providing domain separation (Evers et al., 2006; J. Zhang et al., 2009). The procedure for insertion of the VGB sequence will be outlined in later sections. A basic visualization of VGB peptide insertion within the L1 sequence is illustrated in Figures 12A and B. The full DNA-VLP sequences can be found in Appendix A.

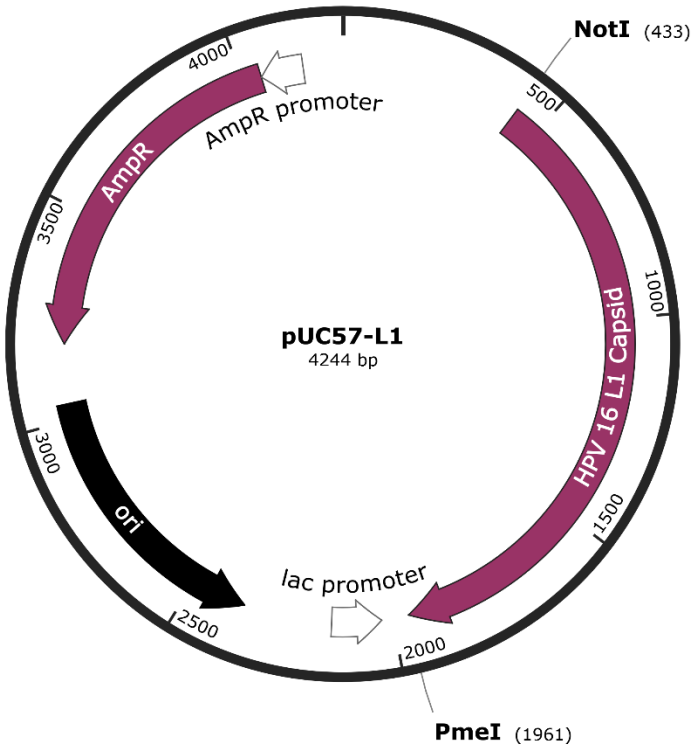

Figure 11. pUC57 L1 plasmid. The pUC57 L1 plasmid map containing the HPV16 L1 sequence. The pUC57 plasmid also contains a bacterial origin of replication (ori), ampicillin resistance marker (AmpR) and lac promoter. The NotI and the PmeI restriction enzyme sites were added to the 5' and 3' ends of the HPV16 L1 sequence, respectively, as identified in the image. The final size of the plasmid is ~ 4.3 kb.

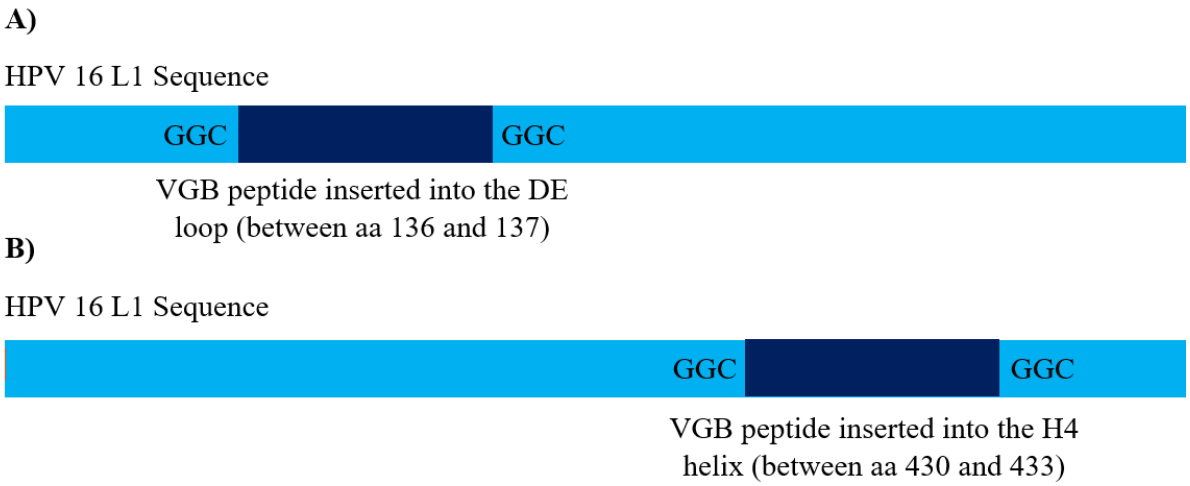

Figure 12. HPV16 L1 sequence with VGB insertions. The light blue bars represent the L1 sequence, and the dark blue bars represent the VGB sequence fusion in the translational frame (not to scale) of the gene. The image depicts the general location of the VGB sequence within the **A)** DE loop and the **B)** H4 helix of the L1 sequence.

3.2.2 HPV16 L1 DNA-VLP and control plasmids

The backbone of the pGL2-CMV-gfp plasmid, previously designed by Dr. Nafisseh Nafissi (Nafissi & Slavcev, 2012; Figure 13), was used for insertion of the DNA-VLP sequences, outlined in Table 4. Table 4 also outlines the strains used for the expression and storage of these plasmids. pGL2-CMV-gfp encodes for green fluorescent protein (GFP), which was used as a control to visually verify for transfection and measure transfection efficiency. The backbone (pGL2-CMV) of this plasmid was used to control the expression of the DNA-VLP sequences within mammalian cells, by replacement of the *gfp* gene. The pGL2-CMV-gfp plasmid contains a strong viral cytomegalovirus (CMV) promoter that is used extensively for ubiquitous transgene expression in mammalian cells (Xia et al., 2006). The super sequences (SS) contain polyomavirus simian virus (SV) 40 enhancer sequences that have been shown to facilitate nuclear translocation (Nafissi et al., 2014). The polyadenylation (polyA) site is used for mRNA stability and translation (Gallie, 1991). This plasmid also contains an ampicillin resistance (AmpR) marker for antibiotic selection.

Table 4. HPV16 L1 DNA-VLP plasmids, control plasmids, and cell strains

Plasmids				
	Gene	**Encodes For**	**DNA-VLP gene cassette (within the pGL2-CMV mammalian expression plasmid)**	**Plasmid Name**
	gfp (Control #1)	-green fluorescent protein (GFP)	*ss-cmv-gfp-ss*	pGL2-CMV-gfp
	l1 (Control #2)	-HPV16 L1 capsid protein (L1)	*ss-cmv-l1-ss*	pGL2-CMV-L1
	l1-vgb -de	-HPV16 L1 capsid protein with the VGB peptide inserted into the DE loop region of L1 (L1-VGB-DE)	*ss-cmv-l1-vgb-de-ss*	pGL2-CMV-L1-VGB-DE
	l1-vgb-h4	-HPV16 L1 capsid protein with the	*ss-cmv-l1-vgb-h4-ss*	pGL2-CMV-L1-VGB-H4

		VGB peptide inserted into the H4 helix region of L1 (L1-VGB-H4)		
Strains				
	Name	**Cell Type**	**Source**	**Use**
	JM109	-Bacterial cell line (prokaryotic)	NEB (Ipswich, USA)	For the long-term storage and extraction of plasmids
	HEK 293T	-Mammalian cell line (eukaryotic)	ATCC (Manassas, USA)	For the expression of the DNA-VLP plasmids

ATCC: American Type Cell Culture Collection; CMV: cytomegalovirus; DNA: deoxyribonucleic acid; GFP: green fluorescent protein; HEK: human embryonic kidney; HPV: human papillomavirus; NEB: New England Biolabs; SS: super sequence.

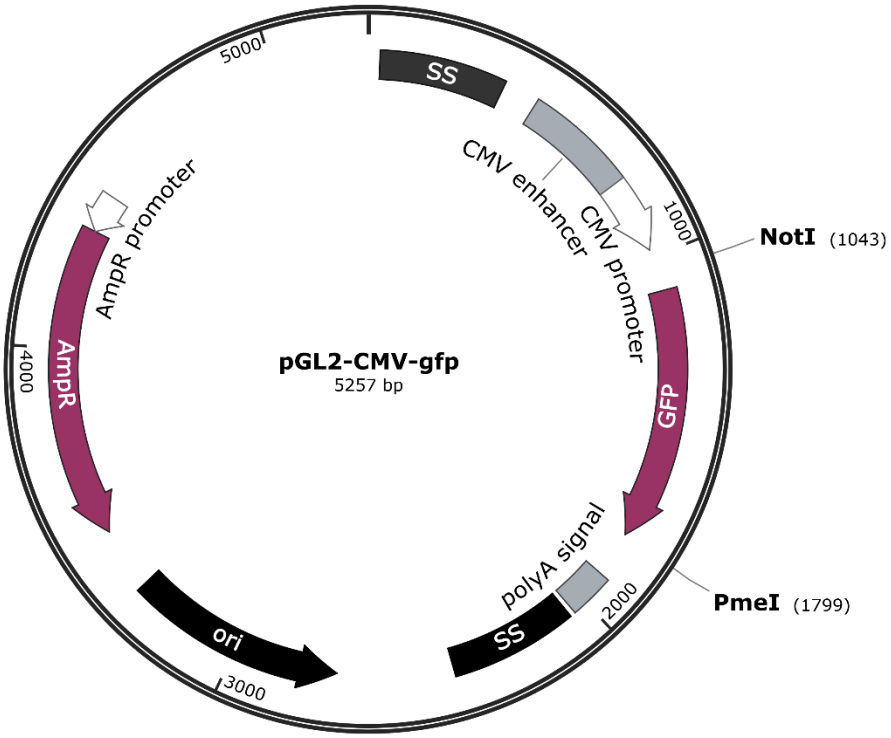

Figure 13. pGL2-CMV-gfp plasmid. Mammalian expression vector which contains a ubiquitous cytomegalovirus (CMV) promoter for control of the expression of the green fluorescent protein (*gfp*) gene. This vector also contains super sequences (SS), a polyadenylation (polyA) tail, and an ampicillin resistance (AmpR) marker for antibiotic selection. The NotI and PmeI restriction enzymes sites at the 5' end and the 3' end of the *gfp* gene are identified in the image. The final size of the plasmid is ~ 5.3 kb.

3.3 Cloning of the HPV16 L1 DNA-VLP sequence into the mammalian expression plasmid

This section outlines the steps taken to clone the sequence encoding the L1 capsid protein contained in the standard pUC57 vector, into the pGL2-CMV backbone using RE cloning to produce the final plasmid, pGL2-CMV-L1, identified in Table 4.

3.3.1 RE digestion of plasmids

The pUC57-L1 plasmid (Table 4; Figure 11), and the pGL2-CMV-gfp plasmid (Table 4; Figure 13) were both digested with the same REs. These enzymes were NotI HF and PmeI, purchased from NEB (Ipswich, USA). In each reaction, 1 ug of plasmid DNA was digested with 10 units of each enzyme in a total reaction volume of 30 uL by incubating at 37°C for 30 min. The reaction was then inactivated at 65°C for 25 min and run on a 0.8% gel for ~ 1 h and 30 min at 88 volts (V) (Appendix D). The bands observed for the pGL2-CMV backbone (~ 4.5 kilobases (kb)) and the L1 sequence (~1.5 kb) were then gel extracted using the Qiagen (Hilden, Germany) QIAquick Gel Extraction Kit. The concentration and purity of gel-extracted DNA was measured using the Thermo Fisher Scientific (Waltham, USA) NanoDrop 2000.

3.3.2 Ligation and transformation of plasmids

The gel-extracted bands for the pGL2-CMV backbone and the L1 sequence were ligated using the NEB (Ipswich, USA) T4 DNA ligase, in a total reaction volume of 20 uL by incubating at 16°C overnight. The reaction was then inactivated at 65°C for 15 min. The vector: insert ratio used for the ligation reaction was 1:5 by using 50 ng of vector DNA (pGL2-CMV backbone) and ~ 87 ng of insert DNA (L1 sequence). The amount of insert DNA required for a vector: insert ratio of 1:5 was calculated using the online NEBioCalculator tool.

The next day, calcium competent JM109 *E. coli* cells (Table 4) were thawed on ice for 30 min. Subsequently, 5 uL of the ligation reaction was added to the competent cells for 30 min. The cells

were then transformed via heat shock at 42°C for 90 seconds (sec) and placed on ice for 3 min. 900 uL of Luria Burtani (LB) broth was added and the cells were kept within a 37°C shaking incubator (at 250 revolutions per min (rpm)) for 1 h. The cells were then plated on LB agar plates containing ampicillin (Amp) (LB + Amp) and left overnight in a 37°C incubator. Two negative control ligation reactions were also transformed into competent cells, including that which did not contain the addition of any DNA and that which contained only the addition of the backbone vector, and subsequently plated. An additional negative control was plated using competent cells without the addition of the ligation reaction to detect for the presence of contamination. The next day the plates were observed for the growth of colonies (Appendix D).

3.3.3 Confirmation of pGL2-CMV-L1 formation

To confirm the ligation of the pGL2-CMV backbone and the L1 sequence to generate the final pGL2-CMV-L1 plasmid (Table 4), colonies that grew on LB + Amp agar plates were cultured in 5 mL of LB + Amp broth overnight. Subsequently, a plasmid extraction was conducted using the NEB (Ipswich, USA) Monarch Plasmid Miniprep Kit and digested with the same REs used to digest the initial plasmids for cloning of the L1 sequence (PmeI and NotI HF). The restriction digestion was then run on a gel to confirm for DNA fragment lengths that corresponded to the size of the pGL2-CMV backbone (~ 4.5 kb) and the L1 sequence (~ 1.5 kb). Sequencing was also conducted to verify the insertion of the L1 sequence into the vector by sanger sequencing, conducted by the Sick Kids Centre for Applied Genomics TCAG Facility (Toronto, CA).

3.4 VGB insertion into the L1 sequence

This section outlines the steps conducted for insertion of the VGB sequence into the L1 sequence within the pGL2-CMV backbone vector using PCR amplification, ligation, and subsequent transformation into competent *E. coli* cells.

3.4.1 pGL2-CMV-L1 PCR amplification

The primer sequences indicated in Table 5 include the forward and reverse primers used for VGB insertion into the L1 sequence. Each primer contains a GGC linker sequence, part of the VGB gene sequence, and an annealing sequence targeted towards a specific location of the L1 sequence. For PCR amplification, the Bio-Rad (Hercules, USA) C1000 Thermal Cycler was used. A PCR reaction was conducted using the pUC57 L1 plasmid (for insertion of the VGB sequence into the DE loop) and the pGL2-CMV-L1 plasmid (for insertion of the VGB sequence into the H4 helix). The PCR reaction contained 12.5 uL of the Thermo Fisher Scientific (Waltham, USA) Phusion Flash High Fidelity PCR Master Mix, 5 ng of plasmid DNA, 0.5 uM of forward and reverse primers, and sterile water within a final reaction volume of 25 uL. Table 6 outlines the settings applied for the conduction of the PCR cycle. The PCR amplified products were then run on a 0.8% gel for approximately 1 h and 30 min at 88 V (Appendix D) to verify for amplification of a ~ 6.1 kb sized fragment, and gel-extracted using the Qiagen (Hilden, Germany) QIAquick Gel Extraction Kit (Appendix D). The concentration and purity of gel-extracted DNA was measured using the Thermo Fisher Scientific (Waltham, USA) NanoDrop 2000.

Table 5. Forward and reverse primers for VGB insertion into the L1 sequence

Primer	Sequence
VGB DE Forward	5’GCCAGCACATCTGCAACGACGAGGGCgccaacgccggcgtggacaacag3’
VGB DE Reverse	5’CCTGGTGGGGCTTGATGCAGGCggcgtaggcgctggcgttct3’
VGB H4 Forward	5’GCCCAGCACATCTGCAACGACGAGGGCccccccgcccccaaggag3’
VGB H4 Reverse	5’CTGGTGGGGCTTGATGCAGGCcttctggcaggcgatggcct3’

[1]The text highlighted in yellow indicates the linker sequence which flanks the VGB sequence. The text highlighted in blue indicates the VGB sequence, in which each forward and reverse primer contains approximately half of the full sequence. The green highlighted text contains the annealing component of the primers which were designed to anneal within a specific location of the DE loop region or the H4 helix region of the L1 sequence.

Table 6. PCR steps for VGB insertion into the L1 sequence

Cycle Step	Temperature	Time	Number of Cycles
Initial Denaturation	98˚C	10 sec	1 cycle
Denaturation	98˚C	5 sec	35 cycles
Annealing	• 70˚C (using VGB H4 primers) •73˚C (using VGB DE primers)	5 sec	
Extension	72˚C	• 92 sec (15 sec/kb; for the pGL2-CMV-L1 plasmid) • 65 sec (15 sec/kb; for the pUC57 L1 plasmid)	
Final Extension	72˚C	60 sec	1 cycle
Incubation	4˚C	Incubate	N/A

[1]The PCR cycle that was conducted using the primers listed in Table 5 for amplification of plasmid DNA for VGB insertion into the L1 sequence.

3.4.2 Phosphorylation and cleanup of the PCR amplified product

The gel-extracted bands of the amplified pGL2-CMV-L1 and pUC57 L1 plasmids, flanked with the VGB sequence, were then phosphorylated using the NEB (Ipswich, USA) T4 Polynucleotide Kinase (PNK) in a 50 uL final reaction volume. Each reaction contained ~ 250 ng of DNA, 1 uL of T4 PNK, 5 uL of 10X T4 PNK Buffer, 5 uL of 10 uM ATP, and remaining sterile water. This was conducted to provide an available 3' phosphate group to the PCR amplified product at either end to enable successful ligation. The reaction was set on ice and then incubated at 37˚C for 30 min. The reaction was then inactivated at 60˚C for 20 min. The phosphorylated DNA product was subsequently cleaned using the NEB (Ipswich, USA) Monarch PCR & DNA Cleanup kit.

3.4.3 Ligation and transformation of the PCR amplified product

The ends of the cleaned phosphorylated PCR amplified product (which contained the VGB sequence within the DE loop region or the H4 helix region) was ligated using the NEB (Ipswich, USA) T4 DNA ligase by incubating with 100 ng of DNA at 16˚C overnight. The reaction was then

inactivated at 65°C for 15 min. The cells were then transformed in the same manner as outlined in Section 3.3.2.

3.4.4 Confirmation of VGB sequence insertion

To confirm the insertion of the VGB sequence into the L1 gene to generate the final plasmids named pGL2-CMV-L1-VGB-DE and pGL2-CMV-L1-VGB-H4, as outlined in Table 4, colonies that grew on LB + Amp agar plates were cultured in 5 mL of LB + Amp broth overnight. Subsequently, a plasmid extraction was conducted using the NEB (Ipswich, USA) Monarch Plasmid Miniprep Kit and digested with the same REs used to digest the original plasmids for cloning of the L1 sequence (PmeI and NotI HF). The restriction digestion was then run on a 0.8% gel to confirm for DNA fragment lengths corresponding to the size of the pGL2-CMV backbone (~ 4.5 kb) and the L1 sequence with the VGB insertions in either the DE loop or the H4 helix region (~ 1.55 kb).

Additionally, primers surrounding the location of the VGB sequence were designed and used for PCR amplification to verify for VGB sequence insertion. This was also performed using the pGL2-CMV-L1 plasmid (without VGB sequence insertion) to compare band sizes with the plasmids containing the VGB insertions within the L1 sequence (pGL2-CMV-L1-VGB-DE and pGL2-CMV-L1-VGB-H4). For PCR amplification, the Bio-Rad (Hercules, USA) C1000 Thermal Cycler was used. A PCR reaction was conducted using the NEB (Ipswich, USA) One-Taq 2X Master Mix with Standard Buffer. Each reaction contained 12.5 uL of the One-Taq 2X Master Mix with Standard Buffer, 5 ng of plasmid DNA, 0.5 uM of forward and reverse primers, and sterile water within a final reaction volume of 25 uL. Table 7 outlines the settings applied for the conduction of the PCR cycle. The PCR amplified products were then run on a 3% gel for ~ 1 h and 30 min at 80 V and visualized.

Plasmids extracted from colonies that showed correct DNA band lengths after RE digestion and PCR amplification were then sent to the Sick Kids Centre for Applied Genomics TCAG Facility (Toronto, CA) for sanger sequencing to verify for VGB sequence insertion.

Table 7. PCR steps for verification of VGB insertion in the L1 sequence

Cycle Step	Temperature	Time	Number of Cycles
Initial Denaturation	94˚C	30 sec	1 cycle
Denaturation	94˚C	30 sec	30 cycles
Annealing	56-58˚C	60 sec	
Extension	68˚C	6-8 sec	
Final Extension	68˚C	5 min	1 cycle
Incubation	4˚C	Incubate	N/A

3.5 Mammalian cell line maintenance

The cell line used for the testing of the DNA-VLP sequences (Table 4) were Human Embryonic Kidney cells (HEK). The specific strain used, HEK 293T, are adherent cells and was purchased from ATCC (Manassas, USA). The media used for HEK 293T cell maintenance was Dulbecco's Modified Eagle Media (DMEM) (purchased from ATCC) + 10% fetal bovine serum (FBS). Cell maintenance of the HEK 293T cells was conducted within a Biosafety Cabinet.

3.5.1 HEK 293T cell maintenance

The purchased HEK 293T cells (Table 4) were stored in 1.5 mL of DMEM + 10% FBS within a liquid nitrogen tank. To thaw cells, they were quickly placed in a 37˚C water bath for 5 min. This was then added to 8.5 mL of pre-warmed DMEM + 10% FBS and mixed gently. The cells were then spun down using the Eppendorf (Hamburg, Germany) 0804 R Centrifuge for 6 min at 110 g. The supernatant was discarded, and the cells were then mixed with pre-warmed DMEM + 10% FBS. This was then transferred to a T-75 flask and placed in a 37˚C + 5% CO_2 incubator.

The cells were continually maintained in a T-75 flask for the duration of the experiments. To maintain cells, old media was first removed from the cells. The cells were then washed with 10

mL of sterile Dulbecco's Phosphate-Buffered Saline (D-PBS) solution and trypsinized with 2.5 mL of TripleE to detach the cells from the adherent side of the flask by incubating at 37°C + 5% CO_2 for 5 min. Subsequently, 7.5 mL of pre-warmed DMEM + 10% FBS media was added and mixed with the cells. Around 0.5 mL of cells were aliquoted to check for cell size (μm), cell viability (%), and cell count (cells/mL) using the Thermo Fisher Scientific (Waltham, USA) Countess II FL Automated Cell Counter. The remaining portion of cells were centrifuged for 6 min at 110 g. The supernatant was then discarded, and the cells were mixed with new pre-warmed DMEM + 10% FBS media. Based on the cell count, a specified number of cells was added to a T-75 flask containing 10 mL of pre-warmed DMEM + 10% FBS for seeding at 1 x 10^6 cells. The cells were then incubated at 37°C + 5% CO_2 and passaged every 3 days.

3.6 Transfection efficiency of the pGL2-CMV-gfp plasmid

This section outlines the steps taken to determine the transfection efficiency of the pGL2-CMV-gfp plasmid using the SignaGen Laboratories (Maryland, USA) GenJet™ Plus transfection reagent, as a means to approximate the transfection efficiency using the same reagent for the DNA-VLP plasmids (Table 4).

3.6.1 Transfection of HEK 293T cells using the pGL2-CMV-gfp plasmid

For transfection efficiency determination, HEK 293T cells were seeded onto 6-well plates at a concentration of ~ 1.5 x 10^6 cells/mL. After 18-24 h, 1 ug of plasmid DNA (pGL2-CMV-gfp) (diluted in DMEM) was added subsequent to mixing with the GenJet™ plus transfection reagent (diluted in DMEM) and incubating at room temperature for 15 min. The ratio of transfection reagent: plasmid DNA was 3:1 for all wells, as suggested by the manufacturer of the reagent. After transfection, the cells were harvested at 24, 48, 72, 96, and 120 h. To harvest the cells, they were first washed twice with sterile D-PBS. Next, 1 mL of TripleE was added to the cells and incubated

at 37°C + 5% CO_2 for 5 min. 1 mL of prewarmed DMEM + 10% FBS was then added to inactivate the TripleE. 0.5 mL of each sample was aliquoted to check for cell viability (%), cell size (μm), and cell count (cells/mL). The remaining cells were centrifuged at 110 g at room temperature for 6 min. The supernatant was discarded, and the pellet was kept for fixation.

3.6.2 Flow cytometry analysis

On the same day of cell harvesting, cells were fixed with 1 mL of 4% paraformaldehyde diluted in D-PBS and incubated at 4°C for 1 h. The fixed cells were then run through the BD Biosciences (San Jose, CA, USA) FACSCalibur flow cytometer. Green fluorescence emitted by the GFP protein was detected using the FL1 detector. Non-transfected HEK 293T cells were also run through the flow cytometer as a control to detect for background signals. The flow cytometer settings were inputted to detect a maximum of 10 000 events (detectable cells) at a slow fluidic rate. Analysis of the number of events (cells), mean fluorescence intensity, and percent of fluorescent cells was carried out using the FlowJo Software (Ashland, USA) to measure transfection efficiency. Transfection efficiency was calculated as a percent of the number of cells emitting fluorescence divided by the total number of cells detected.

3.7 Production and collection of HPV16 L1 VLPs

This section outlines how the HPV16 L1 VLPs were produced within HEK 293T mammalian cells beginning from initial transfection to cell lysis and retrieval of lysate.

3.7.1 Transfection of HEK 293T cells with the HPV16 L1 DNA-VLP plasmids

The HEK 293T cells, maintained in T-75 flasks, were seeded onto T-25 flasks at a cell count of ~ 4 x 10^6 cells. After 18-24 h, 5 ug of DNA (diluted in DMEM) was added to the flasks after mixing with the GenJet™ Plus reagent (diluted in DMEM) and incubating at room temperature for 15 min. The ratio of transfection reagent: plasmid DNA was 3:1, as suggested by the manufacturer of

the reagent. The cells were transfected with the following plasmids: pGL2-CMV-gfp, pGL2-CMV-L1, pGL2-CMV-L1-VGB-DE, and pGL2-CMV-L1-VGB-H4 (Table 4). The pGL2-CMV-gfp and pGL2-CMV-L1 plasmids were used as negative and positive controls, respectively.

3.7.2 Cell harvesting and lysis

At 72 h post-transfection, the media from transfected HEK 293T cells was removed and stored at -20°C. The adherent cells were then washed twice with sterile D-PBS. Subsequently, 1 mL of TripleE was added to the cells and incubated at 37°C + 5% CO_2 for 5 min. After this, 4 mL of pre-warmed DMEM + 10% FBS was added to inactivate the TripleE and the cells were then transferred to 15 mL falcon tubes. 0.5 mL of each sample was aliquoted to check for cell viability (%), cell size (μm), and cell count (cells/mL). The tubes were then centrifuged at 110 g for 6 min. The supernatant was transferred to a new sterile falcon tube and stored at -20°C. The cell pellet was also stored at -20°C for subsequent lysis.

To lyse the cells, lysis buffer was prepared using a modified recipe of the Thermo Fisher Scientific (Waltham, USA) RIPA Lysis and Extraction Buffer (Catalogue No. 89900), by omitting the addition of sodium deoxycholate and SDS to promote stabilization of the L1 protein. The altered RIPA buffer preparation was composed of 25 mM Tris HCl pH 7.6, 150 mM NaCl, and 1% NP-50. Following the RIPA Lysis and Extraction Buffer protocol, for every 1 x 10^6 cells, 1 mL of RIPA buffer was added to the cell pellet. The RIPA buffer was gently mixed with the cells and left on ice with occasional gentle mixing for ~ 15 min. The mixture was then centrifuged at 4000 g for 50 min to pellet the cell debris. The supernatant (cell lysate) was then transferred to a new 15 mL sterile falcon tube and stored at -20°C.

3.8 Purification of HEK 293T-transfected cell lysates and protein quantification

Purification of the HPV16 L1 VLPs from HEK 293T cell lysates was conducted using iodixanol (OptiPrep^{TM}) density gradient ultracentrifugation, following a previously conducted protocol, specifically for HPV VLPs and pseudovirions (Buck et al., 2005). These steps will be briefly outlined in this section. Firstly, the iodixanol gradient was prepared. OptiPrep^{TM} dilutions of 27%, 33% and 39% dilutions were made from an initial 60% OptiPrep^{TM} stock solution in D-PBS/0.8M NaCl. Subsequently, 1.4 mL of each dilution was transferred to a Beckman Coulter (Brea, USA) polystyrene thin-walled centrifuge starting with the lowest dilution (39%) to the highest dilution (27%). This was then kept at room temperature for 2 h to allow gradient diffusion to occur. During this incubation, salt extraction of the cell lysates was performed. The cell lysates were chilled on ice and then mixed with 0.17 volumes (850 uL for each 5 mL of cell lysate) of 5M NaCl. This was incubated on ice for ~ 10 - 20 min. The salt lysate was then clarified by centrifugation for 15 min at 2000 g and the supernatant was transferred to the gradient (2 h after incubation at room temperature). This was then centrifuged using the Beckman Coulter (Brea, USA) Optima XPN-100 Ultracentrifuge SW41 rotor at 40 000 rpm at 16°C for 5 h. After ultracentrifugation, 12 fractions (with a volume of ~ 1 mL each) were collected for each sample by puncturing a hole within the centrifuge tubes starting from the top of the tube to the bottom of the tube.

To determine the amount of protein present in the purified fractions, the Thermo Fisher Scientific (Waltham, USA) Pierce BCA Protein Assay Kit was used. Following their protocol, the albumin protein standards were prepared at concentrations ranging from 2000 ug/mL to 0 ug/mL. Next, 10 uL of the standards and samples were plated on Thermo Fisher Scientific (Waltham, USA) non-treated Nunc 96 flat-well plates. 200 uL of working reagent (Reagent A and Reagent B at a 50:1 ratio) was then added to each well, mixed with the samples, and incubated at 37°C for 30 min. The

absorbances were subsequently read at 562 nm using the Biotek plate reader (Winooski, USA). The concentration of protein within the purified samples was calculated using the line of best-fit equation determined from the albumin protein standards.

3.9 Characterization of HPV16 L1 VLPs

This section outlines the steps taken to characterize the production of L1 protein with and without the insertion of the VGB peptide from the iodixanol density gradient purified fractions. Moreover, this section describes the experiments conducted to identify for the formation of L1 VLPs and to evaluate the display of the inserted VGB peptide. For all the experiments conducted in this section, a positive control was run alongside the experimental samples. This positive control was a recombinant HPV16 L1 protein purchased from Abcam (Cambridge, UK, Catalogue No. ab119880), which will be henceforth referred to as RL1.

3.9.1 SDS-PAGE and western blot analysis

The SDS resolving and stacking gels (1.0 mm and 1.5 mm) were prepared using the Bio-Rad (Hercules, USA) MINI PROTEAN TGX Stain-Free Precast Gel Kit. These solutions were then transferred to SDS gel plates and allowed to solidify. Approximately 10 ug of protein sample was mixed with the Bio-Rad (Hercules, USA) 4x Laemeli buffer (10 uL) and 2-mercaptoethanol in a total volume of 40 uL and subsequently heated at 95°C for 5-10 min. The samples were then loaded into each well along with the Thermo Fisher Scientific (Waltham, USA) PageRuler^{TM} Plus Prestained Protein Ladder (10 to 250 kilodaltons (kDa)). The gels were run at 80 V for 15 min and then at 200 V for ~ 45 min within 1X running buffer.

The proteins on the gel were then transferred onto Bio-Rad (Hercules, USA) ImmunoBlot Polyvinylidene difluoride (PVDF) membranes using the Bio-Rad (Hercules, USA) Trans-Blot Turbo machine at a voltage of 25 V for 3 min, following the Turbo MP TGX Mini Protein Gel

Mixed MW protocol. Prior to this, PVDF membranes were placed within methanol and 1X transfer buffer (diluted from the Bio-Rad (Hercules, USA) 5X Turbo Transfer Buffer solution), to facilitate protein transfer. The membranes were then directly stained with ponceau stain to verify that the proteins within the samples successfully ran through the gel and transferred to the membrane, and subsequently washed with MilliQ water to remove the stain. The membranes were then blocked with blocking buffer (5% skim milk) for 1 h and washed three times with 1X wash buffer (1X Tris-HCl buffered saline/Tween 20 (TBS-T)) for 10 min each, while shaking. After this, the membranes were incubated with Novus Biologics (Centennial, USA) Camvir-1 (primary Ab) (Catalogue No. NB100-2732SS) at a concentration of 1 ug/mL (diluted in blocking buffer) and left overnight at 4˚C while spinning. The next day, the membranes were washed with 1X wash buffer three times (10 min each) while shaking. Secondary anti-mouse IgG (whole molecule) – horse radish peroxidase (HRP) Ab (Sigma Aldrich, St. Louis, USA, Catalogue No. SLCG4695) diluted in blocking buffer at a ratio of 1:10 000, was added to the membranes and incubated for 1 h at room temperature while shaking. The membranes were then washed again three times (10 min each) with 1X wash buffer while shaking. To visualize for the presence of the L1 protein, 15 mL of the Kernentec Solutions (Amherst, USA) tetramethylbenzidine (TMB) PLUS2 solution was added to each of the membranes, covered in foil, and incubated at room temperature for ~ 30 min while shaking. The presence of L1 protein was verified by the observation of a blue band at ~ 56 kDa.

3.9.2 Non-denaturing PAGE and western blot analysis

The same process outlined in Section 3.9.1 was conducted for this experiment, however, the composition of the stacking and resolving gels were altered (non-denaturing) to preserve the assembly of L1 VLPs. The non-denaturing gels did not contain SDS, and were composed of 0.375

M Tris HCl, pH 7.6, 30% acrylamide, ammonium persulfate (APS) and tetramethylethylenediamine (TEMED). These samples were run on non-denaturing gels in the same manner as outlined in Section 3.9.1, however, the samples were mixed with 4X Laemli Buffer in the absence of 2-mercaptoethanol, and not heated at 95°C prior to loading onto the gel. Protein transfer was conducted at 25 V for 25 min. Blocking and primary/secondary Ab incubation of the membranes, in addition to band visualization, was conducted as outlined in Section 3.9.1. However, an additional primary Ab was used (H16.U4), gifted from Dr. Neil D Christensen (Department of Pathology, The Pennsylvania State University College of Medicine, Hershey, Pennsylvania, USA), to detect for the formation of L1 VLPs.

3.9.3 Indirect ELISA

Samples were first diluted in 1X phosphate buffered saline (PBS) and plated at varying concentrations onto a Thermo Fisher Scientific (Waltham, USA) 96-well Immunol 2 High-Binding plate. The plates were then left overnight at 4°C to allow for binding of the protein samples to the bottom of each well. The next day, the samples were removed and washed three times with 1X wash buffer (1X phosphate buffered saline/Tween 20 (PBS-T)) using the Biotek (Winooski, USA) 50^{TM} TS microplate washer. The plate was then blocked with 300 uL of blocking buffer (5% skim milk) for 1 h. The blocking buffer was removed and washed once with 1X wash buffer.

The plate was then incubated with 100 uL of primary Ab (Camvir-1 and/or H16.U4) at a concentration of 1 ug/mL (diluted in blocking buffer) and kept at room temperature for 2 h. After this, the primary Ab was removed and washed three times with 1X wash buffer. Then, 100 uL of secondary anti-mouse IgG HRP Ab diluted in blocking buffer at a ratio of 1:10 000, was added to the plate and incubated for 1 h at room temperature. The secondary Ab was then removed and washed three times with 1X wash buffer. 100 uL of TMB PLUS2 (Kernentec Solutions, Amherst,

USA) substrate was then added to the plate and covered with aluminum foil and left for shaking at room temperature for 30 min. To stop the reaction, 100 uL of stop solution (0.3M H_2SO_4) was added to each well, inducing a colour change that was visually detected if binding of the L1 protein and/or L1 VLPs towards the primary Abs occurred. Absorbance values of the colour changes were measured at 450 nm using the BioTek (Winooski, USA) plate reader.

3.9.4 VEGFR ELISA

To determine the binding capability of VGB-displaying VLPs to VEGFR, the Abcam (Cambridge, UK) recombinant human VEGFR-2 protein (Catalogue No. ab281825) was diluted in 1X PBS and coated onto a Thermo Fisher Scientific (Waltham, USA) 96-well Immunol 4 High Binding plate at a concentration of 5 ug/mL and incubated at 4˚C overnight. The next day, the plate was washed with 1X wash buffer (1X PBS-T) and subsequently blocked with 300 uL of blocking buffer (5% skim milk) in each well for 1 h at room temperature. Protein samples, diluted in 1X PBS, were added to the plate, and incubated at room temperature for 2 h. The plate was then washed three times with 1X wash buffer and incubated with 100 uL of the Camvir-1 Ab diluted in blocking buffer for 2 h at room temperature. The plate was then washed three times with 1X wash buffer and subsequently incubated with 100 uL of secondary anti-mouse IgG HRP Ab diluted in blocking buffer at a ratio of 1:10 000, for 1 h at room temperature. After a final wash, TMB PLUS2 (Kernentec Solutions, Amherst, USA) substrate was added to each of the wells and the plate was subsequently covered with aluminum foil and incubated at room temperature for ~ 30 min while shaking. To stop the reaction, 100 uL of stop solution (0.3M H_2SO_4) was added to each well inducing a colour change that was visually detected if binding of the VBG-displaying VLPs towards VEGFR-2 occurred. Absorbance values of the colour changes were measured at 450 nm using the BioTek (Winooski, USA) plate reader. The mean absorbance readings obtained from the

non-transfected control lysate sample was used to subtract absorbance values contributed by background signals. Statistical analysis was conducted using the two-sample t-test assuming unequal variances. For each sample group, the mean absorbance measurements were assessed for statistical significance compared to the non-transfected control lysate sample group. Additionally, the mean absorbance measurements were also assessed for statistical significance between VGB-displaying VLP sample groups and non VGB-displaying VLP sample groups. Sample groups demonstrating statistical significance were visualized with an asterix symbol on the prepared graphs.

3.9.5 TEM

Fractions displaying the presence of the L1 protein, detected using western blot analysis (Section 3.9.1), were used for visualization of potential VLP formation using TEM. To conduct this, a protocol outlined by Gulati et al., (2019) was employed and is briefly outlined in this section. Samples (20 uL each) were placed onto Electron Microscopy Sciences (Hatfield, USA) formvar carbon-coated copper grids (purchased from Thermo Fisher Scientific, Waltham, USA) and incubated for 1-2 min. The samples were then removed using Whatman Cellulose Filter Paper to soak up the sample solutions from the grid. To wash the grids, 40 uL of MilliQ water was added to each grid, incubated for 1 min, and removed using filter paper. The grids were subsequently stained using 20 uL of 2% phosphotungstic acid for each sample. The stain was left for ~ 1 min and then removed using filter paper. The stain was removed by washing with 40 uL of MilliQ water five times, in the same manner as aforementioned. The grids were finally left to air dry overnight, and subsequently imaged using the Phillips CM10 transmission electron microscope at a magnification of 64 000X.

3.10 Characterization of the accumulation and release of HPV16 L1 VLPs

To determine if the VLPs were released from transfected HEK 293T cells, media was collected at 24, 48, 72, 96, and 120 h post-transfection to detect for the presence of L1 protein via western blot analysis (outlined in Section 3.9.1). The cells were also collected (outlined in Section 3.7.2) for measurement of decreased cell viability (%) and cell counts (cells/mL) over the time periods previously indicated.

4. Results

4.1 Comparative study of viruses for the selection of HPV as the VLP of study

Candidate VLPs for this study were assessed based on collected background information (Section 1.5) and subsequent comparative analysis (Table 8; Appendix C). VLPs were studied in terms of their ease of characterization/production, immunogenicity, and tolerance of peptide fusions. Based on these features, each VLP candidate was assigned a score (Table 8). According to this assessment rubric, HPV was ultimately selected as the VLP of study as it was given the highest score (+5). A more in-depth analysis outlining the reasoning behind the assigned scores can be found in Appendix C. Based on the reviewed papers, an extensive number of studies have been conducted for HPV VLPs considering the commercial availability of three licensed HPV VLP vaccines (Buonaguro et al., 2011). Clinical trials of these vaccines have been shown to induce both cellular and humoral immune responses in patients (Schiller & Lowy, 2012; Suzich et al., 1995), giving HPV VLPs an overall immunogenicity score of +1. Various studies have also confirmed the successful display of peptides on the surface of HPV VLPs, as aforementioned (Huber et al., 2017; Schellenbacher et al., 2009; Varsani et al., 2003), giving HPV VLPs an overall peptide fusion tolerance score of +1. Furthermore, HPV is easily characterizable given the fact that it is a non-enveloped virus and only requires the expression of the L1 major capsid protein for VLP assembly (Hagensee et al., 1993; Kirnbauer et al., 1992; Schellenbacher et al., 2009), giving HPV VLPs an overall characterizable score of +3. Upon weighing all considerations, an L1-based HPV VLP was chosen for design and characterization for the purposes of this project, to assess its future potential as a DNA-VLP immunotherapeutic.

Table 8. Benefits and limitations of previously studied viruses for VLP applications

Virus	Ease of Characterization/ Production	Immunogenicity	Peptide Fusion Tolerance	Final Score
HPV	+ 3	+1	+1	+5
AAV	+1	-1	+1	+1
HBV	+2	+1	+1	+4
IV	-1	0	-1	-2
CoV	-4	+1	-1	-4
CPMV	-2	+2	+1	+1
HIV	0	0	+1	+1

AAV: adeno-associated virus; CoV: coronavirus; CPMV: cowpea mosaic virus; HBV: hepatitis B virus; HIV: human immunodeficiency virus; HPV: human papillomavirus; IV: influenza virus

[1]The scores ((+) = positive attribute; (-) = negative attribute) indicate the level of the major features (ease of characterization/production, immunogenicity, and peptide fusion tolerance) that are characteristic of each virus listed for VLP formation based on their benefits and limitations outlined in previous studies.

4.2 Generation of DNA-VLP plasmids

The selection of HPV16 L1 VLPs for this study led to the design and genetic engineering of the DNA-VLP plasmids including the L1 capsid sequence. The maps of the cloned DNA-VLP plasmids will be outlined along with agarose gels to visually verify the successful construction of these plasmids. The agarose gels presented in this section demonstrate the cloning of the L1 capsid sequence into the pGL2-CMV mammalian expression backbone vector and the insertion of the VGB sequence into the L1 gene.

4.2.1 Generation of the pGL2-CMV-L1 plasmid

The pGL2-CMV-L1 plasmid was generated after cloning the L1 sequence (~ 1.5 kb) into the pGL2-CMV backbone vector (~ 4.5 kb) (Figure 14; Table 4).

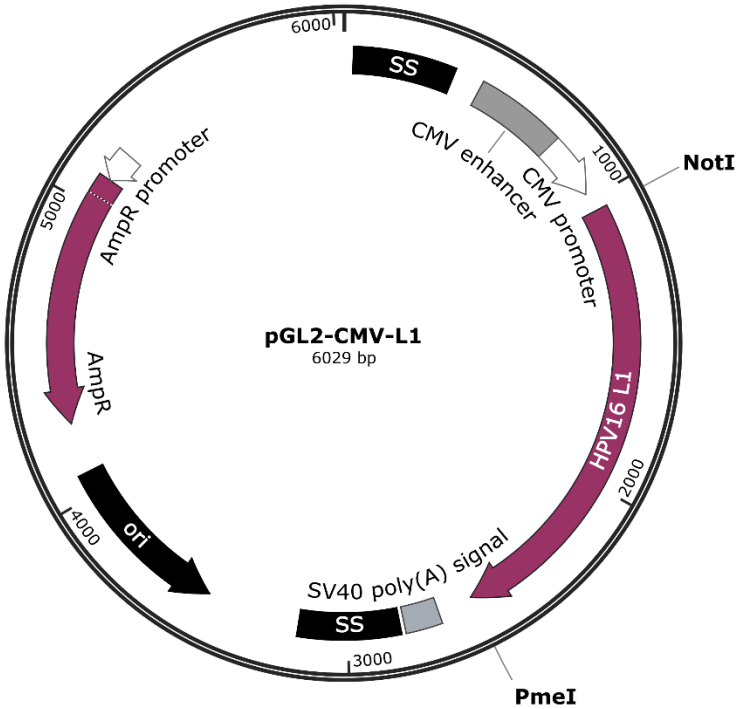

Figure 14. pGL2-CMV-L1 plasmid. DNA-VLP plasmid containing the HPV16 L1 sequence in the pGL2-CMV vector backbone. The pGL2-CMV backbone contains a ubiquitous cytomegalovirus (CMV) promoter for control of the expression of the L1 gene. This vector also contains super sequences (SS), a polyadenylation (polyA) tail, and an ampicillin resistance (AmpR) marker for antibiotic selection. The NotI and PmeI sequences at the 5' and 3' ends of the L1 gene are identified in the image. The final size of the plasmid is ~ 6 kb.

Confirmation of insertion of the L1 gene into the pGL2-CMV backbone to produce the pGL2-CMV-L1 plasmid, was conducted using RE analysis, which demonstrated the expected fragments at ~ 4.5 kb (pGL2-CMV backbone) and ~ 1.5 kb (L1 gene) in lane 2 (Figure 15). The bands in lane 4 demonstrate the digested original pGL2-CMV-gfp plasmid with one band visualized as the size of the pGL2-CMV backbone vector at ~ 4.5 kb, and the other band visualized as the size of the *gfp* gene at ~ 0.75 kb (as outlined in the map in Figure 13). The *gfp* gene in Lane 4 at ~ 0.75 kb demonstrated successful replacement with the L1 sequence indicated in Lane 2 at ~ 1.5 kb (Figure 15). However, RE analysis alone cannot adequately confirm the insertion of the gene of interest. Therefore, sequencing of the cloned L1 sequence was conducted by the Sick Kids Centre for Applied Genomics and demonstrated successful insertion within the pGL2-CMV backbone vector.

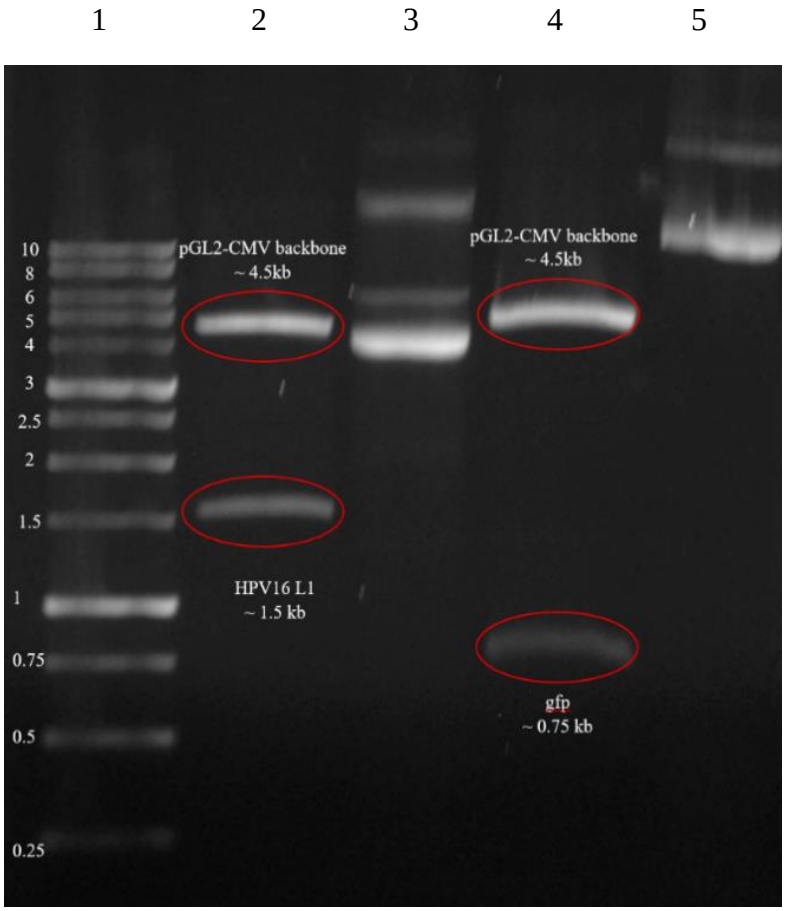

Figure 15. Confirmation of pGL2-CMV-L1 plasmid generation using restriction enzyme digestion. Plasmids extracted from transformed cells were digested with NotI HF and PmeI and subsequently run on a 0.8% gel for ~ 1 h and 30 min at 88 V. Lane 1: 1kb DNA FroggoBio (Concord, CA) Ladder (Catalogue No. DM010-R500). The size of the DNA ladder bands is indicated on the left side of the image in kb; Lane 2: pGL2-CMV-L1 restriction digest reaction; Lane 3: Uncut pGL2-CMV-L1 plasmid; Lane 4: pGL2-CMV-gfp restriction digest reaction; Lane 5: Uncut pGL2-CMV-gfp plasmid.

4.2.2 Generation of the pGL2-CMV-L1 plasmid with VGB sequence insertion

Upon cloning of the HPV16 L1 sequence into the pGL2-CMV backbone, the VGB sequence was inserted into the DE loop and H4 helix region of L1. The pGL2-CMV-L1-VGB-DE and pGL2-CMV-L1-VGB-H4 plasmids were generated, containing the L1-VGB-DE (Table 4) and L1-VGB-H4 (Table 4) sequences (~ 1.55 kb) within the pGL2-CMV backbone (~ 4.5 kb) (Figures 16A and B).

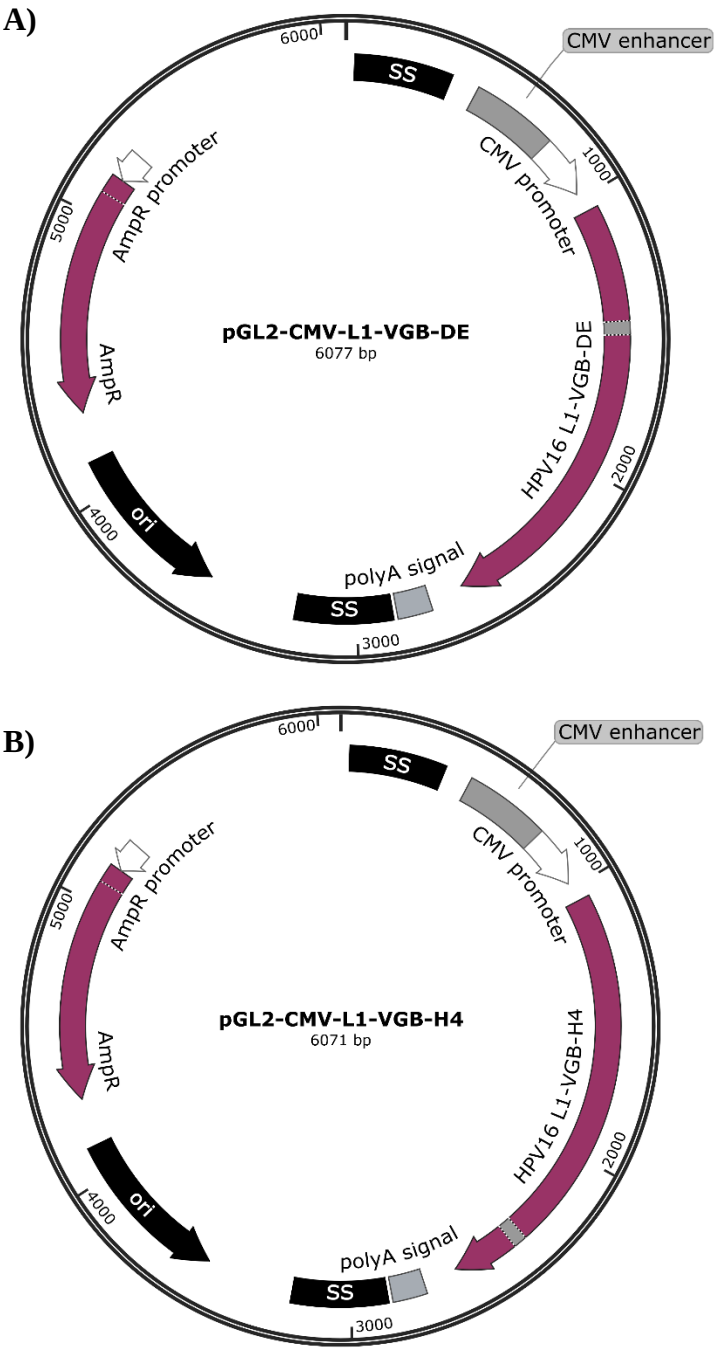

Figure 16. pGL2-CMV-L1 plasmids with VGB sequence insertions. A) pGL2-CMV-L1-VGB-DE plasmid. The HPV16 L1-VGB-DE sequence labelled on the image contains the 42 base pair (bp) VGB sequence inserted in the DE loop of L1 indicated by the grey coloured box. **B)** pGL2-CMV-L1-VGB-H4 plasmid. The HPV16 L1-VGB-H4 sequence labelled on the image contains the 42 bp VGB sequence inserted in the H4 helix of L1 indicated by the grey coloured box. Both plasmids contain the pGL2-CMV backbone which consists of the ubiquitous cytomegalovirus (CMV) promoter for control of the expression of the L1-VGB-DE and L1-VGB-H4 genes. This vector also contains super sequences (SS), a polyadenylation (polyA) tail, and an ampicillin resistance marker (AmpR) for antibiotic selection. The final size of the plasmids are ~ 6.1 kb.

The newly constructed plasmids demonstrated typical banding patterns when run on agarose gel and a similar banding pattern compared to the previously generated pGL2-CMV-L1 plasmid, as three distinct high molecular weight bands (Figure 17A). This promoted the confirmation of pGL2-CMV-L1-VGB-DE and pGL2-CMV-L1-VGB-H4 plasmid formation. The banding pattern observed is attributed to the different forms of plasmids that naturally exist, including covalently closed circular DNA (supercoiled), open circle DNA (nicked) and linear DNA. The contrasting shapes and structures of these three major plasmid forms causes them to migrate through agarose gels at alternative rates. Moreover, accurate DNA fragment sizes (~ 4.5 kb and ~ 1.55 kb) subsequent to digestion with NotI HF and PmeI REs was observed, similar to the previously constructed pGL2-CMV-L1 upon RE digestion (Figure 17B). This further validated the insertion of the L1-VGB-DE and L1-VGB-H4 sequences into the pGL2-CMV backbone. For the plasmids containing the VGB sequence within L1, the L1 sequence displayed a slight increase in size (~ 1.55 kb) in comparison to the control L1 sequence (~ 1.5 kb), due to the increase in the number of bases contributed by the inserted VGB sequence, which was expected (Figure 17B).

To additionally confirm for VGB insertion, primers designed outside of the DE loop and H4 helix region were used to amplify the area of interest, which verified for sequence insertion upon running on agarose gels based on the band size of the amplified products (Figure 18). For VGB sequence insertion into the DE loop region and the H4 helix region, a band size of ~ 128 bp (lane 2) and ~ 136 bp (lane 4), respectively, was observed, as expected. For the control L1 sequence (without VGB insertion), amplification using the designed primers demonstrated a smaller band on the agarose gel, due to the absence of the inserted VGB sequence, at a size of ~ 80 bp (lane 3) within the DE loop region and ~ 88 bp (lane 5) within the H4 helix region. Considering the control L1 plasmid, pGL2-CMV-L1, did not contain the VGB sequence, the amplified product should be ~

50 bp less than the plasmids containing the VGB insertion in the L1 sequence (pGL2-CMV-L1-DE and pGL2-CMV-L1-H4), which was observed (Figure 18). In general, these combined methods (plasmid banding pattern analysis, RE digestion analysis, and PCR amplification) cannot completely verify for VGB insertion into the L1 sequence. Therefore, sequencing was conducted to validate this, which verified the intended outcome.

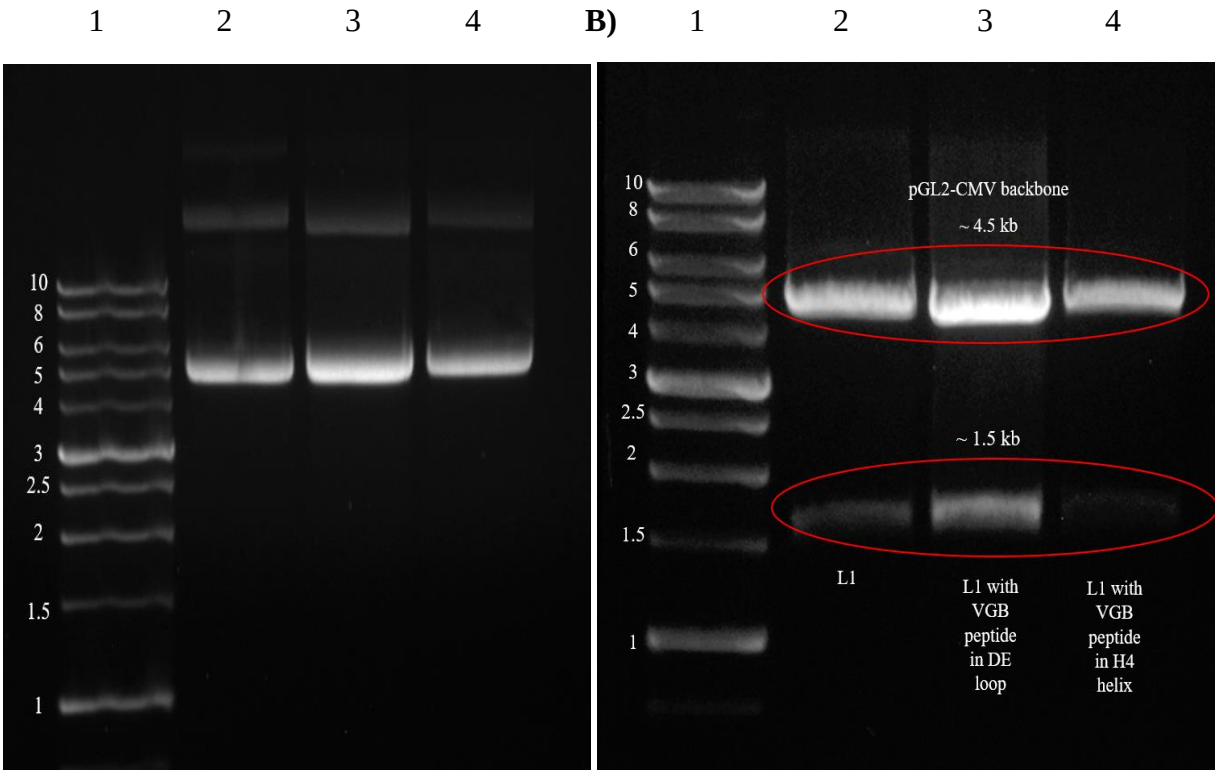

Figure 17. Confirmation of pGL2-CMV-L1-VGB-DE and pGL2-CMV-L1-VGB-H4 plasmid generation. The plasmids and restriction enzyme digest reactions with NotI HF and PmeI were run on 0.8% gels for ~ 1 h and 30 min at 88 V. **A)** Undigested DNA-VLP plasmids. Lane 1: 1 kb FroggoBio (Concord, CA) DNA Ladder (Catalogue No. DM010-R500). The size of the DNA ladder bands is indicated on the left side of the image in kb; Lane 2: Undigested pGL2-CMV-L1 plasmid; Lane 3: Undigested pGL2-CMV-L1-VGB-DE plasmid; Lane 4: Undigested pGL2-CMV-L1-VGB-H4 plasmid. **B)** Digested DNA-VLP plasmids. Lane 1: 1kb DNA FroggBio (Concord, CA) Ladder (Catalogue No. DM010-R500). The size of the DNA ladder bands is indicated on the left side of the image in kb; Lane 2: Digested pGL2-CMV-L1 plasmid; Lane 3: Digested pGL2-CMV-L1-VGB-DE plasmid; Lane 4: Digested pGL2-CMV-L1-VGB-H4 plasmid.

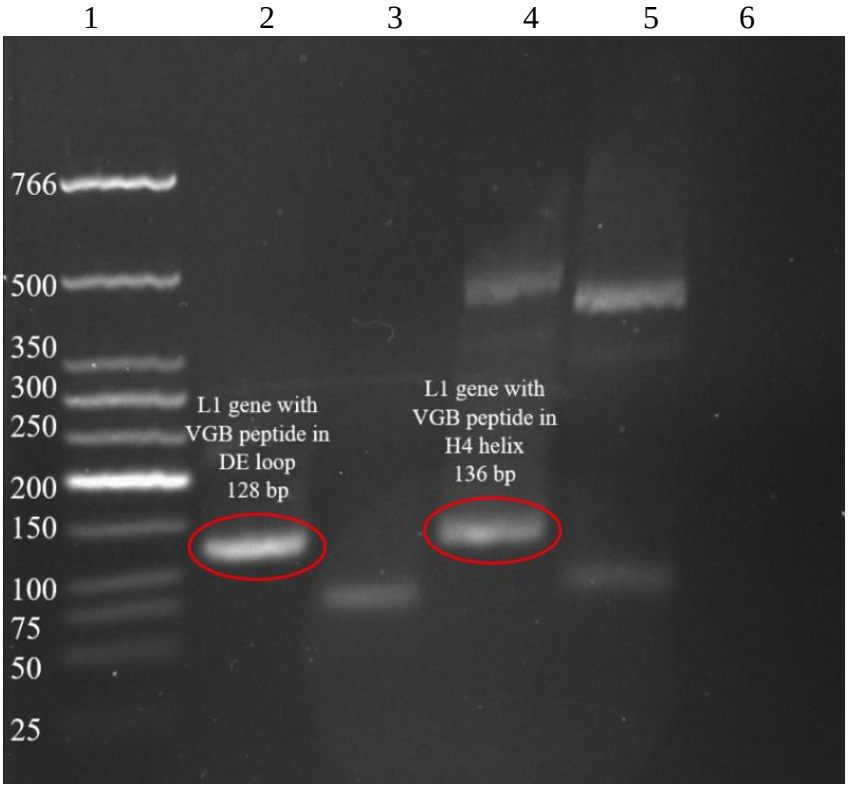

Figure 18. Confirmation of VGB sequence insertion using PCR. The PCR reactions were run on a 3% gel for ~ 1 h and 30 min at 82 V. Lane 1: NEB (Ipswich, USA) Quick-Load Purple Low Molecular Weight DNA Ladder (Catalogue No. N-557S). The size of the DNA ladder bands are indicated on the left side of the image in bp; Lane 2: pGL2-CMV-L1-DE plasmid PCR reaction with primers around the VGB sequence in the DE loop region of the L1 sequence; Lane 3: pGL2-CMV-L1 PCR reaction with primers in the DE loop region of the L1 sequence; Lane 4: pGL2-CMV-L1-H4 PCR reaction with primers around the VGB sequence in the H4 helix region of the L1 sequence; Lane 5: pGL2-CMV-L1 PCR reaction with primers in the H4 helix region of the L1 sequence; Lane 6: Control PCR reaction with no template DNA.

4.3 Increased fluorescence intensity and stabilized transfection efficiency of the pGL2-CMV-gfp plasmid

Prior to transfection with the generated DNA-VLP plasmids, HEK 293T cells were transfected with the control pGL2-CMV-gfp plasmid and run through the flow cytometer to evaluate transfection efficiency. The mean fluorescence intensity values were calculated for duplicates of transfected and non-transfected HEK 293T cells at each time point (24, 48, 72, 96, and 120 h) and increased gradually over time, indicating that increased lengths of time upon plasmid transfection

promoted enhanced GFP expression (Figure 19). The mean percent (%) of fluorescent cells (transfection efficiency) stayed relatively consistent over time at percentage values generally within the range of 40 - 60%, indicating that within the first 24 h, most of the plasmid DNA was taken up by the HEK293T cells, however, not evenly by all cells (Figure 20).

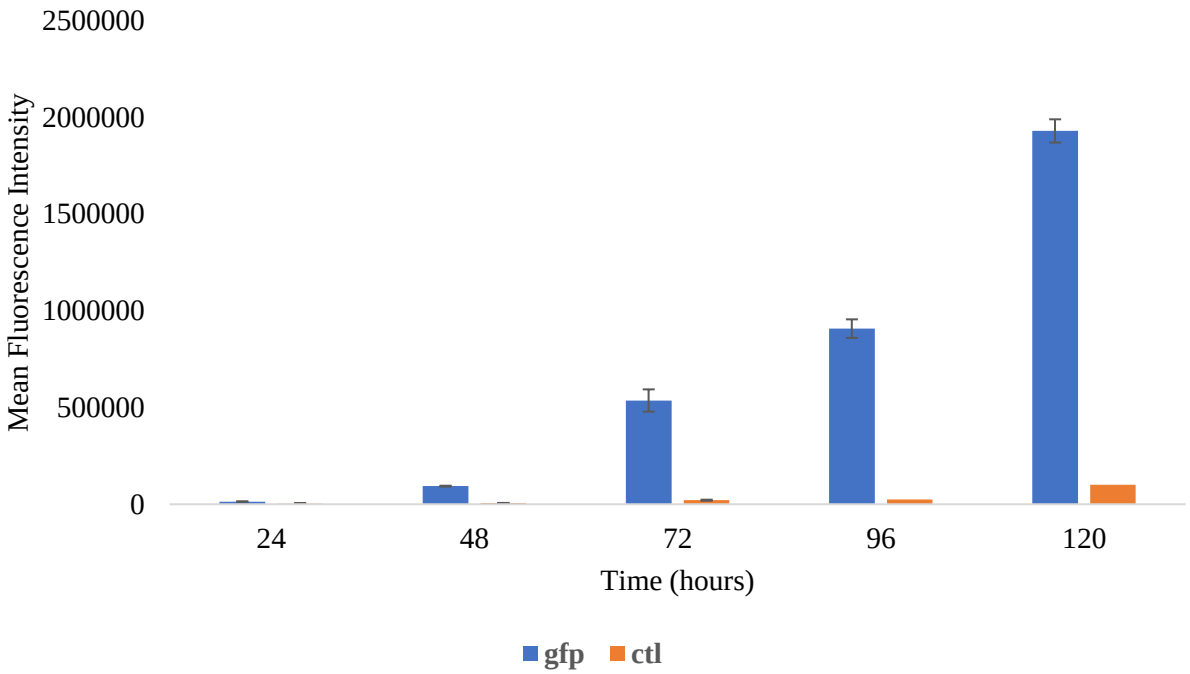

Figure 19. Fluorescence intensity of HEK 293T cells transfected with pGL2-CMV-gfp. Data is presented as mean fluorescence intensity +/- standard error of the mean (SEM) for duplicate samples (10 000 events (cells) per sample) at each time point (24, 48, 72, 96, and 120 h) for pGL2-CMVgfp-transfected cells (represented as blue bars) and control non-transfected cells (represented as orange bars).

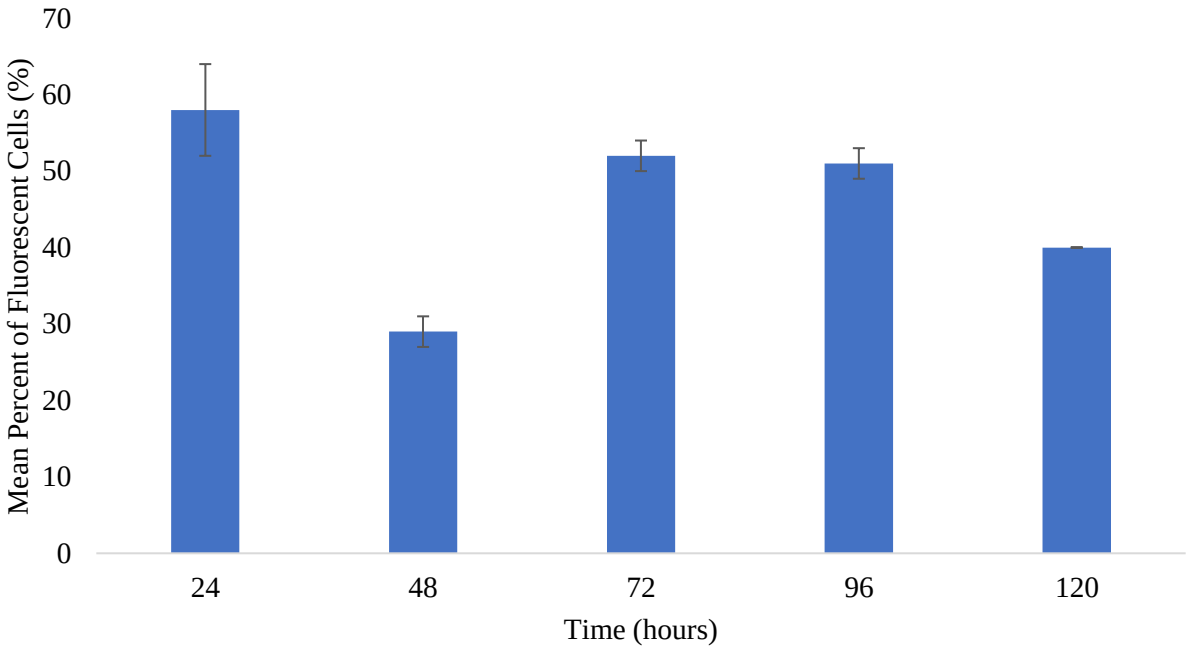

Figure 20. Percent of fluorescent HEK 293T cells transfected with pGL2-CMV-gfp. Data is presented as the mean percent (%) of fluorescent cells +/- standard error of the mean (SEM) for duplicate samples (10 000 events (cells) per sample) at each time point (24, 48, 72, 96, and 120 h) for pGL2-CMV-gfp-transfected cells (represented as blue bars).

4.4 Detection of HPV16 L1 protein expression from purified fractions

Confirmation of transfection efficiency led to the transfection of HEK 293T cells using the DNA-VLP plasmids and subsequent purification. VLPs were purified using an iodixanol density gradient and all fractions were assayed for L1 protein expression by denaturing SDS-PAGE and western blot analysis using the Camvir-1 linear epitope-specific Ab. The results outlined in this section verified L1 protein expression (with and without inserted VGB sequences) within HEK 293T cells.

4.4.1 HPV16 L1 protein with and without VGB insertions was expressed in HEK 293T cells

L1 protein expression was confirmed by the Camvir-1 linear epitope-specific Ab by western blot analysis (Figures 21A-C) by the presence of bands at ~ 56 kDa, primarily in fraction 11, and faintly

in fractions 8-10 and 12. This confirms that the L1 protein was successfully produced from the control construct. The presence of VGB in either site (DE loop and H4 helix) of the L1 capsid did not alter the linear specificity for the Camvir-1 Ab, regardless of the site of insertion (Figures 21B and C). This was expected as the sites of insertion for VGB are not within the determinant sequence identified by Camvir-1. The RL1 protein also showed a more prominent band at ~ 56 kDa, however, some smearing above and below this band can be observed (Figure 21A). Control (non-transfected) cell lysate from HEK 293T cells exhibited no indication of L1 protein expression, as expected, considering no L1 protein was expressed in these cells (Figures 21A-C).

A)

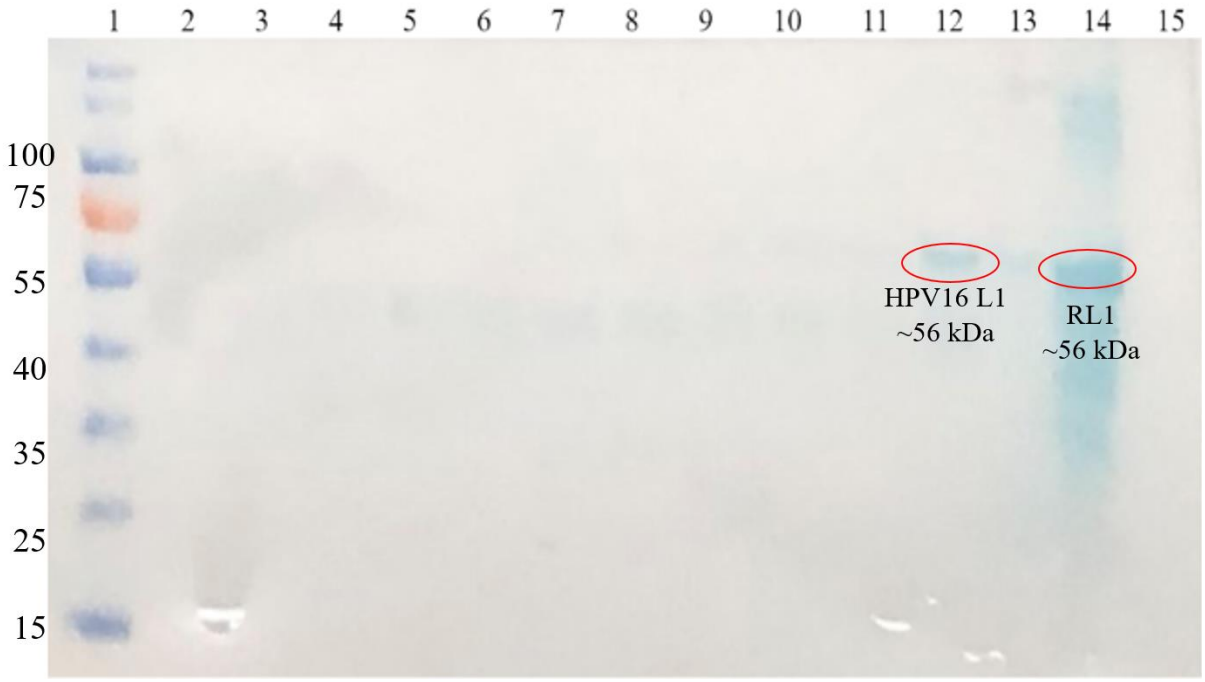

B)


1 2 3 5 5 6 7 8 9 10 11 12 13 14
100
75
55
40
35
25
15
HPV16
L1-VGB-DE
~56 kDa

C)


1 2 3 4 5 6 7 8 9 10 11 12 13 14
100
75
55
40
35
25
15
HPV16
L1-VGB-H4
~56 kDa

Figure 21. Western blot detection of HPV16 L1 protein production with and without VGB insertions. A) Western blot of iodixanol density gradient purified L1 fractions 1 – 12. Lane 1: Prestained PageRuler^{TM} Protein Ladder (Catalogue No. PI26616). The protein ladder sizes are indicated to the left of the image in kDa; Lane 2: Fraction 1; Lane 3: Fraction 2; Lane 4: Fraction 3; Lane 5: Fraction 4; Lane 6: Fraction 5; Lane 7: Fraction 6; Lane 8: Fraction 7; Lane 9: Fraction 8; Lane 10: Fraction 9; Lane 11: Fraction 10; Lane 12: Fraction 11; Lane 13: Fraction 12; Lane 14: RL1 protein (ab119880); Lane 15: Non-transfected HEK 293T cell lysate. **B)** Western blot of iodixanol density gradient purified L1-VGB-DE fractions 1 - 12. Lane 1: Prestained PageRuler^{TM} Protein Ladder (Catalogue No. PI26616). The protein ladder sizes are indicated to the left of the image in kDa; Lane 2: Fraction 1; Lane 3: Fraction 2; Lane 4: Fraction 3; Lane 5: Fraction 4; Lane 6: Fraction 5; Lane 7: Fraction 6; Lane 8: Fraction 7; Lane 9: Fraction 8; Lane 10: Fraction 9; Lane 11: Fraction 10; Lane 12: Fraction 11; Lane 13: Fraction 12; Lane 14: Non-transfected HEK 293T cell lysate. **C)** Western blot of iodixanol density gradient purified L1-VGB-H4 fractions 1 - 12. Lane 1: Prestained PageRuler^{TM} Protein Ladder (Catalogue No. PI26616). The protein ladder sizes are indicated to the left of the image in kDa; Lane 2: Non-transfected HEK 293T cell lysate; Lane 3: Fraction 1; Lane 4: Fraction 2; Lane 5: Fraction 3; Lane 6: Fraction 4; Lane 7: Fraction 5; Lane 8: Fraction 6; Lane 9: Fraction 7; Lane 10: Fraction 8; Lane 11: Fraction 9; Lane 12: Fraction 10; Lane 13: Fraction 11; Lane 14: Fraction 12. For all western blots, protein was detected using the Camvir-1 Ab.

4.5 Detection of HPV16 L1 VLP formation from purified fractions

Next, we sought to investigate whether the expressed L1 proteins could spontaneously form VLPs. To evaluate this, a combination of western blot analysis and ELISA experimentation was conducted using the conformationally dependent H16.U4 Ab. Additionally, visualization of VLPs was observed using TEM. The results obtained suggested potential VLP assembly within HEK 293T cells.

4.5.1 HPV16 L1 trimer formation with and without VGB insertions was observed using non-denaturing PAGE and western blot analysis

The non-denaturing gel and subsequent western blot analysis using the H16.U4 primary Ab was not sufficient to confirm for VLP formation within fraction 11 of the purified samples, as the molecular weight of the VLP would be considerably higher than the largest molecular weight band of the protein ladder. This was confirmed by the absence of notable bands on the western blot (Figure 22A). However, potential configuration/interaction of multiple L1 proteins was observed

when the same experiment was conducted using the Camvir-1 Ab, which demonstrated bands on the western blot with a molecular weight above 130 kDa, for all purified samples (L1, L1-VGB-DE and L1-VGB-H4) (Figure 22B). This is approximately three times the molecular weight of the L1 protein in monomer form (~ 56 kDa), which could possibly be indicative of trimerization of the L1 proteins in non-denaturing form. No bands were observed after incubation with H16.U4 and Camvir-1 Abs for both of the negative controls (pGL2-CMV-gfp transfected lysate and non-transfected lysate samples), as expected, considering no L1 protein was expressed in these cells (Figures 22A and B).

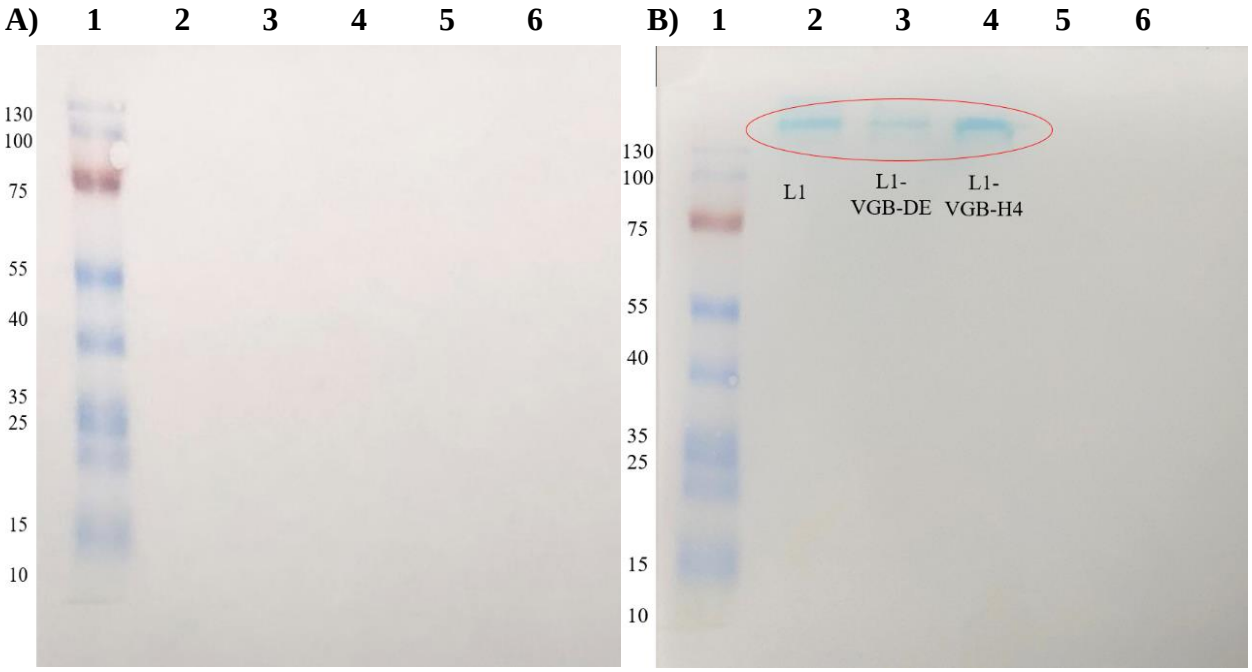

Figure 22. Western blot from a non-denaturing gel for detection of non-denatured HPV16 L1 protein with and without VGB insertions. A) Non-denaturing gel-based western blot using the H16.U4 Ab. Lane 1: Prestained PageRuler^{TM} Protein Ladder (Catalogue No. PI26616). The protein ladder sizes are indicated to the left of the image in kDa; Lane 2: L1 fraction 11; Lane 3; L1-VGB-DE fraction 11; Lane 4: L1-VGB-H4 fraction 11; Lane 5: pGL2-CMV-gfp transfected HEK 293T cell lysate; Lane 6: non-transfected HEK 293T cell lysate **B)** Non-denaturing gel-based western blot using the Camvir-1 Ab. Lane 1: Prestained PageRuler^{TM} Protein Ladder (Catalogue No. PI26616). The protein ladder sizes are indicated to the left of the image in kDa; Lan e2: L1 fraction 11; Lane 3: L1-VGB-DE fraction 11; Lane 4: L1-VGB-H4 fraction 11; Lane 5: pGL2-CMV-gfp transfected HEK 293T cell lysate; Lane 6: non-transfected HEK 293T cell lysate.

4.5.2 HPV16 L1 VLPs with and without VGB insertions were detected using indirect ELISA experimentation

Using indirect ELISA experimentation to supplementarily confirm for HPV16 L1 VLP formation, it was demonstrated that within purified and non purified cell lysate samples, VLP assembly did occur (Figures 23 A-C). The presence of L1 protein and VLP formation within these samples was successfully detected by binding towards Camvir-1 and H16.U4 Abs, respectively, indicated by increased absorbance readings for all samples, including those with VGB insertions (Figures 23A-C). This suggests that VGB peptide insertion did not prohibit the formation of L1 VLPs and did not disrupt the conformational epitope that the H16.U4 Ab specifically recognizes (between aa 422 and 445 of the L1 protein) (Carter et al., 2003; Guan et al., 2015). Wells coated with pGL2-CMV-gfp transfected HEK 293T cell lysate (gfp lysate) and non-transfected HEK 293T cell lysate (ctl lysate), in addition to non-coated wells, demonstrated low absorbance values in comparison to wells coated with the RL1 protein (positive control), fraction 11 of L1, L1-VGB-DE, and L1-VGB-H4, and non-purified L1 lysate samples (Figures 23A-C), indicative of the absence of L1 protein and VLP formation, as expected. Furthermore, it can be noted that non-purified L1 lysate samples (Figure 23A) demonstrated lower binding towards both Abs in comparison to the purified samples (Figure 23C) and the RL1 positive control sample (Figure 23B), suggesting that the purified samples exemplified increased availability and exposure towards the primary Abs applied for consequent recognition and binding.

A)

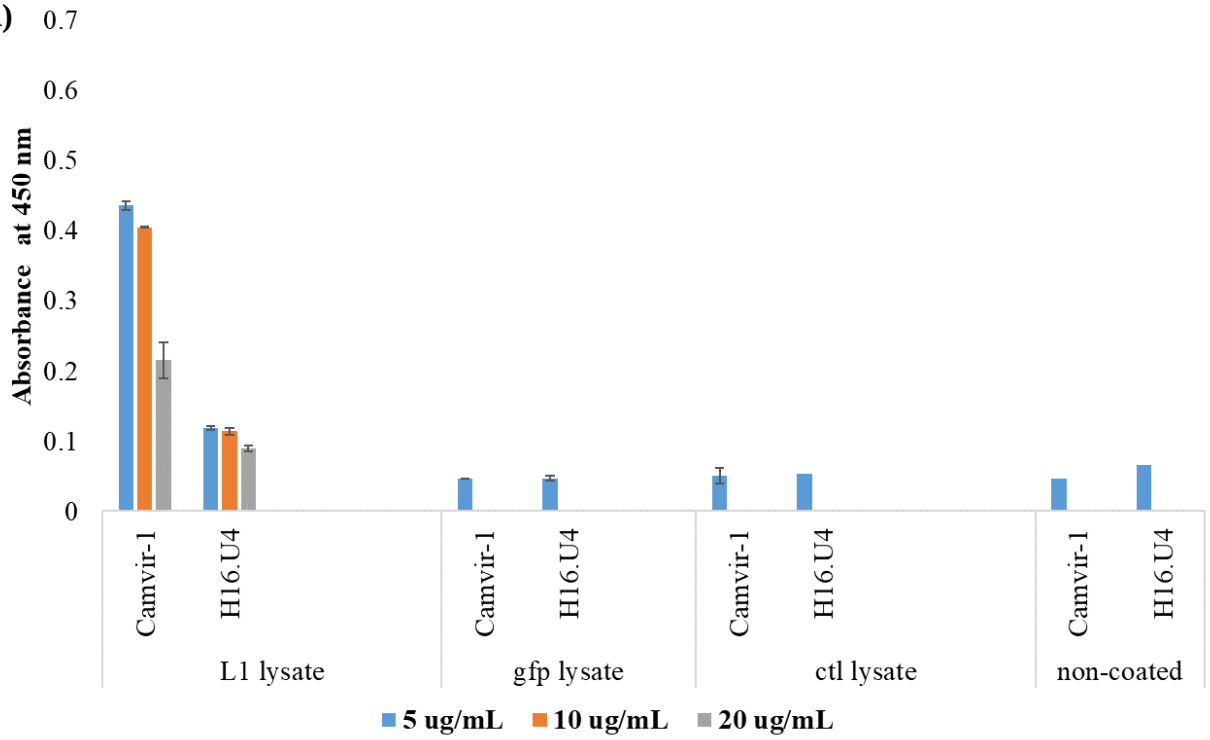
0.7
0.6
0.5
0.4
0.3
0.2
0.1
0
Absorbance at 450 nm
Camvir-1
H16.U4
L1 lysate
gfp lysate
ctl lysate
non-coated
5 ug/mL
10 ug/mL
20 ug/mL

B)

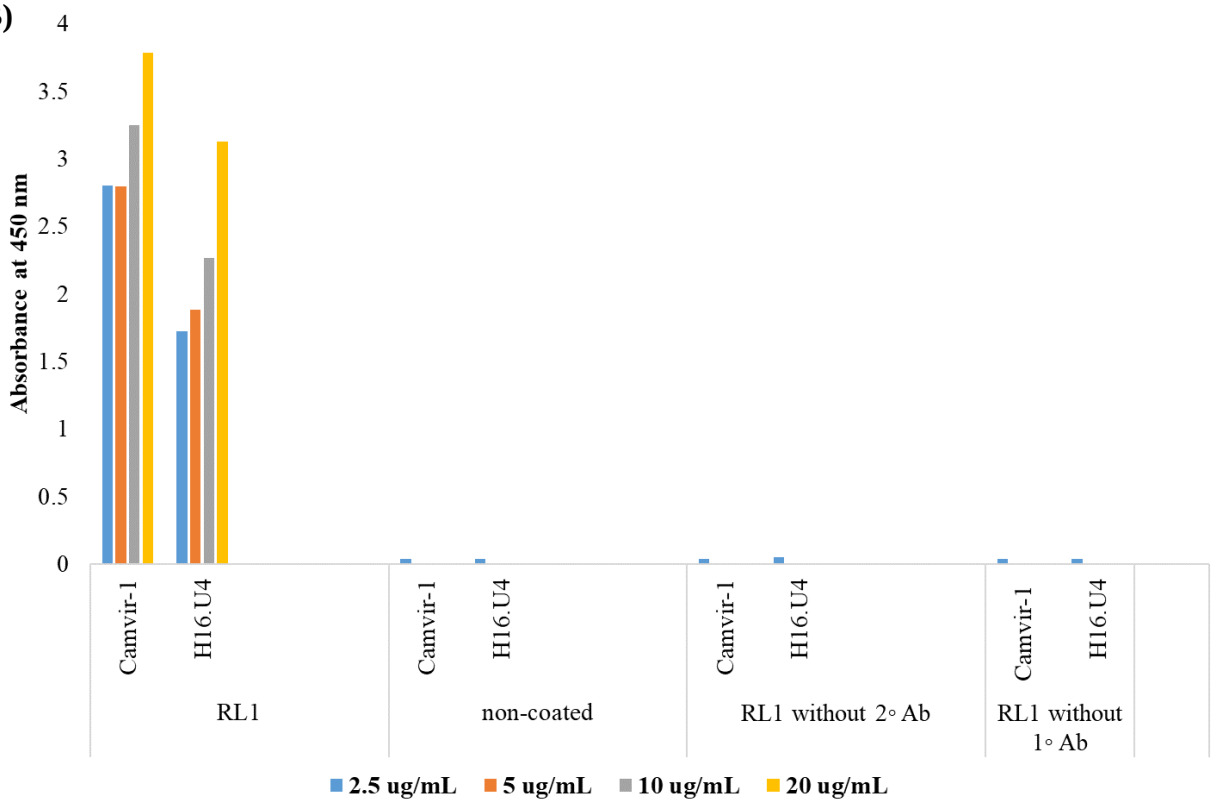
4
3.5
3
2.5
2
1.5
1
0.5
0
Absorbance at 450 nm
Camvir-1
H16.U4
RL1
non-coated
RL1 without 2◦ Ab
RL1 without 1◦ Ab
2.5 ug/mL
5 ug/mL
10 ug/mL
20 ug/mL

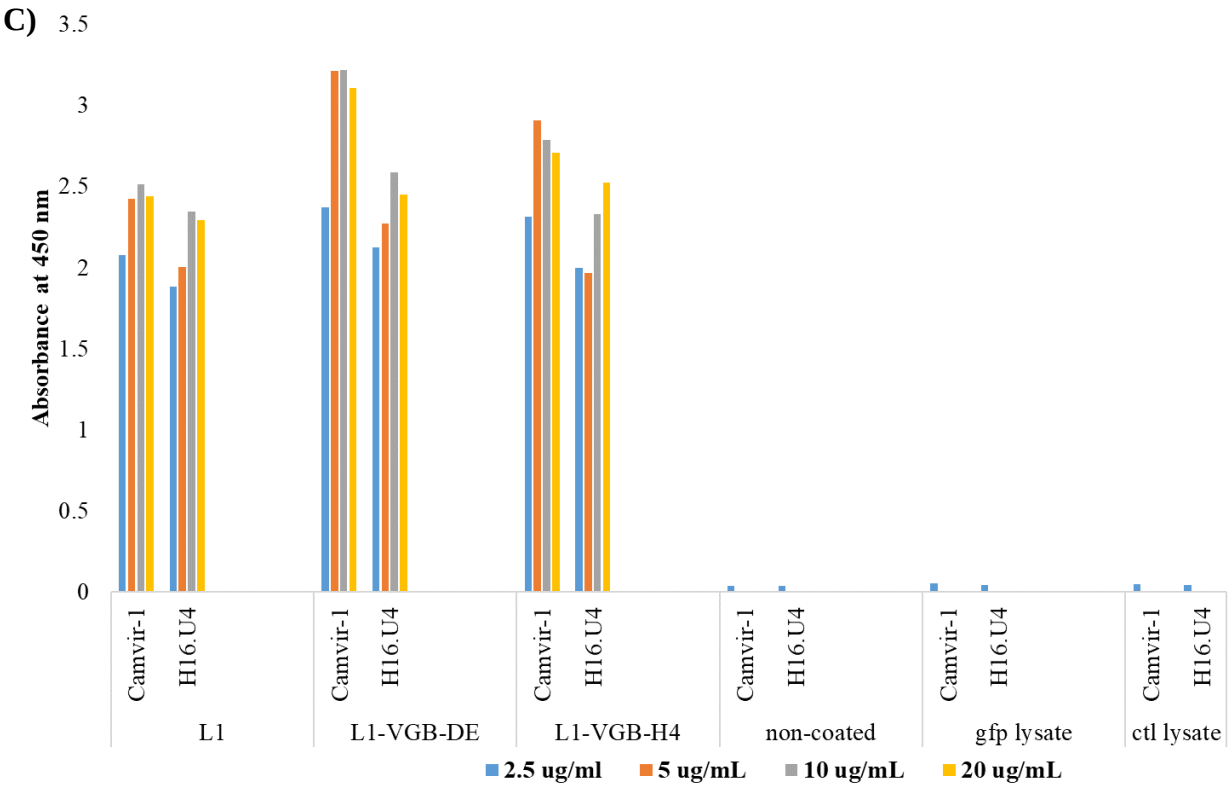

Figure 23. Indirect ELISA detection of HPV16 L1 protein and VLP assembly with and without VGB insertions. A) Detection of L1 protein and VLP assembly from cell lysate. L1 lysate represents lysate collected after pGL2-CMV-L1 transfection. GFP lysate, ctl lysate and non-coated, represents lysate collected after pGL2-CMV-gfp transfection, non-transfected cell lysate, and wells that were not incubated with protein/VLP samples, respectively, as negative controls. The bars represent mean absorbance values of duplicate samples +/- standard error of the mean (SEM) at 450 nm after incubation with either the Camvir-1 or H16.U4 Ab, as labelled in the graph. **B)** Detection of L1 protein and VLP assembly from RL1. RL1 represents the positive control (purchased recombinant HPV16 L1 protein; Catalogue No. 119880). Non-coated, RL1 without 2˚Ab, and RL1 without 1˚ Ab, represents wells not incubated with protein/VLP samples, the RL1 protein coated onto wells but not incubated with secondary Ab, and the RL1 protein coated onto wells but not incubated with primary Ab, respectively, as negative controls. The bars represent absorbance values at 450 nm after incubation with either the Camvir-1 or H16.U4 Ab, as labelled in the graph **C)** Detection of L1 protein and VLP assembly from iodixanol density gradient purified fractions (fraction 11). L1, L1-VGB-DE and L1-VGB-H4 represent fraction 11 of purified L1 protein, L1 protein with the VGB peptide inserted in the DE loop, and L1 protein with the VGB peptide inserted in the H4 helix, respectively. Non-coated, gfp lysate, and ctl lysate, represent wells not incubated with protein/VLP samples, lysate collected after pGL2-CMV-gfp transfection, and non-transfected cell lysate, respectively, as negative controls. The bars represent absorbance values at 450 nm after incubating with the Camvir-1 or H16.U4 Ab, as labelled in the graph. For each graph, the legend indicates the concentration of samples (from 2.5 to 20 ug/mL) coated onto wells indicated by differentially coloured bars.

4.5.3 HPV16 L1 VLP-like structures with and without VGB insertions were observed using TEM

The next step was to visually determine if the binding of the conformationally dependent H16.U4 Ab toward the purified fractions was targeting existent VLPs. Images of the purified L1 fractions (L1, L1-VGB-DE, and L1-VGB-H4) and positive control (RL1 protein), were observed as hollow geometric circular VLP-like structures around 35 – 50 nm in size (Figures 24A, C, E, and F), indicative of potential VLP formation. Additionally, dark-coloured geometric circular structures were observed within the L1 purified fraction (Figure 24D). Considering HPV VLPs are generally observed as hollow circular structures, these structures may be attributed to artifacts in the background of the TEM grid. For the RL1 sample, clusters of very lightly outlined circular structures were observed (Figure 24B), however, this could also be attributed to the background of the TEM grid opposed to actual VLP formation. The negative controls (fraction 1 of the purified L1 fractions, and non-transfected cell lysate) in general, did not demonstrate as visually convincing VLP-like structures, as expected. Some VLP-like structures were observed for fraction 1 of the purified L1 fraction (Figure 24G), however, these structures were not as geometrically defined.

A)

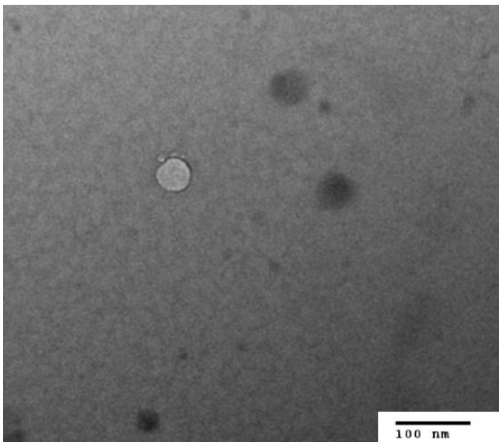

B)

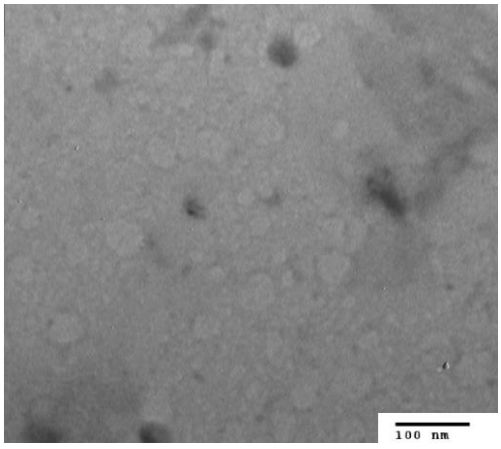

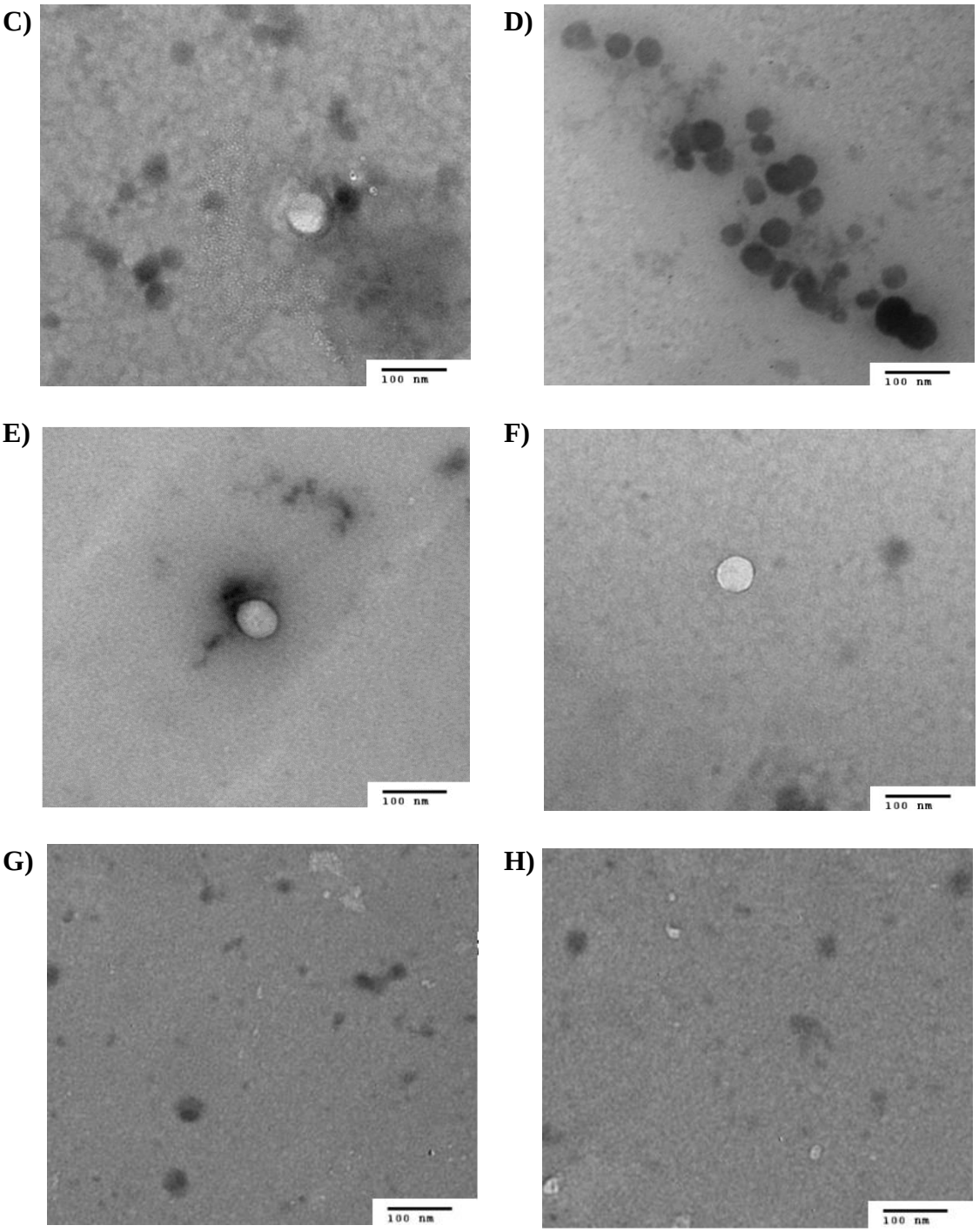

Figure 24. TEM of purified HPV16 L1 fractions. A) TEM image of RL1 (positive control); B) TEM image of RL1 (positive control); C) TEM image of fraction 11 of the purified L1 sample; D) TEM image of fraction 11 of the purified L1 sample; E) TEM image of fraction 11 of the purified L1-VGB-DE sample; F) TEM image of fraction 11 of the purified L1-VGB-H4 sample; G) TEM image of non-transfected HEK 293T cell lysate; H) TEM image of fraction 1 of the purified L1 sample. All images were obtained at a magnification of 64 000X. Bar size: 100 nm.

4.6 HPV16 L1 VLPs with VGB insertions potentially bind to VEGFR

Upon evaluation of HPV16 L1 VLP assembly using indirect ELISA experimentation, VGB-displaying VLP samples (L1-VGB-DE and L1-VGB-H4) demonstrated increased absorbance signals upon incubation with VEGFR compared to non-VGB-displaying samples (L1 and RL1 samples) (Figure 25). The other negative controls (gfp lysate, ctl lysate, L1-VGB-DE without 2° Ab, L1-VGB-DE without 1° Ab, and non-coated) all demonstrated low absorbance measurements, suggesting the lack of specificity of these samples towards VEGFR-2 (Figure 25). However, upon conduction of a two-sample t-test assuming unequal variances between each of the sample groups compared to the negative ctl lysate sample group, significant difference was detected for the L1 and RL1 samples, which was not expected. This decreases the validity of VGB-displaying VLP preferential binding towards VEGFR-2, considering the non-VGB displaying sample mean absorbance levels (L1 and RL1) were statistically different compared to the negative ctl lysate sample mean. Furthermore, for the VGB-displaying samples, only the L1-VGB-H4 sample demonstrated a significantly different mean absorbance measurement compared to the ctl lysate sample group. Significant differences were also not observed between non-VGB displaying samples (RL1 and L1) and the VGB-displaying samples (L1-VGB-DE and L1-VGB-H4), further decreasing the statistical support of VEGFR targeted binding by the VGB-displaying VLPs.

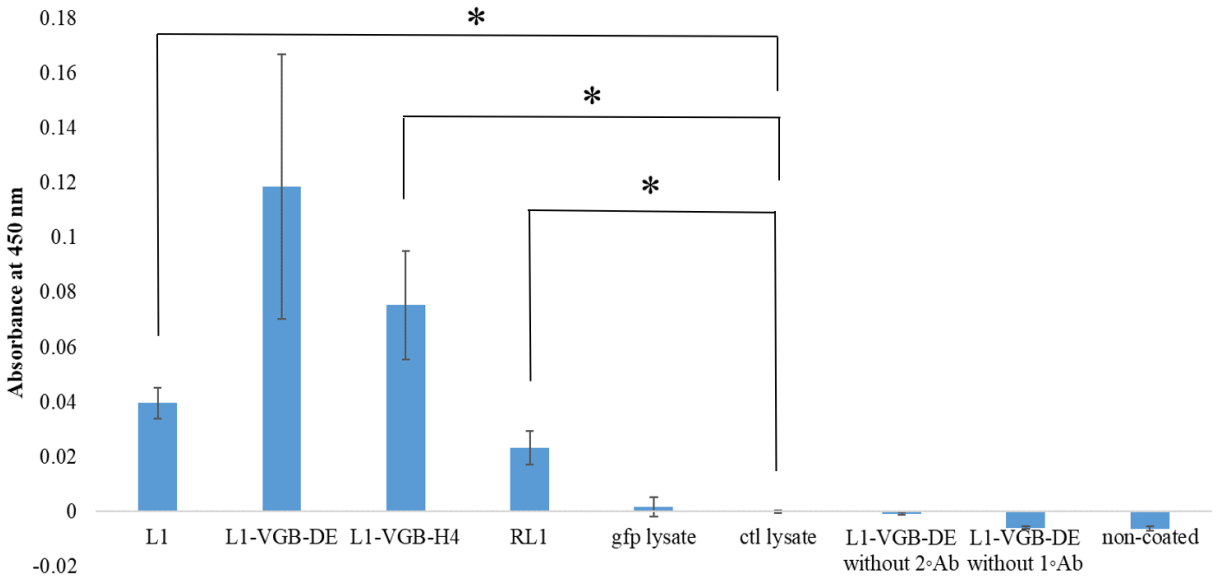

Figure 25. Indirect ELISA detection of potential binding specificity of VGB-displaying HPV16 L1 VLPs toward VEGFR. L1, L1-VGB-DE, and L1-VGB-H4 represents iodixanol density gradient purified L1 protein (fraction 11), L1 protein with the VGB peptide inserted in the DE loop (fraction 11), and L1 protein with the VGB peptide inserted in the H4 helix (fraction 11), respectively. The positive control represents the RL1 (purchased recombinant HPV16 L1 protein). GFP protein lysate, ctl lysate, and non-coated, represents HEK 293T cell lysate collected after pGL2-CMV-gfp transfection, non-transfected HEK 293T cell lysate, and wells not incubated with protein/VLP samples, respectively, as negative controls. L1-VGB-DE without 2^o Ab and L1-VGB-DE without 1^o Ab represents L1-VGB-DE plated onto VEGFR-2 coated wells and incubated without 2^o Ab and L1-VGB-DE plated onto VEGFR-2 coated wells and incubated without 1^oAb, respectively, as negative controls. The bars represent mean absorbance values (subtracted with the mean ctl lysate absorbance value) of triplicate samples +/- standard error of the mean (SEM) at 450 nm after incubation with Camvir-1. Statistical significance was determined using the two-sample t-test assuming unequal variances by comparing the mean values of each of the sample groups to the ctl lysate sample group (non-transfected HEK 293T cell lysate) and indicated by the asterix symbol on the graph.

4.7 HPV16 L1 VLPs do not release from HEK 293T cells

Upon confirming for the potential presence of HPV16 L1 VLP assembly, overviewed in Section 4.5, release of these particles from HEK 293T cells was evaluated post-transfection with the control pGL2-CMV-L1 plasmid at specific points of time. At each time point, the cell count (cells/mL) was recorded and demonstrated a general increase from ~ 1.5 x 10^6 cells/mL to ~ 3.5 x

10^6 cells/mL for all samples (L1, Ctl with reagent and Ctl) that did not considerably differ from one another (Figure 26). The viability of cells was also measured at each time point and demonstrated a slight decrease over time from 95% to around 85% for all samples (L1, Ctl with reagent and Ctl) that also did not considerably differ from one another (Figure 27). These results suggest that the production of L1 protein and L1 VLP formation had a limited effect on the growth and viability of the cells, inferring the absence of the induction of cell lysis.

To further evaluate for the release of HPV16 L1 VLPs, the media of pGL2-CMV-L1 transfected HEK 293T cells was collected at specific points of time, which did not verify for the presence of L1, indicated by the absence of bands at ~ 56 kDa upon western blot analysis (Figure 28). This indicates that the L1 VLPs likely did not release from the cells into the surrounding media. Media collected from non-transfected HEK 293T cells at each of the specified time points, similarly, did not show L1 protein expression, as expected.

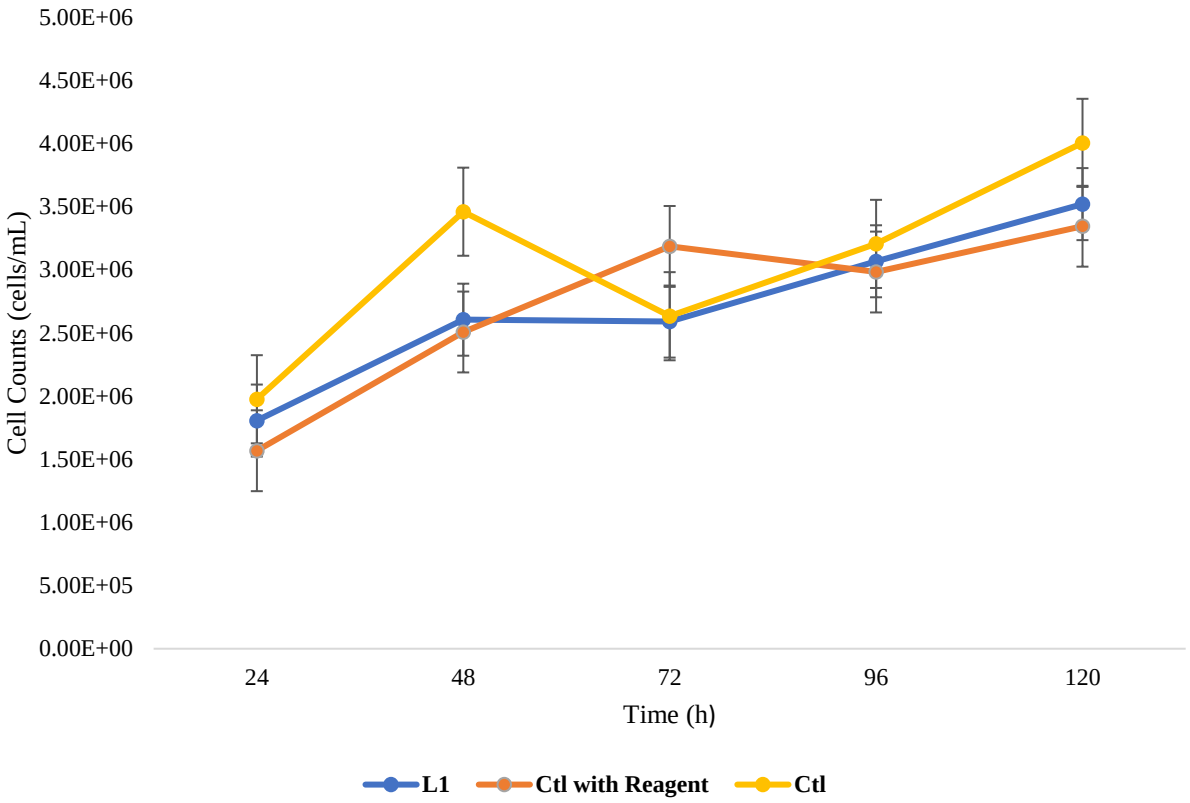

Figure 26. Increased cell counts for pGL2-CMV-L1 transfected HEK 293T cells. L1 represents HEK 293T cells transfected with the pGL2-CMV-L1 plasmid using a transfection reagent. Ctl with reagent represents HEK 293T cells applied with transfection reagent in the absence of DNA. Ctl represents HEK 293T cells that were not applied with transfection reagent and DNA. The legend indicates these samples (L1, Ctl with Reagent and Ctl) differentiated by coloured lines. The cell count values (cells/mL) are presented as mean +/- standard error of the mean (SEM) from quadruplicate samples at each time point for each sample type.

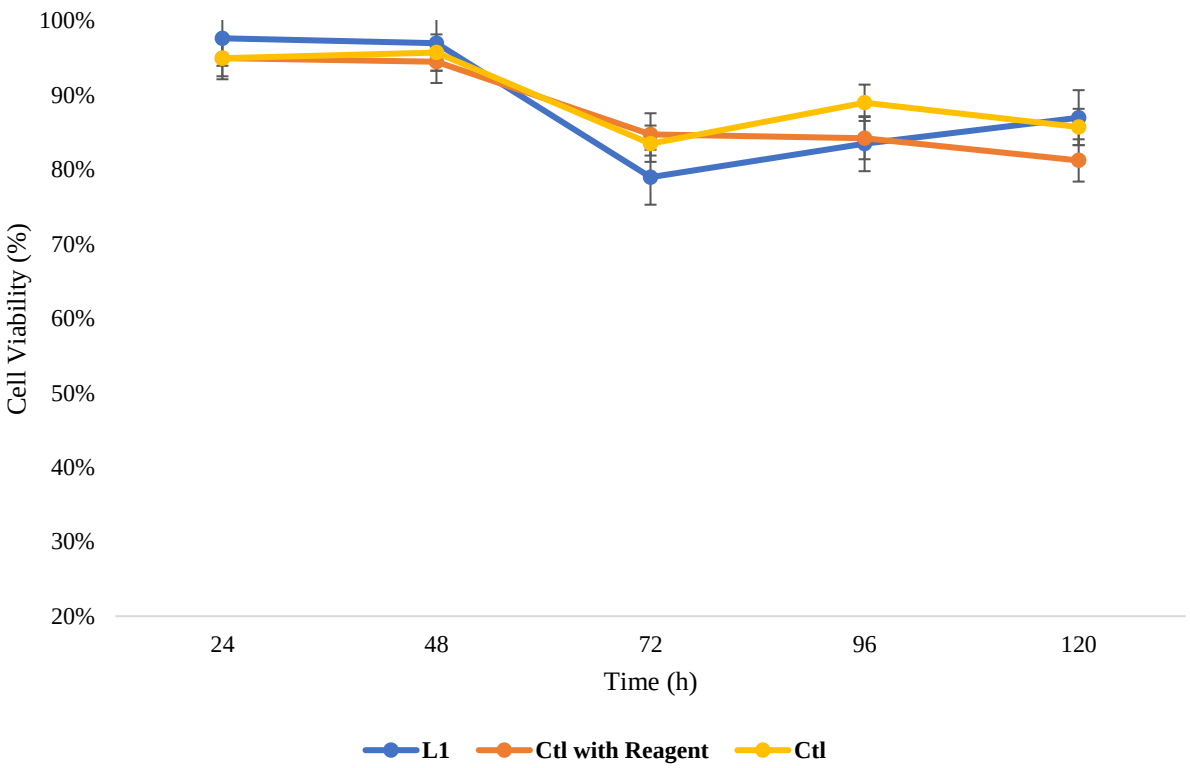

Figure 27. Minimal decrease of cell viability for pGL2-CMV-L1 transfected HEK 293T cells. L1 represents HEK 293T cells transfected with the pGL2-CMV-L1 plasmid using a transfection reagent. Ctl with reagent represents HEK 293T cells applied with transfection reagent in the absence of DNA. Ctl represents HEK 293T cells that were not applied with transfection reagent and DNA. The legend indicates these samples (L1, Ctl with Reagent and Ctl) differentiated by coloured lines. The cell viability values (%) are presented as mean +/- standard error of the mean (SEM) from quadruplicate samples at each time point for each sample type.

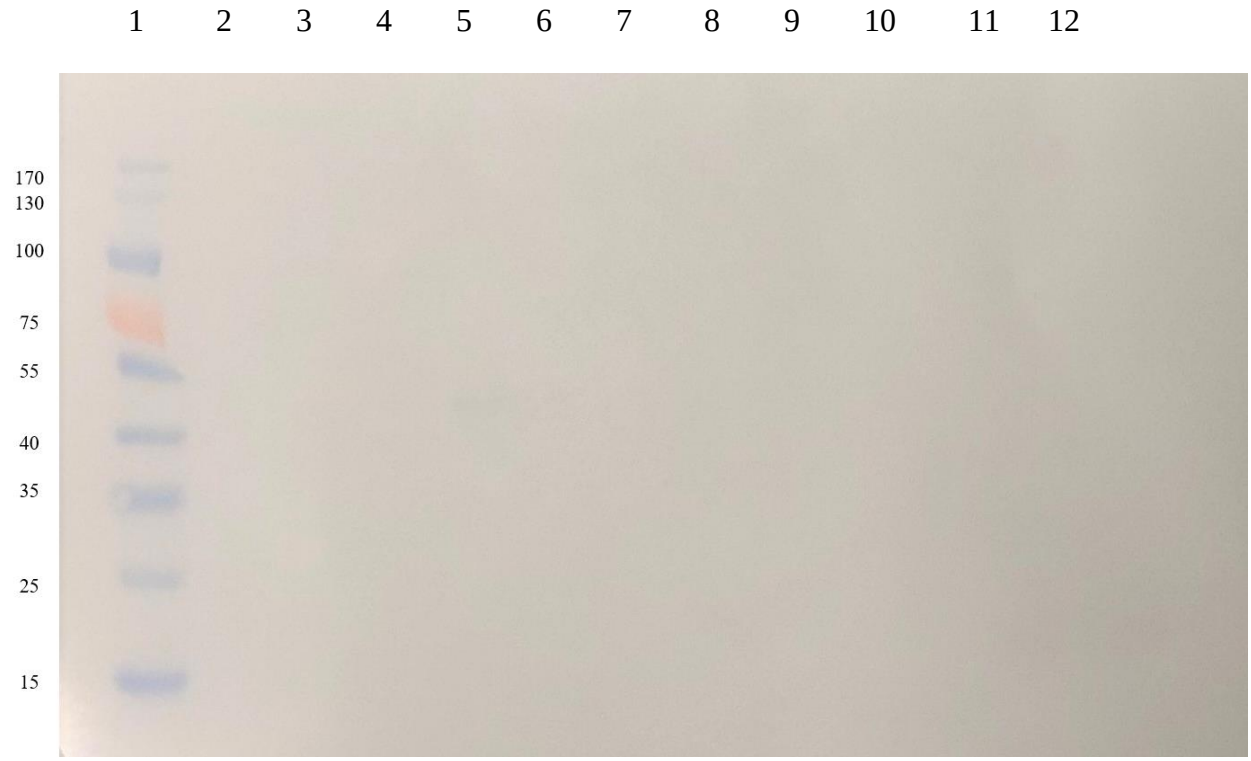

Figure 28. Western blot detected the absence of L1 protein within media from pGL2-CMV-L1 transfected HEK 293T cells. Lane 1: Prestained PageRuler^{TM} Protein Ladder (Catalogue No. PI26616). The protein ladder sizes are indicated to the left of the image in kDa; Lane 2: media from pGL2-CMV-L1 transfected cells at 24 h; Lane 3: media from pGL2-CMV-L1 transfected cells at 48 h; Lane 4: media from pGL2-CMV-L1 transfected cells at 72 h; Lane 5: media from pGL2-CMV-L1 transfected cells at 96 h; Lane 6: media from pGL2-CMV-L1 transfected cells at 120 h; Lane 7: N/A; Lane 8: media from non-transfected cells at 24 h; Lane 9: media from non-transfected cells at 48 h; Lane 10: media from non-transfected cells at 72 h; Lane 11: media from non-transfected cells at 96 h; Lane 12: media from non-transfected cells at 120 h.

5. Discussion

The application of VLPs as a treatment modality for cancer therapeutic administration is currently being advanced at an unprecedented rate, primarily attributed to the ability of VLPs to generate potent cell-mediated immune responses without the added risks that characterize the use of replicative viral treatment (Mohsen et al., 2020; Ong et al., 2017; Tornesello et al., 2022). The ability of these particles to undergo surface modifications to present a variety of peptides and/or ligands further renders them a strong platform for more specific and targeted therapy (Mohsen et al., 2020). The success of preventative VLP vaccine studies led to their FDA approval in the late 1980s (HBV) and the early 2000s (HPV), which was pivotal in branching the use of these particles for therapeutic applications, and more specifically, cancer immunotherapy (Caldeira et al., 2020; Mohsen et al., 2020; Tornesello et al., 2022). Moreover, the success of gene-based vaccine studies in the past has promoted the study of DNA-encoded VLP vaccines (Leder et al., 2001; Rayner et al., 2021; Szécsi et al., 2009; Young et al., 2004), exploiting the benefits of both gene therapy and immunotherapy.

This study included the design of an engineered HPV16 L1 VLP, encoded as a DNA sequence within a eukaryotic expression plasmid, displaying an anti-angiogenic peptide known as, VGB, for the purpose of characterization within mammalian cells (HEK 293T). This peptide prevents downstream signaling pathways for blood vessel formation and has been shown to significantly reduce cancer cell proliferation and tumour growth within mice (Sadremomtaz, Kobarfard, et al., 2018; Sadremomtaz, Mansouri, et al., 2018). Ideally, this VLP was designed to actuate two major anti-cancer responses including the induction of anti-cancer immune responses targeted towards the tumour vasculature, and antagonism of VEGFR signalling, to effectively mitigate tumour

growth. Through molecular genetic engineering, the insertion of the VGB sequence within the L1 capsid sequence was successfully inserted and confirmed. Additionally, we observed that the engineered L1 gene with the inserted VGB sequence was successfully translated to form protein and potentially assembled into VLPs within mammalian cells. The future implications of these findings suggest that this could be employed as a potential immunotherapeutic DNA-VLP vaccine, which has not been licensed to date.

5.1 VLPs can be delivered as a DNA-encoded sequence within a eukaryotic expression plasmid for production in mammalian/human cells

For the purpose of this study, HEK 293T adherent cells were used to express and produce the designed HPV16 L1 VLPs. HEK 293T cells are human embryonic kidney cells and daughter cells of the original HEK 293 cell line, which was generated ~ 40 years ago (Thomas & Smart, 2005; Yuan et al., 2018). In general, HEK 293 cells have been widely used for cell biology experimentation and the production of recombinant proteins for therapeutic and medicinal applications. HEK 293 cells are also highly attractive as they are easy to maintain, grow at accelerated rates compared to other mammalian cells, are highly transfectable, and demonstrate increased levels of genome stability over time (Hu et al., 2018; Stepanenko & Dmitrenko, 2015). Plasmids containing CMV promoters, the promoter used for the expression of the L1 VLPs investigated in this study, in addition to many others promoter types, are able to effectively employ HEK 293's machinery to successfully transcribe and subsequently translate introduced genetic sequences into stabilized protein (Thomas & Smart, 2005). Furthermore, a characteristic feature of these cells includes the fact that they are able to conduct human-like post-translational modifications of proteins, promoting ideal protein formation, conformation and biological activity (Stepanenko & Dmitrenko, 2015; Thomas & Smart, 2005). These combined factors promoted the

selection of HEK 293T cells for expression of the VLPs for this study. Moreover, considering HPV is a virus that inherently infects humans (Humans, 2007), the production of the L1 protein and VLP formation within this human cell line was expected and is a suitable option. Previous studies have also validated the successful production of the L1 protein, in addition to VLP formation within HEK 293 adherent and suspension cells (Leder et al., 2001; Sakauchi et al., 2021). Furthermore, the data obtained from this study supports the finding that L1 protein and VLPs were produced within these cells, which signifies the ability to use DNA-encoded VLPs for expression and assembly within human cells (Figures 21-24). These results will be more explicitly analyzed in later sections.

A distinguishing feature that differentiates HEK293 cells and HEK 293T cells is the presence of an additional temperature-sensitive allele of the SV40 T antigen, which imparts HEK 293T cells with the capability to enhance and increase recombinant protein expression using vectors that specifically contain the SV40 ori (Yuan et al., 2018). The expression of the T-antigen enhances replication of the plasmid containing the SV 40 ori, which in turn augments transcription and translation of introduced genetic sequences into protein (DuBridge et al., 1987; E. Tan et al., 2021). However, for this study, the pGL2-CMV backbone vector was used, which does not contain the SV40 ori. Therefore, the added benefit of using this cell line was not fully exploited. Nonetheless, in future studies, the use of mammalian expression plasmids containing the SV40 ori can be conducted and directly compared to the plasmid employed for this study (pGL2-CMV), to analyze the amount of L1 protein and VLP production within HEK 293T cells.

Although the use of mammalian cells for the expression of VLPs is favourable, as they are able to produce and assemble more complex protein and VLP structures, protein expression levels are considerably lower than other cell types, such as bacterial and yeast cells (Fuenmayor et al., 2017;

Zhu, 2012). This could explain the low levels of VLP-like structures observed via TEM (Figure 24), which will also be more explicitly analyzed in later sections. According to a review (Fuenmayer et al., 2017), bacterial and yeast cells generally can produce proteins within the range of 0.75 to 700 ug of protein/mL of cell culture (Leavitt et al., 1985; Schädlich, Senger, Kirschning et al., 2009). This is notably higher than what has been observed using mammalian cells, which generally produce proteins within the range of 0.1 to 18 ug of protein/L of culture (Holzer et al., 2018; Taube et al., 2005). After purification of the L1 proteins using iodixanol density gradient ultracentrifugation in this study, the protein concentrations within fractions containing the potentially formed L1 VLPs (fraction 11) were within the range of 75 to 100 ug/mL. However, free L1 protein or L1 capsomere formation may migrate to different locations within the iodixanol gradient, as previous studies demonstrate the migration of L1 capsomeres and HPV pseudoviruses towards different density levels compared to VLPs (Buck et al., 2005; Müller et al., 1997). This could also contribute to higher protein concentrations of the L1 capsid produced within the HEK 293T cells. Based on the results obtained, L1 protein concentrations in this study were higher than the aforementioned general protein amounts for VLP formation within mammalian cells (Holzer et al., 2018; Taube et al., 2005). However, the presence of other contaminating proteins within the collected fractions could contribute to the increased protein concentration levels observed. Hence, employing mammalian cells for the industrial large-scale production of VLPs may not be suitable (Fuenmayor et al., 2017; Zhu, 2012), and possibly limited the potential industrial application of this study. Although, the use of mammalian cells grown as suspension cultures, opposed to adherently cultured, can compensate for this. Increasing the scalability of production using adherent cells is generally time consuming and not preferentially employed (McCarron et al., 2016; Rout-Pitt et al., 2018; E. Tan et al., 2021). Considering this, serum free suspension mammalian

cell cultivation for large-scale production purposes have been investigated and used for recombinant AAV production (Ansorge et al., 2009; Nguyen et al., 2021; Segura et al., 2007; E. Tan et al., 2021). A previous study demonstrated that HEK 293 suspension cells have the capability to generate greater than 1 x 10^5 vector genome containing particles/cell when harvested 48 h post-transfection (Grieger et al., 2016). Considering for this study a DNA-VLP strategy is being investigated for future gene delivery into tumours, further applicational studies should employ a mammalian tumour cell model to determine how the VLPs grow within these cell types and their anti-tumour efficacy. If proven successful, HEK 293 suspension cells could subsequently be used for their amplification and production in the large-scale setting.

The choice of mammalian expression plasmid and design of the DNA-VLP sequences (Appendix A; Table 4) was carefully considered in order to achieve maximal L1 protein production and VLP assembly within mammalian cells. In a previous study, the pGL2 (Promega, Madison, WI) vector derivative was constructed to express *gfp* under the control of an SV40 promoter (pNN7). SV40 enhancer sequences (SS) were also inserted into this plasmid upstream of the SV40 promoter and downstream of the polyA sequence to enhance the nuclear translocation of the gene of interest (Nafissi et al., 2014; Nafissi & Slavcev, 2012). It was shown that transfection efficiency with plasmids containing SV40 enhancer sequences is significantly greater in comparison to plasmids not containing these sequences in HEK 293 cells, in addition to a cancer cell line (OVCAR-3). Furthermore, increasing the number of SV40 enhancer units within vectors was also shown to increase the transfection efficiency (Nafissi et al., 2014; Nafissi & Slavcev, 2012). Based on this information, the presence of these sequences within the DNA-VLP plasmids should ideally allow for enhanced nuclear translocation and transcription of plasmid DNA, and consequently greater L1 protein production and VLP formation. To assess for the influence of these enhancer units,

plasmids could be designed containing DNA-VLP gene cassettes in the absence of these sequences to evaluate for differences in L1 protein production and L1 VLP formation. Additionally, to promote higher protein production and assembly of VLPs, different promoters, enhancer elements, and delivery systems could be investigated for comparative analysis.

In summary, the information assessed in this section signifies that HPV16 L1 VLPs can be delivered as a DNA sequence for formation within human cells. The use of the adherent HEK 293T cell line for characterization of the VLPs was successful, however for large-scale production in the future, expression within suspension cells may be more suitable. Moreover, to enhance the quantity of protein and VLPs produced, variations of the design of the eukaryotic expression cassette can be further investigated.

5.2 HPV16 L1 DNA-VLP sequences assemble into potential functional VLPs, but do not induce cell-lysing effects

The production of L1 protein, in addition to L1 protein with VGB insertions was confirmed (Figures 21A-C), as expected, considering previous studies have shown the expression of the L1 protein within the HEK 293 cell line (Leder et al., 2001; Sakauchi et al., 2021). This was also expected as earlier studies have additionally demonstrated the expression of the L1 protein with peptides inserted within the DE loop and H4 helix region (Boxus et al., 2016; Huber et al., 2017; McGrath et al., 2013; Pineo et al., 2013; Varsani et al., 2003). Additionally, the L1 VLPs were expected to migrate towards the bottom of the gradient, at a density level between ~ 1.25 to 1.29 g/cm^3 (Buck et al., 2005; Sapp et al., 1998; Touze et al., 1998; Zahin et al., 2016), which was observed as the L1 protein was detected primarily in fraction 11 (Figures 21A-C). However, as aforementioned, free L1 protein or L1 capsomere formation may migrate to different locations within the iodixanol gradient (Buck et al., 2005; Müller et al., 1997). However, this was not

observed, as the L1 protein was not detected in earlier fractions (Figures 21A-C). Considering this, chemiluminescence detection of the L1 protein from all fractions obtained from the gradients may have verified the presence of the L1 protein contained within earlier fractions, as this method for protein detection is highly sensitive (Mathews et al., 2009).

According to the western blot images visualized, a faint additional band ~ 35 kDa was observed for the L1, L1-VGB-DE and L1-VGB-H4 purified fractions (Figures 21A-C), which could be attributed to partial degradation of the samples over time after being subject to freeze/thaw events over the course of the conduction of these experiments (Jain et al., 2021). The RL1 protein additionally demonstrated a considerable amount of smearing (Figure 21A), also likely attributed to degradation of the protein over time (Jain et al., 2021). Another possible explanation for the presence of additional bands on the presented western blots could be contributed by differentially spliced variants of the L1 protein (Hitzeroth et al., 2018; Wu et al., 2017), producing altered protein sizes, while keeping the linear epitope that the Camvir-1 Ab binds to intact. Moreover, some proteins of HPV are subject to cleavage subsequent to production. The minor capsid protein of HPV, known as, L2, as aforementioned, gets cleaved by furin at the N-terminus region of the protein to expose a binding site for a secondary receptor (Buck et al., 2013; Cerqueira & Schiller, 2017; Cruz et al., 2015). The L1 capsid protein gets cleaved by kallikrein-8, a secreted serine protease, on its C-terminal arm, which facilitates HPV infection (Cerqueira & Schiller, 2017; DiGiuseppe et al., 2017). However, both the capsid proteins of HPV (L1 and L2) are cleaved extracellularly, prior to entry into host cells (Cerqueira & Schiller, 2017; Cruz et al., 2015; DiGiuseppe et al., 2017). Therefore, this cleavage step is an unlikely explanation for the presence of the additional band at ~ 35 kDa on the western blots presented in Figures 21A-C, considering the L1 protein in this study was produced intracellularly. Another possible explanation for the

presence of an additional band within the fractions could be attributed to the specificity of the Camvir-1 Ab. As aforementioned, this Ab binds to a linear epitope of the L1 protein, however, the aa sequence that it binds to (residues 204 to 210) does not span a large section of the protein (Carter et al., 2003). Conformationally dependent Abs on the other hand, depend on both the linear sequence of aa residues in addition to the tertiary structure of the protein, thereby making it more specific compared to linear-epitope binding Abs and less likely to bind to undesirable non-specific proteins (Najar et al., 2017). Based on this information, this could increase the probability that other present proteins within the fraction samples collected prior to and subsequent to purification bound to the linear-epitope binding Camvir-1 Ab, due to the presence of a similar/same set of aa residues. This may explain the presence of the additional faint banding pattern observed on the western blots. However, it is worth noting that the likelihood of this is quite low as Camvir-1 is a mAb, which generally exemplify low levels of cross-reactivity compared to polyclonal Abs (Frank, 2002).

The verification of L1 protein production within HEK 293T cells, as previously outlined, suggests that the formed L1 proteins would spontaneously assemble into VLPs (Buck et al., 2013), which was observed in this study. No L1 VLPs were detected using the H16.U4 Ab after running on a non-denaturing gel (Figure 22A), as expected, as the HPV16 capsid contains 360 copies of the L1 protein arranged in pentamer formation (Buck et al., 2005). This causes the VLPs to confer a high molecular weight that would render it non-detectable using the gels and protein ladders employed in this study. Additionally, the detection of the VLPs using this method would likely disrupt the conformation of the VLPs, potentially attributed to the unstable nature of VLPs in solution (Zahin et al., 2016). Therefore, the absence of VLP detection on the western blot is likely not due to the absence of HPV16 L1 VLP formation. However, it should be noted that high molecular weight

bands (above 130 kDa) were observed on the western blots obtained from the non-denaturing gel when incubated with Camvir-1 (Figure 22B), which could be indicative of VLP formation. A previous study observed that HPV VLPs run on non-reducing gels demonstrate a distinct banding pattern with ~ 50% of L1 migration as monomers (displaying a band at ~ 50 kDa) and ~ 50% of L1 migration as trimer oligomers (displaying a band at ~ 150-160 kDa) (Sapp et al., 1998). Therefore, Figure 22B could be indicative of potential VLP formation, as the aforementioned study concluded that trimerization of L1 is required for VLP assembly (Sapp et al., 1998). This was observed as the mutation of specifically conserved cysteine residues prevented trimerization, and consequently, VLP construction (Sapp et al., 1998). Therefore, based on the results, it is possible that trimerization of the L1 protein is occurring and remained stabilized throughout the conduction of the experiment. In addition to this, it is worth noting that additional bands around 280 kDa (5 times the molecular weight of the L1 protein) was not detected, which could have potentially confirmed for L1 capsomere formation. However, it is likely that if present, L1 capsomere formation did not remain intact (Schädlich, Senger, Gerlach et al., 2009), or was not able to be detected due to non-suitable gel percentage conditions and difficulties during transfer onto the membrane, which is characteristic of high-molecular weight proteins (Bolt & Mahoney, 1997).

To further evaluate for L1 VLP formation, a less invasive method in compared to western blot analysis was employed (indirect ELISA experimentation) (Figures 23A-C). The Camvir-1 Ab bound more significantly to the transfected cell lysate samples compared to the H16.U4 Ab at all protein concentrations, and slightly more to the purified samples (L1, L1-VGB-DE and L1-VGB-H4), which was expected. This was expected as 100% of L1 protein produced within the cells would likely not assemble into VLPs, which is generally what has been previously observed (Sapp et al., 1998). The presence of increased free L1 protein opposed to assembled VLPs could

potentially be attributed to several plausible reasons. First, in general, the lack of the presence of a viral genome renders VLPs less stable, making them more prone to disassembly during downstream processing events (Dai et al., 2018; Vicente et al., 2011). Additionally, the expression level of proteins also determines how efficiently and readily available the proteins are to assemble into VLPs (Dai et al., 2018). A previous study indicated that in order for efficient levels of HPV L1 VLPs to form, a critical L1 protein level needs to be attained within cells (Senger et al., 2009). Furthermore, HPV VLP formation requires the production of stabilized disulphide binding interactions between L1 proteins which needs to be kept intact for VLPs to remain in proper conformation (Palucha et al., 2005; Sapp et al., 1998). In general, these factors limit the conservation of VLP assembly in comparison to free individual protein formation.

Previous studies generally show more consistent formation of VLPs when peptides are inserted into the DE loop region (Huber et al., 2017; Varsani et al., 2003), as opposed to the H4 helix region (Boxus et al., 2016; McGrath et al., 2013; Pineo et al., 2013; Varsani et al., 2003). A comparison could be made to determine the level of VLP formation based on the level of binding of the H16.U4 Ab by the level of absorbance measured subsequent to substrate addition. It was observed that a slightly higher level of binding towards H16.U4 was detected for L1-VGB-DE samples compared to L1-VGB-H4 samples (Figure 23C), which was expected, considering VLPs with peptides inserted in the DE loop region of L1 show more consistent VLP formation (Huber et al., 2017; Pineo et al., 2013; Schellenbacher et al., 2009; Varsani et al., 2003), as aforementioned. However, the level of binding that occurred towards the L1-VGB-DE sample was also higher compared to the control non-altered L1 sample (Figure 23C), which was not expected, indicating that the indirect ELISA conducted may not be an accurate method to estimate relative levels of VLP

formation. More suitable methods for VLP quantification have been conducted including nanoparticle tracking analysis and size exclusion chromatography (Steppert et al., 2017).

It is important to note that the H16.U4 Ab is targeted towards the region of VGB peptide insertion within the H4 helix (at aa residues between 422 to 445) (Carter et al., 2003; Guan et al., 2015), hence, it would be expected that insertion of a peptide within the H4 helix would disrupt the conformational epitope that this Ab binds to. Although, based on the results obtained, despite VGB peptide insertion into the H4 helix, it is likely that the L1 pentamers assembled into VLPs and maintained the structural configuration required for the H16.U4 Ab to bind to the VLP in between formed L1 capsomers. This was additionally observed in a previous study assessing chimeric HPV L1 VLP binding towards conformationally dependent Abs (Varsani et al., 2003).

We observed by TEM that the RL1 protein, L1, L1-VGB-DE and L1-VGB-H4 samples all displayed similar VLP-like structures (Figure 24). Based on previously imaged L1 VLPs negatively stained using 2% PTA, 35 - 50 nm circular formations characterized by a dark outer lining and inner lighter area were visualized (Olcese et al., 2004; D. Wang et al., 2020; Zahin et al., 2016). This structure is generally observed for viruses and VLPs, as the negative stain solution coats the TEM grid to surround the particle without infiltrating the capsid structure, generating a dark border, outlining its geometrical circular shape (Blancett et al., 2017; S. Brenner & Horne, 1959; González-Domínguez et al., 2020; Monninger et al., 2016). Similar structures were visualized for the RL1 protein, L1, L1-VGB-DE and L1-VGB-H4 samples (Figure 24A, C, E, and F), suggesting potential VLP formation. However, it should be noted that the VLP-like structures were observed as single particles rather than as clusters, differentiating these images to what has been predominantly examined in previous studies and suggesting low levels of VLP formation (Zahin et al. 2016; Wang et al., 2016; Leder et al., 2001). This could be attributed to low levels of

produced VLPs within the HEK 293T cell line, or possibly deformation of the VLPs during TEM sample preparation (Nooraei et al., 2021). Only one of the samples (RL1 protein samples) (Figure 26B) displayed clusters of circular structures, although, these structures were very lightly defined, and could be contributed by the background of the grid. Some similar VLP-like structures were observed within the samples without L1 protein expression; however, the structures were not as symmetrically geometric and well-defined compared to what has previously been observed (Olcese et al., 2004; Zahin et al., 2016). One of the L1 transfected samples (Figure 24D) additionally illustrated clusters of circular structures, however, the negative stain appears to have infiltrated the particle, which should not generally occur with negatively stained viruses (Blancett et al., 2017; S. Brenner & Horne, 1959; Monninger et al., 2016). Therefore, what was observed in Figure 24D could be artifact structures within the background of the grids, although the circular symmetrical geometric shape is characteristic of VLPs (González-Domínguez et al., 2020). Moreover, the size of VLP-like structures was also between 35 - 50 nm, which is specifically characteristic of HPV16 L1 VLPs (Leder et al., 2001; Sanchooli et al., 2020; Zahin et al., 2016). Accordingly, it can be concluded that the images observed potentially display HPV16 L1 VLP structures. However, due to the presence of some similar geometric VLP-like structures observed for samples without L1 VLPs, it is important to verify that the VLP-like structures observed for the purified VLP samples was not debris or other artifacts contributed by the grid. In order to validate this, samples stained with L1-specific primary Ab and gold-labelled secondary Ab, can be visualized on the TEM grid as dark black dots specifically within the vicinity of the L1 VLP/protein formations (Lucocq, 2008).

The potential assembly of VLPs based on western blot analysis, ELISA experimentation and visualization via TEM was observed, and therefore, the possibility for the accumulation of VLPs

within cells promoting subsequent cell lysis, was assessed. Non-enveloped VLP accumulation and release into the extracellular environment has not been significantly investigated to date based on previous review papers (Dai et al., 2018; Fuenmayor et al., 2017). Generally, non-enveloped VLPs remain intracellular. For their production and collection within cells, a cell lysis step is conducted to release the VLPs (Dai et al., 2018). In general, studies investigating L1 VLPs apply lysis treatment 72 h post-transfection, which provides enough time for the VLPs to collect within the cell to a certain degree without greatly diminishing the viability of the transfected cells (García-Piñeres et al., 2009; Leder et al., 2001; Mossadegh et al., 2004; Sakauchi et al., 2021). Based on this, it was hypothesized that allowing the VLPs to form post 72 h (96 to 120 h) would enable the VLPs to accumulate and in doing so, potentially burst the mammalian cells or induce cell lysis for their release, however, this did not occur. This was not inferred as a decrease in cell viability and cell growth did not occur after transfection with the DNA-VLP plasmid (Figures 26 and 27), in addition to the absence of L1 protein detection within the cell culture media (Figure 28). In spite of this, it is important to be aware that the trypan blue assay can overestimate the level of viable cells, considering it depends on the fact that live cells contain intact cell membranes, while dead cells do not (Strober, 2015). This does not necessarily always occur as apoptotic cells may still maintain an intact cell membrane (Strober, 2015), which could have contributed to the minimal decrease in cell viability that was observed.

In general, previous studies have shown a significant reduction in cell viability upon viral particle formation over time (Aucoin et al., 2006; Mena et al., 2007). Therefore, it was expected that this would occur post-transfection with the DNA-VLP plasmids. Furthermore, release of the L1 VLPs was also expected to occur considering during the normal life cycle of HPV, the virus gets released from host cells subsequent to assembly into virions. The actual mechanism of release of HPV

virions has not yet been fully characterized, however, it has been stated that certain cytoskeletal rearrangements in the cell are required for this to occur (Pinidis et al., 2016), which likely did not occur within the HEK 293T cells to enable VLP release. Moreover, it has been shown that HPV VLPs assemble within the nucleus subsequent to L1 protein expression in the cytoplasm, which infers an additional barrier for accumulation of VLPs in the cytoplasm, potentially limiting the cell-lysing inducibility of these VLPs (Leder et al., 2001). Overall, these results suggest that the VLPs likely did not accumulate to a high enough degree to induce cell lysis, and thus did not affect the viability and growth of the HEK 293T cells considerably.

In summary, the information assessed in this section signifies that the insertion of the VGB peptide within the L1 protein did not prevent L1 protein and potential L1 VLP formation within human cells. Although, the display of the VGB peptide on the surface of the VLPs still requires further validation. Furthermore, the stability of VLPs can be greatly influenced by handling and preparation procedures (Dai et al., 2018), which may have promoted the observation of low VLP-like structures visualized by TEM. This promotes the increased need for proper techniques and handling procedures during the conduction of these processes for enhanced VLP collection. Considering the accumulation of the VLPs within the cells did not impact cell viability and growth to a considerable degree, inferring the absence of cell lysis, different methods should be taken into consideration to increase the delivery of the DNA-VLP gene cassettes to promote increased amounts of L1 VLP formation within cells. This could further enhance the impact of this treatment as an oncolytic-based treatment.

5.3 VGB insertions within the assembled HPV16 L1 VLPs could enable preferential binding towards VEGFR

The specificity of the VGB-displaying HPV VLPs towards VEGFR was assessed using an indirect ELISA. As aforementioned, VGB specifically binds toward VEGFR1 and VEGFR2 simultaneously and individually (Sadremomtaz, Kobarfard, et al., 2018; Sadremomtaz, Mansouri, et al., 2018). L1-VGB-DE and L1-VGB-H4 samples demonstrated increased absorbance levels upon incubation with VEGFR-2 compared to the negative controls (L1, RL1, control lysate and gfp lysate) (Figure 25), which could be indicative of specific binding of the VGB-displaying VLPs towards VEGFR-2. Nevertheless, it should be noted that the standard error of the mean for the L1-VGB-DE and L1-VGB-H4 samples was higher compared to the other sample groups tested. This suggests the need for further confirmatory testing to validate the binding specificity of VGB-displaying VLPs towards VEGFR-2. Moreover, non-VGB-displaying samples (L1 and RL1) demonstrated a significant difference in absorbance means compared to the negative ctl lysate group (Figure 25). However, based on this information, it cannot be concluded that the VGB-displaying VLPs do not preferentially bind towards VEGFR, as the VGB-displaying VLP samples showed higher absorbance readings compared to all other sample groups (Figure 25). Although the L1 and the RL1 samples demonstrated statistically significant mean absorbance levels in comparison to the ctl lysate, this could be attributed to insufficient washing subsequent to sample incubation and primary/secondary Ab incubation, or non-specific binding of the Camvir-1 Ab. To more definitively confirm for VEGFR-2 targeted binding of the VGB-displaying VLPs and the validity of this assay, a positive control sample needs to be tested. This positive control ideally should be a purchased VGB peptide or a native VEGF ligand, which specifically binds to VEGFR-2. Furthermore, additional DNA-VLP gene cassettes could be generated which would contain the

L1 sequence with scramble peptide sequence insertions to help eliminate the possibility of non-VGB-specific binding towards VEGFR-2. A concentration range of samples could also be employed to evaluate the relationship between sample concentration and VEGFR-2 targeted binding. In summary, the information assessed in this section signifies the possible use of the designed VLPs as an anti-angiogenic treatment, however, further confirmatory testing is still required to validate this.

6. Conclusions and Future Research

The main objective of this project was to characterize the *in vitro* assembly and release of HPV16 L1 VLPs displaying VGB within mammalian cells via transfection with DNA-VLP plasmids. The DNA-VLP sequences were designed and successfully cloned into a mammalian expression plasmid (pGL2-CMV), confirmed by RE digestion, PCR, and sequencing. Following this, transfection of the plasmids containing the DNA-VLP gene cassettes was conducted using HEK 293T cells and analyzed for L1 protein expression. The L1 protein and modified L1 proteins containing VGB insertions within the DE loop or the H4 helix region, transcribed and translated from the DNA-VLP plasmids, were produced within HEK 293T cells, verified by western blot analysis and ELISA experimentation.

Assembly and formation of VGB-displaying HPV16 L1 VLPs was observed via ELISA experimentation using a conformationally-dependent and VLP-specific Ab known as, H16.U4. TEM was additionally used to confirm VLP formation. The images indicate possible VLP formation as circular geometric structures were observed at comparable sizes to what has previously been observed (35 - 50 nm) upon TEM visualization. The display of VGB on the surface of HPV16 L1 VLPs was assessed by evaluating its specificity towards VEGFR. The VLPs demonstrated potential preferential binding towards VEGFR-2, however, further testing is required to infer statistically significant VEGFR-2 binding specificity.

The release of VLPs, indicative of potential VLP-induced cell lysis, was assessed by collecting culture media at varied points of time post-transfection. However, based on the results, it can be concluded that the accumulation of HPV16 L1 VLPs within HEK 293T cells does not induce their release into the extracellular environment, as no L1 protein was detected.

The outcomes of this project suggest that the *in vitro* assembly of VGB-displaying HPV16 L1 VLPs occurs within HEK 293T cells subsequent to transfection with the designed DNA-VLP plasmids. However, the VLPs were not released from the HEK 293T cells, which would have ideally further enabled targeting toward VEGFRs within growing tumours, subsequent to patient treatment application. Nevertheless, the designed HPV16 L1 DNA-VLP plasmids could still be applied as potential DNA immunotherapeutic vaccines for *in vivo* assembly within humans. Moreover, this could also be applied as a VLP immunotherapeutic by direct application of the VGB-displaying HPV16 L1 VLPs to solid tumours. This would still enable the impartation of dual-anti-cancer promoting outcomes via the targeting of VEGFRs expressed on the tumour vasculature and immune response stimulation.

The future of this study requires repetition of all the aforementioned experiments within a tumour cell model to compare the degree of VLP formation and direct influence on cancer cell growth. The application of assembled VLPs and DNA-VLP plasmids toward a 3D spheroid cancer cell model, as opposed to a 2D cancer cell line, could additionally be conducted. These 3D spheroid cancer cell models more accurately represent the TME architecture and *in vivo* cellular environment (Barbosa et al., 2021). Therefore, this would permit an enhanced and more accurate analysis of the effectiveness of the designed treatment on cancer cell growth.

Further testing needs to be conducted to confirm the specificity of VGB-displaying VLPs toward VEGFR, as briefly outlined in the discussion. In order to do so, a positive control needs to be employed to confirm the validity of the indirect ELISA assay. Additionally, insertion of scramble peptides within the DE loop and H4 helix region of the L1 protein needs to be conducted to eliminate the possibility of non-specific binding towards VEGFR. Upon confirmation and assessment of the binding affinity of VGB-displaying VLPs toward VEGFR, application toward

tumour cell lines specifically over-expressing VEGFR could also be completed to evaluate the anti-cancer enhancing ability of these VLPs in comparison to non-VGB-displaying VLPs. This could be assessed by the conduction of cell proliferation assays, in addition to assays evaluating the formation of blood vessels, including tube formation and collagen-cytodex angiogenesis assays, which were previously conducted using the VGB peptide (Sadremomtaz, Kobarfard, et al., 2018; Sadremomtaz, Mansouri, et al., 2018).

Upon characterization and evaluation of the VLPs within tumour cell models, investigation of the delivery of the DNA-VLP plasmids should be conducted to enhance L1 protein production and consequently, VLP formation within cells. Bacteriophages, which are bacterial viruses, have been studied extensively for their application as vectors for gene therapy, as their coat proteins are able to protect encapsulated genomes from degradation (Hosseinidoust, 2017). Additionally, they are also safe for human application considering they are present in many compartments of the human body (Huh et al., 2019). Other forms of targeted gene delivery systems could also be investigated to maximize the delivery and production of VLPs.

In future clinical applications of this treatment, trials within *in vivo* tumour animal models needs to be conducted to test for its safety and efficacy. Real-time visualization of blood vessels within the tumours of animal models upon treatment administration would enable validation of the anti-angiogenic ability of the VGB-displaying VLPs (Xing & Zhang, 2012).

References

Alhajj, M., & Farhana, A. (2022). Enzyme Linked Immunosorbent Assay. In *StatPearls*. StatPearls Publishing. http://www.ncbi.nlm.nih.gov/books/NBK555922/

Alitalo, K., & Carmeliet, P. (2002). Molecular mechanisms of lymphangiogenesis in health and disease. *Cancer Cell*, *1*(3), 219–227.

Almåsbak, H., Aarvak, T., & Vemuri, M. C. (2016). CAR T Cell Therapy: A Game Changer in Cancer Treatment. *Journal of Immunology Research*, *2016*, 5474602.

Amanna, I. J., & Slifka, M. K. (2010). Mechanisms that determine plasma cell lifespan and the duration of humoral immunity. *Immunological Reviews*, *236*(1), 125–138.

André, T., Shiu, K.-K., Kim, T. W., Jensen, B. V., Jensen, L. H., Punt, C., Smith, D., Garcia-Carbonero, R., Benavides, M., Gibbs, P., de la Fouchardiere, C., Rivera, F., Elez, E., Bendell, J., Le, D. T., Yoshino, T., Van Cutsem, E., Yang, P., Farooqui, M. Z. H., … Diaz, L. A. (2020). Pembrolizumab in Microsatellite-Instability–High Advanced Colorectal Cancer. *New England Journal of Medicine*, *383*(23), 2207–2218.

Ansorge, S., Lanthier, S., Transfiguracion, J., Durocher, Y., Henry, O., & Kamen, A. (2009). Development of a scalable process for high-yield lentiviral vector production by transient transfection of HEK293 suspension cultures. *The Journal of Gene Medicine*, *11*(10), 868–876.

Arevalo, M. T., Wong, T. M., & Ross, T. M. (2016). Expression and Purification of Virus-like Particles for Vaccination. *Journal of Visualized Experiments : JoVE*, *112*.

Aucoin, M. G., Perrier, M., & Kamen, A. A. (2006). Production of adeno-associated viral vectors in insect cells using triple infection: Optimization of baculovirus concentration ratios. *Biotechnology and Bioengineering*, *95*(6), 1081–1092.

Balkwill, F. R., Capasso, M., & Hagemann, T. (2012). The tumor microenvironment at a glance. *Journal of Cell Science*, *125*(23), 5591–5596. https://doi.org/10.1242/jcs.116392

Barbosa, M. A. G., Xavier, C. P. R., Pereira, R. F., Petrikaitė, V., & Vasconcelos, M. H. (2021). 3D Cell Culture Models as Recapitulators of the Tumor Microenvironment for the Screening of Anti-Cancer Drugs. *Cancers*, *14*(1), 190.

Bates, D. O., Cui, T.-G., Doughty, J. M., Winkler, M., Sugiono, M., Shields, J. D., Peat, D., Gillatt, D., & Harper, S. J. (2002). VEGF165b, an inhibitory splice variant of vascular endothelial growth factor, is down-regulated in renal cell carcinoma. *Cancer Research*, *62*(14), 4123–4131.

Begum, A. A., Toth, I., Hussein, W. M., & Moyle, P. M. (2019). Advances in Targeted Gene Delivery. *Current Drug Delivery*, *16*(7), 588–608.

Belardelli, F., & Gresser, I. (1996). The neglected role of type I interferon in the T-cell response: Implications for its clinical use. *Immunology Today*, *17*(8), 369–372.

Bellone, S., El-Sahwi, K., Cocco, E., Casagrande, F., Cargnelutti, M., Palmieri, M., Bignotti, E., Romani, C., Silasi, D.-A., Azodi, M., Schwartz, P. E., Rutherford, T. J., Pecorelli, S., & Santin, A. D. (2009). Human papillomavirus type 16 (HPV-16) virus-like particle L1-specific CD8+ cytotoxic T lymphocytes (CTLs) are equally effective as E7-specific CD8+ CTLs in killing autologous HPV-16-positive tumor cells in cervical cancer patients: Implications for L1 dendritic cell-based therapeutic vaccines. *Journal of Virology*, *83*(13), 6779–6789.

Bird, S. W., & Kirkegaard, K. (2015). Escape of non-enveloped virus from intact cells. *Virology*, *0*, 444–449.

Blancett, C. D., Monninger, M. K., Nguessan, C. A., Kuehl, K. A., Rossi, C. A., Olschner, S. P., Williams, P. L., Goodman, S. L., & Sun, M. G. (2017). Utilization of Capsules for Negative Staining of Viral Samples within Biocontainment. *Journal of Visualized Experiments : JoVE*, *125*, 56122.

Boehme, K. W., & Compton, T. (2004). Innate Sensing of Viruses by Toll-Like Receptors. *Journal of Virology*, *78*(15), 7867–7873.

Bolli, E., O'Rourke, J. P., Conti, L., Lanzardo, S., Rolih, V., Christen, J. M., Barutello, G., Forni, M., Pericle, F., & Cavallo, F. (2017). A Virus-Like-Particle immunotherapy targeting Epitope-Specific anti-xCT expressed on cancer stem cell inhibits the progression of metastatic cancer in vivo. *Oncoimmunology*, *7*(3).

Bolt, M. W., & Mahoney, P. A. (1997). High-efficiency blotting of proteins of diverse sizes following sodium dodecyl sulfate-polyacrylamide gel electrophoresis. *Analytical biochemistry*, *247*(2), 185–192.

Bonilla, F. A., & Oettgen, H. C. (2010). Adaptive immunity. *Journal of Allergy and Clinical Immunology*, *125*(2), S33–S40.

Boxus, M., Fochesato, M., Miseur, A., Mertens, E., Dendouga, N., Brendle, S., Balogh, K. K., Christensen, N. D., & Giannini, S. L. (2016). Broad Cross-Protection Is Induced in Preclinical Models by a Human Papillomavirus Vaccine Composed of L1/L2 Chimeric Virus-Like Particles. *Journal of Virology*, *90*(14), 6314–6325.

Brenner, D. R., Poirier, A., Woods, R. R., Ellison, L. F., Billette, J.-M., Demers, A. A., Zhang, S. X., Yao, C., Finley, C., Fitzgerald, N., Saint-Jacques, N., Shack, L., Turner, D., & Holmes, E. (2022). Projected estimates of cancer in Canada in 2022. *CMAJ : Canadian Medical Association Journal*, *194*(17), E601–E607.

Brenner, S., & Horne, R. W. (1959). A negative staining method for high resolution electron microscopy of viruses. *Biochimica et Biophysica Acta*, *34*, 103–110.

Brisse, M., Vrba, S. M., Kirk, N., Liang, Y., & Ly, H. (2020). Emerging Concepts and Technologies in Vaccine Development. *Frontiers in Immunology*, *11*.

Brown, L. F., Berse, B., Jackman, R. W., Tognazzi, K., Manseau, E. J., Senger, D. R., & Dvorak, H. F. (1993). Expression of Vascular Permeability Factor (Vascular Endothelial Growth Factor) and Its Receptors in Adenocarcinomas of the Gastrointestinal Tract. *Cancer Research*, *53*(19), 4727–4735.

Brunel, F. M., Lewis, J. D., Destito, G., Steinmetz, N. F., Manchester, M., Stuhlmann, H., & Dawson, P. E. (2010). Hydrazone ligation strategy to assemble multifunctional viral nanoparticles for cell imaging and tumor targeting. *Nano Letters*, *10*(3), 1093–1097.

Buck, C. B., Day, P. M., & Trus, B. L. (2013). The Papillomavirus Major Capsid Protein L1. *Virology*, *445*(0), 169–174.

Buck, C. B., Pastrana, D. V., Lowy, D. R., & Schiller, J. T. (2005). Generation of HPV pseudovirions using transfection and their use in neutralization assays. *Methods in Molecular Medicine*, *119*, 445–462.

Buijs, P. R., Verhagen, J. H., van Eijck, C. H., & van den Hoogen, B. G. (2015). Oncolytic viruses: From bench to bedside with a focus on safety. *Human Vaccines & Immunotherapeutics*, *11*(7), 1573–1584.

Buonaguro, L., Tagliamonte, M., Tornesello, M. L., & Buonaguro, F. M. (2011). Developments in virus-like particle-based vaccines for infectious diseases and cancer. *Expert Review of Vaccines*, *10*(11), 1569–1583.

Burd, E. M., & Dean, C. L. (2016). Human Papillomavirus. *Microbiology Spectrum*, *4*(4).

Caldeira, J. C., Perrine, M., Pericle, F., & Cavallo, F. (2020). Virus-Like Particles as an Immunogenic Platform for Cancer Vaccines. *Viruses*, *12*(5).

Campoli, M., & Ferrone, S. (2008). HLA antigen changes in malignant cells: Epigenetic mechanisms and biologic significance. *Oncogene*, *27*(45), 5869–5885.

Carpenter, R. O., Evbuomwan, M. O., Pittaluga, S., Rose, J. J., Raffeld, M., Yang, S., Gress, R. E., Hakim, F. T., & Kochenderfer, J. N. (2013). B-cell Maturation Antigen is a Promising Target for Adoptive T-cell Therapy of Multiple Myeloma. *Clinical Cancer Research : An Official Journal of the American Association for Cancer Research*, *19*(8), 2048–2060.

Carretero, R., Sektioglu, I. M., Garbi, N., Salgado, O. C., Beckhove, P., & Hämmerling, G. J. (2015). Eosinophils orchestrate cancer rejection by normalizing tumor vessels and enhancing infiltration of CD8 + T cells. *Nature Immunology*, *16*(6), Article 6.

Carter, J. J., Wipf, G. C., Benki, S. F., Christensen, N. D., & Galloway, D. A. (2003). Identification of a Human Papillomavirus Type 16-Specific Epitope on the C-Terminal Arm of the Major Capsid Protein L1. *Journal of Virology*, *77*(21), 11625–11632.

Cercek, A., Lumish, M., Sinopoli, J., Weiss, J., Shia, J., Lamendola-Essel, M., El Dika, I. H., Segal, N., Shcherba, M., Sugarman, R., Stadler, Z., Yaeger, R., Smith, J. J., Rousseau, B., Argiles, G., Patel, M., Desai, A., Saltz, L. B., Widmar, M., … Diaz, L. A. (2022). PD-1 Blockade in Mismatch Repair-Deficient, Locally Advanced Rectal Cancer. *The New England Journal of Medicine*, *386*(25), 2363–2376.

Cerqueira, C., & Schiller, J. T. (2017). Papillomavirus assembly: An overview and perspectives. *Virus Research*, *231*, 103–107.

Chabeda, A., van Zyl, A. R., Rybicki, E. P., & Hitzeroth, I. I. (2019). Substitution of Human Papillomavirus Type 16 L2 Neutralizing Epitopes Into L1 Surface Loops: The Effect on Virus-Like Particle Assembly and Immunogenicity. *Frontiers in Plant Science*, *10*.

Chackerian, B., Durfee, M. R., & Schiller, J. T. (2008). Virus-Like Display of a Neo-Self Antigen Reverses B Cell Anergy in a B Cell Receptor Transgenic Mouse Model. *Journal of Immunology (Baltimore, Md. : 1950)*, *180*(9), 5816–5825.

Chakraborty, S., & Rahman, T. (2012). The difficulties in cancer treatment. *Ecancermedicalscience*, *6*.

Chen, X., Du, Y., Hu, Q., & Huang, Z. (2017). Tumor-derived CD4+CD25+regulatory T cells inhibit dendritic cells function by CTLA-4. *Pathology, Research and Practice*, *213*(3), 245–249.

Chen, X., Liu, H., Wang, Z., Wang, S., Zhang, T., Hu, M., Qiao, L., & Xu, X. (2017). Human papillomavirus 16L1-58L2 chimeric virus-like particles elicit durable neutralizing antibody responses against a broad-spectrum of human papillomavirus types. *Oncotarget*, *8*(38), 63333–63344.

Chen, X., Zhang, T., Liu, H., Hao, Y., Liao, G., & Xu, X. (2018). Displaying 31RG-1 peptide on the surface of HPV16 L1 by use of a human papillomavirus chimeric virus-like particle induces cross-neutralizing antibody responses in mice. *Human Vaccines & Immunotherapeutics*, *14*(8), 2025–2033.

Chidambaram, M., Manavalan, R., & Kathiresan, K. (2011). Nanotherapeutics to Overcome Conventional Cancer Chemotherapy Limitations. *Journal of Pharmacy & Pharmaceutical Sciences*, *14*(1), Article 1.

Chmielewski, M., Hombach, A. A., & Abken, H. (2013). Antigen-Specific T-Cell Activation Independently of the MHC: Chimeric Antigen Receptor-Redirected T Cells. *Frontiers in Immunology*, *4*.

Chowell, D., Morris, L. G. T., Grigg, C. M., Weber, J. K., Samstein, R. M., Makarov, V., Kuo, F., Kendall, S. M., Requena, D., Riaz, N., Greenbaum, B., Carroll, J., Garon, E., Hyman, D. M., Zehir, A., Solit, D., Berger, M., Zhou, R., Rizvi, N. A., & Chan, T. A. (2018). Patient HLA class I genotype influences cancer response to checkpoint blockade immunotherapy. *Science (New York, N.Y.)*, *359*(6375), 582–587.

Christensen, N. D., Dillner, J., Eklund, C., Carter, J. J., Wipf, G. C., Reed, C. A., Cladel, N. M., & Galloway, D. A. (1996). Surface Conformational and Linear Epitopes on HPV-16 and HPV-18 L1 Virus-like Particles as Defined by Monoclonal Antibodies. *Virology*, *223*(1), 174–184.

Combita, A.-L., Touzé, A., Bousarghin, L., Christensen, N. D., & Coursaget, P. (2002). Identification of Two Cross-Neutralizing Linear Epitopes within the L1 Major Capsid Protein of Human Papillomaviruses. *Journal of Virology*, *76*(13), 6480–6486.

Compton, T., Kurt-Jones, E. A., Boehme, K. W., Belko, J., Latz, E., Golenbock, D. T., & Finberg, R. W. (2003). Human Cytomegalovirus Activates Inflammatory Cytokine Responses via CD14 and Toll-Like Receptor 2. *Journal of Virology*, *77*(8), 4588–4596.

Costache, M. I., Ioana, M., Iordache, S., Ene, D., Costache, C. A., & Săftoiu, A. (2015). VEGF Expression in Pancreatic Cancer and Other Malignancies: A Review of the Literature. *Romanian Journal of Internal Medicine = Revue Roumaine De Medecine Interne*, *53*(3), 199–208.

Crisci, E., Bárcena, J., & Montoya, M. (2012). Virus-like particles: The new frontier of vaccines for animal viral infections. *Veterinary Immunology and Immunopathology*, *148*(3), 211–225.

Cross, D., & Burmester, J. K. (2006). Gene Therapy for Cancer Treatment: Past, Present and Future. *Clinical Medicine and Research*, *4*(3), 218–227.

Cruz, L., Biryukov, J., Conway, M. J., & Meyers, C. (2015). Cleavage of the HPV16 Minor Capsid Protein L2 during Virion Morphogenesis Ablates the Requirement for Cellular Furin during De Novo Infection. *Viruses*, *7*(11), 5813–5830.

Cubas, R., Zhang, S., Li, M., Chen, C., & Yao, Q. (2011). Chimeric Trop2 virus-like particles: A potential immunotherapeutic approach against pancreatic cancer. *Journal of Immunotherapy (Hagerstown, Md.: 1997)*, *34*(3), 251–263.

Dai, S., Wang, H., & Deng, F. (2018). Advances and challenges in enveloped virus-like particle (VLP)-based vaccines. *Journal of Immunological Sciences*, *2*(2).

Das, S. K., Menezes, M. E., Bhatia, S., Wang, X.-Y., Emdad, L., Sarkar, D., & Fisher, P. B. (2015). Gene Therapies for Cancer: Strategies, Challenges and Successes. *Journal of Cellular Physiology*, *230*(2), 259–271.

De Bock, K., Cauwenberghs, S., & Carmeliet, P. (2011). Vessel abnormalization: Another hallmark of cancer?: Molecular mechanisms and therapeutic implications. *Current Opinion in Genetics & Development*, *21*(1), 73–79.

De Falco, S., Gigante, B., & Persico, M. G. (2002). Structure and function of placental growth factor. *Trends in Cardiovascular Medicine*, *12*(6), 241–246.

de Lima Farah, J., Sano, R., Maugéri, I. M. L., Teixeira, D., Ishimura, M. E., Martins, G., Mimica, L. M. J., da Silva, C. B., Meyer, C. H., de Oliveira Dias, J. R., de Andrade, G.

C., & Farah, M. E. (2018). Evaluation of aflibercept and ziv-aflibercept binding affinity to vascular endothelial growth factor, stability and sterility after compounding. *International Journal of Retina and Vitreous*, *4*.

Deeks, E. D. (2016). Pembrolizumab: A Review in Advanced Melanoma. *Drugs*, *76*(3), 375–386.

Dehghanian, F., Hojati, Z., & Kay, M. (2014). New Insights into VEGF-A Alternative Splicing: Key Regulatory Switching in the Pathological Process. *Avicenna Journal of Medical Biotechnology*, *6*(4), 192–199.

Deng, X., Storz, U., & Doranz, B. J. (2018). Enhancing antibody patent protection using epitope mapping information. *MAbs*, *10*(2), 204–209.

Des Guetz, G., Uzzan, B., Nicolas, P., Cucherat, M., Morere, J.-F., Benamouzig, R., Breau, J.-L., & Perret, G.-Y. (2006). Microvessel density and VEGF expression are prognostic factors in colorectal cancer. Meta-analysis of the literature. *British Journal of Cancer*, *94*(12), 1823–1832.

DiGiuseppe, S., Bienkowska-Haba, M., Guion, L. G. M., Keiffer, T. R., & Sapp, M. (2017). Human Papillomavirus Major Capsid Protein L1 Remains Associated with the Incoming Viral Genome throughout the Entry Process. *Journal of Virology*, *91*(16), e00537-17.

Donaldson, B., Lateef, Z., Walker, G. F., Young, S. L., & Ward, V. K. (2018). Virus-like particle vaccines: Immunology and formulation for clinical translation. *Expert Review of Vaccines*, *17*(9), 833–849.

Doorbar, J., Ely, S., Sterling, J., McLean, C., & Crawford, L. (1991). Specific interaction between HPV-16 E1-E4 and cytokeratins results in collapse of the epithelial cell intermediate filament network. *Nature*, *352*(6338), 824–827.

Du, Z., & Lovly, C. M. (2018). Mechanisms of receptor tyrosine kinase activation in cancer. *Molecular Cancer*, *17*(1), 58.

DuBridge, R. B., Tang, P., Hsia, H. C., Leong, P. M., Miller, J. H., & Calos, M. P. (1987). Analysis of mutation in human cells by using an Epstein-Barr virus shuttle system. *Molecular and Cellular Biology*, *7*(1), 379–387.

Duffy, A. M., Bouchier-Hayes, D. J., & Harmey, J. H. (2013). Vascular Endothelial Growth Factor (VEGF) and Its Role in Non-Endothelial Cells: Autocrine Signalling by VEGF. In *Madame Curie Bioscience Database [Internet]*. Landes Bioscience.

Dzopalic, T., Rajkovic, I., Dragicevic, A., & Colic, M. (2012). The response of human dendritic cells to co-ligation of pattern-recognition receptors. *Immunologic Research*, *52*(1–2), 20–33.

Ellyard, J. I., Simson, L., & Parish, C. R. (2007). Th2-mediated anti-tumour immunity: Friend or foe? *Tissue Antigens*, *70*(1), 1–11.

Eruslanov, E. B., Bhojnagarwala, P. S., Quatromoni, J. G., Stephen, T. L., Ranganathan, A., Deshpande, C., Akimova, T., Vachani, A., Litzky, L., Hancock, W. W., Conejo-Garcia, J. R., Feldman, M., Albelda, S. M., & Singhal, S. (2014). Tumor-associated neutrophils stimulate T cell responses in early-stage human lung cancer. *The Journal of Clinical Investigation*, *124*(12), 5466–5480.

Esfahani, K., Roudaia, L., Buhlaiga, N., Del Rincon, S. V., Papneja, N., & Miller, W. H. (2020). A review of cancer immunotherapy: From the past, to the present, to the future. *Current Oncology*, *27*(Suppl 2), S87–S97.

Evers, T. H., van Dongen, E. M. W. M., Faesen, A. C., Meijer, E. W., & Merkx, M. (2006). Quantitative understanding of the energy transfer between fluorescent proteins connected via flexible peptide linkers. *Biochemistry*, *45*(44), 13183–13192.

Fan, J., Feng, Y., Tao, Z., Chen, J., Yang, H., Shi, Q., Li, Z., She, T., Li, H., Jin, Y., Cheng, J., & Lu, X. (2021). A versatile platform for the tumor-targeted delivery of immune checkpoint-blocking immunoglobin G. *Journal of Controlled Release*, *340*, 243–258.

Farhood, B., Najafi, M., & Mortezaee, K. (2019). CD8+ cytotoxic T lymphocytes in cancer immunotherapy: A review. *Journal of Cellular Physiology*, *234*(6), 8509–8521.

Farlow, M. R., Andreasen, N., Riviere, M.-E., Vostiar, I., Vitaliti, A., Sovago, J., Caputo, A., Winblad, B., & Graf, A. (2015). Long-term treatment with active Aβ immunotherapy with CAD106 in mild Alzheimer's disease. *Alzheimer's Research & Therapy*, *7*(1), 23.

Farzaneh Behelgardi, M., Zahri, S., Gholami Shahvir, Z., Mashayekhi, F., Mirzanejad, L., & Asghari, S. M. (2020). Targeting signaling pathways of VEGFR1 and VEGFR2 as a potential target in the treatment of breast cancer. *Molecular Biology Reports*, *47*(3), 2061–2071.

Fendly, B. M., Kotts, C., Vetterlein, D., Lewis, G. D., Winget, M., Carver, M. E., Watson, S. R., Sarup, J., Saks, S., & Ullrich, A. (1990). The extracellular domain of HER2/neu is a potential immunogen for active specific immunotherapy of breast cancer. *Journal of Biological Response Modifiers*, *9*(5), 449–455.

Ferrara, N., Gerber, H.-P., & LeCouter, J. (2003). The biology of VEGF and its receptors. *Nature Medicine*, *9*(6), 669–676.

Ferreira, A. R., Ramalho, A. C., Marques, M., & Ribeiro, D. (2020). The Interplay between Antiviral Signalling and Carcinogenesis in Human Papillomavirus Infections. *Cancers*, *12*(3), Article 3.

Ferrone, C., & Dranoff, G. (2010). Dual Roles for Immunity in Gastrointestinal Cancers. *Journal of Clinical Oncology*, *28*(26), 4045–4051.

Fiebiger, E., Meraner, P., Weber, E., Fang, I. F., Stingl, G., Ploegh, H., & Maurer, D. (2001). Cytokines regulate proteolysis in major histocompatibility complex class II-dependent antigen presentation by dendritic cells. *The Journal of Experimental Medicine*, *193*(8), 881–892.

Foekens, J. A., Peters, H. A., Grebenchtchikov, N., Look, M. P., Meijer-van Gelder, M. E., Geurts-Moespot, A., van der Kwast, T. H., Sweep, C. G., & Klijn, J. G. (2001). High tumor levels of vascular endothelial growth factor predict poor response to systemic therapy in advanced breast cancer. *Cancer Research*, *61*(14), 5407–5414.

Folkman, J. (2002). Role of angiogenesis in tumor growth and metastasis. *Seminars in Oncology*, *29*(6, Supplement 16), 15–18.

Fong, G. H., Rossant, J., Gertsenstein, M., & Breitman, M. L. (1995). Role of the Flt-1 receptor tyrosine kinase in regulating the assembly of vascular endothelium. *Nature*, *376*(6535), 66–70.

Forsström, B., Bisławska Axnäs, B., Rockberg, J., Danielsson, H., Bohlin, A., & Uhlen, M. (2015). Dissecting Antibodies with Regards to Linear and Conformational Epitopes. *PLoS ONE*, *10*(3), e0121673.

Frank, S. A. (2002). Specificity and Cross-Reactivity. In *Immunology and Evolution of Infectious Disease*. Princeton University Press.

Frietze, K. M., Peabody, D. S., & Chackerian, B. (2016). Engineering virus-like particles as vaccine platforms. *Current Opinion in Virology*, *18*, 44–49.

Fuenmayor, J., Gòdia, F., & Cervera, L. (2017). Production of virus-like particles for vaccines. *New Biotechnology*, *39*(Pt B), 174–180.

Gallie, D. R. (1991). The cap and poly(A) tail function synergistically to regulate mRNA translational efficiency. *Genes & Development*, *5*(11), 2108–2116.

García-Foncillas, J., Sunakawa, Y., Aderka, D., Wainberg, Z., Ronga, P., Witzler, P., & Stintzing, S. (2019). Distinguishing Features of Cetuximab and Panitumumab in Colorectal Cancer and Other Solid Tumors. *Frontiers in Oncology*, *9*, 849.

García-Piñeres, A. J., Hildesheim, A., Dodd, L., Kemp, T. J., Yang, J., Fullmer, B., Harro, C., Lowy, D. R., Lempicki, R. A., & Pinto, L. A. (2009). Gene Expression Patterns Induced by HPV-16 L1 VLP in Leukocytes from Vaccine Recipients. *Journal of Immunology (Baltimore, Md. : 1950)*, *182*(3), 1706–1729.

Gardlík, R., Pálffy, R., Hodosy, J., Lukács, J., Turna, J., & Celec, P. (2005). Vectors and delivery systems in gene therapy. *Medical Science Monitor: International Medical Journal of Experimental and Clinical Research*, *11*(4), RA110-121.

Gias, E., Nielsen, S. U., Morgan, L. A. F., & Toms, G. L. (2008). Purification of human respiratory syncytial virus by ultracentrifugation in iodixanol density gradient. *Journal of Virological Methods*, *147*(2–2), 328–332.

Giatromanolaki, A., Koukourakis, M. I., Sivridis, E., Chlouverakis, G., Vourvouhaki, E., Turley, H., Harris, A. L., & Gatter, K. C. (2007). Activated VEGFR2/KDR pathway in tumour cells and tumour associated vessels of colorectal cancer. *European Journal of Clinical Investigation*, *37*(11), 878–886.

Gille, J., Heidenreich, R., Pinter, A., Schmitz, J., Boehme, B., Hicklin, D. J., Henschler, R., & Breier, G. (2007). Simultaneous blockade of VEGFR-1 and VEGFR-2 activation is necessary to efficiently inhibit experimental melanoma growth and metastasis formation. *International Journal of Cancer*, *120*(9), 1899–1908.

Goldinger, S. M., Dummer, R., Baumgaertner, P., Mihic-Probst, D., Schwarz, K., Hammann-Haenni, A., Willers, J., Geldhof, C., Prior, J. O., Kündig, T. M., Michielin, O., Bachmann, M. F., & Speiser, D. E. (2012). Nano-particle vaccination combined with TLR-7 and -9 ligands triggers memory and effector CD8+ T-cell responses in melanoma patients. *European Journal of Immunology*, *42*(11), 3049–3061.

Goldufsky, J., Sivendran, S., Harcharik, S., Pan, M., Bernardo, S., Stern, R. H., Friedlander, P., Ruby, C. E., Saenger, Y., & Kaufman, H. L. (2013). Oncolytic virus therapy for cancer. *Oncolytic Virotherapy*, *2*, 31–46.

Gong, B., Liang, D., Chew, T.-G., & Ge, R. (2004). Characterization of the zebrafish vascular endothelial growth factor A gene: Comparison with vegf-A genes in mammals and Fugu. *Biochimica Et Biophysica Acta*, *1676*(1), 33–40.

Gonzalez, H., Hagerling, C., & Werb, Z. (2018). Roles of the immune system in cancer: From tumor initiation to metastatic progression. *Genes & Development*, *32*(19–20), 1267–1284.

González-Domínguez, I., Puente-Massaguer, E., Cervera, L., & Gòdia, F. (2020). Quality Assessment of Virus-Like Particles at Single Particle Level: A Comparative Study. *Viruses*, *12*(2).

Gotink, K. J., & Verheul, H. M. W. (2010). Anti-angiogenic tyrosine kinase inhibitors: What is their mechanism of action? *Angiogenesis*, *13*(1), 1–14.

Gotwals, P., Cameron, S., Cipolletta, D., Cremasco, V., Crystal, A., Hewes, B., Mueller, B., Quaratino, S., Sabatos-Peyton, C., Petruzzelli, L., Engelman, J. A., & Dranoff, G. (2017). Prospects for combining targeted and conventional cancer therapy with immunotherapy. *Nature Reviews. Cancer*, *17*(5), 286–301.

Grgacic, E. V. L., & Anderson, D. A. (2006). Virus-like particles: Passport to immune recognition. *Methods (San Diego, Calif.)*, *40*(1), 60–65.

Grieger, J. C., Soltys, S. M., & Samulski, R. J. (2016). Production of Recombinant Adeno-associated Virus Vectors Using Suspension HEK293 Cells and Continuous Harvest of Vector From the Culture Media for GMP FIX and FLT1 Clinical Vector. *Molecular Therapy*, *24*(2), 287–297.

Grosse-Hovest, L., Hartlapp, I., Marwan, W., Brem, G., Rammensee, H.-G., & Jung, G. (2003). A recombinant bispecific single-chain antibody induces targeted, supra-agonistic CD28-stimulation and tumor cell killing. *European Journal of Immunology*, *33*(5), 1334–1340.

Guan, J., Bywaters, S. M., Brendle, S. A., Lee, H., Ashley, R. E., Christensen, N. D., & Hafenstein, S. (2015). The U4 Antibody Epitope on Human Papillomavirus 16 Identified by Cryo-electron Microscopy. *Journal of Virology*, *89*(23), 12108–12117.

Gulati, N. M., Torian, U., Gallagher, J. R., & Harris, A. K. (2019). Immunoelectron Microscopy of Viral Antigens. *Current Protocols in Microbiology*, *53*(1), e86.

Guo, C., Manjili, M. H., Subjeck, J. R., Sarkar, D., Fisher, P. B., & Wang, X.-Y. (2013). Therapeutic Cancer Vaccines: Past, Present and Future. *Advances in Cancer Research*, *119*, 421–475.

Guo, S., Colbert, L. S., Fuller, M., Zhang, Y., & Gonzalez-Perez, R. R. (2010). Vascular Endothelial Growth Factor Receptor -2 in Breast Cancer. *Biochimica et Biophysica Acta*, *1806*(1), 108–121.

Haabeth, O. A. W., Lorvik, K. B., Yagita, H., Bogen, B., & Corthay, A. (2015). Interleukin-1 is required for cancer eradication mediated by tumor-specific Th1 cells. *Oncoimmunology*, *5*(1).

Hagensee, M. E., Yaegashi, N., & Galloway, D. A. (1993). Self-assembly of human papillomavirus type 1 capsids by expression of the L1 protein alone or by coexpression of the L1 and L2 capsid proteins. *Journal of Virology*, *67*(1), 315–322.

Halford, Z., Anderson, M. K., Bennett, L. L., & Moody, J. (2021). Tisagenlecleucel in Acute Lymphoblastic Leukemia: A Review of the Literature and Practical Considerations. *Annals of Pharmacotherapy*, *55*(4), 466–479.

Harper, S. J., & Bates, D. O. (2008). VEGF-A splicing. *Nature Reviews. Cancer*, *8*(11), 880–887.

Harris, A. L. (1991). Growth factors and receptors in cancer. *Current Opinion in Biotechnology*, *2*(2), 260–268.

Hemminki, O., dos Santos, J. M., & Hemminki, A. (2020). Oncolytic viruses for cancer immunotherapy. *Journal of Hematology & Oncology*, *13*(1), 84.

Hermens, W. T., ter Brake, O., Dijkhuizen, P. A., Sonnemans, M. A., Grimm, D., Kleinschmidt, J. A., & Verhaagen, J. (1999). Purification of recombinant adeno-associated virus by iodixanol gradient ultracentrifugation allows rapid and reproducible preparation of vector stocks for gene transfer in the nervous system. *Human Gene Therapy*, *10*(11), 1885–1891.

Hicklin, D. J., & Ellis, L. M. (2005). Role of the Vascular Endothelial Growth Factor Pathway in Tumor Growth and Angiogenesis. *Journal of Clinical Oncology*, *23*(5), 1011–1027.

Hiratsuka, S., Maru, Y., Okada, A., Seiki, M., Noda, T., & Shibuya, M. (2001). Involvement of Flt-1 Tyrosine Kinase (Vascular Endothelial Growth Factor Receptor-1) in Pathological Angiogenesis. *Cancer Research*, *61*(3), 1207–1213.

Hitzeroth, I. I., Chabeda, A., Whitehead, M. P., Graf, M., & Rybicki, E. P. (2018). Optimizing a Human Papillomavirus Type 16 L1-Based Chimaeric Gene for Expression in Plants. *Frontiers in Bioengineering and Biotechnology*, *6*, 101.

Holash, J., Davis, S., Papadopoulos, N., Croll, S. D., Ho, L., Russell, M., Boland, P., Leidich, R., Hylton, D., Burova, E., Ioffe, E., Huang, T., Radziejewski, C., Bailey, K., Fandl, J. P., Daly, T., Wiegand, S. J., Yancopoulos, G. D., & Rudge, J. S. (2002). VEGF-Trap: A VEGF blocker with potent antitumor effects. *Proceedings of the National Academy of Sciences of the United States of America*, *99*(17), 11393–11398.

Holmes, D. I., & Zachary, I. (2005). The vascular endothelial growth factor (VEGF) family: Angiogenic factors in health and disease. *Genome Biology*, *6*(2), 209.

Holmgren, S. C., Patterson, N. A., Ozbun, M. A., & Lambert, P. F. (2005). The Minor Capsid Protein L2 Contributes to Two Steps in the Human Papillomavirus Type 31 Life Cycle. *Journal of Virology*, *79*(7), 3938–3948.

Holzer, B., Morgan, S. B., Matsuoka, Y., Edmans, M., Salguero, F. J., Everett, H., Brookes, S. M., Porter, E., MacLoughlin, R., Charleston, B., Subbarao, K., Townsend, A., & Tchilian, E. (2018). Comparison of Heterosubtypic Protection in Ferrets and Pigs Induced by a Single-Cycle Influenza Vaccine. *Journal of Immunology (Baltimore, Md.: 1950)*, *200*(12), 4068–4077.

Hosseinidoust, Z. (2017). Phage-Mediated Gene Therapy. *Current Gene Therapy*, *17*(2), 120–126.

Hsu, D. S., Kim, M. K., Balakumaran, B. S., Acharya, C. R., Anders, C. K., Clay, T., Lyerly, H. K., Drake, C. G., Morse, M. A., & Febbo, P. G. (2010). Immune Signatures Predict Prognosis in Localized Cancer. *Cancer Investigation*, *28*(7), 765–773.

Hu, J., Han, J., Li, H., Zhang, X., Liu, L. lan, Chen, F., & Zeng, B. (2018). Human Embryonic Kidney 293 Cells: A Vehicle for Biopharmaceutical Manufacturing, Structural Biology, and Electrophysiology. *Cells Tissues Organs*, *205*(1), 1–8.

Huber, B., Schellenbacher, C., Shafti-Keramat, S., Jindra, C., Christensen, N., & Kirnbauer, R. (2017). Chimeric L2-Based Virus-Like Particle (VLP) Vaccines Targeting Cutaneous Human Papillomaviruses (HPV). *PloS One*, *12*(1), e0169533.

Huh, H., Wong, S., St. Jean, J., & Slavcev, R. (2019). Bacteriophage interactions with mammalian tissue: Therapeutic applications. *Advanced Drug Delivery Reviews*, *145*, 4–17.

Humans, I. W. G. on the E. of C. R. to. (2007). Human Papillomavirus (HPV) Infection. In *Human Papillomaviruses*. International Agency for Research on Cancer.

Jain, K., Salamat-Miller, N., & Taylor, K. (2021). Freeze–thaw characterization process to minimize aggregation and enable drug product manufacturing of protein based therapeutics. *Scientific Reports*, *11*(1), Article 1.

Janeway, C. A. (2001). How the immune system works to protect the host from infection: A personal view. *Proceedings of the National Academy of Sciences*, *98*(13), 7461–7468.

Jarnicki, A. G., Lysaght, J., Todryk, S., & Mills, K. H. G. (2006). Suppression of Antitumor Immunity by IL-10 and TGF-β-Producing T Cells Infiltrating the Growing Tumor:

Influence of Tumor Environment on the Induction of CD4+ and CD8+ Regulatory T Cells. *The Journal of Immunology*, *177*(2), 896–904.

Javle, M., Smyth, E. C., & Chau, I. (2014). Ramucirumab: Successfully Targeting Angiogenesis in Gastric Cancer. *Clinical Cancer Research : An Official Journal of the American Association for Cancer Research*, *20*(23), 5875–5881.

Jegerlehner, A., Storni, T., Lipowsky, G., Schmid, M., Pumpens, P., & Bachmann, M. F. (2002). Regulation of IgG antibody responses by epitope density and CD21-mediated costimulation. *European Journal of Immunology*, *32*(11), 3305–3314.

Jentschke, M., Kampers, J., Becker, J., Sibbertsen, P., & Hillemanns, P. (2020). Prophylactic HPV vaccination after conization: A systematic review and meta-analysis. *Vaccine*, *38*(41), 6402–6409.

Jiang, S.-S., Tang, Y., Zhang, Y.-J., Weng, D.-S., Zhou, Z.-G., Pan, K., Pan, Q.-Z., Wang, Q.-J., Liu, Q., He, J., Zhao, J.-J., Li, J., Chen, M.-S., Chang, A. E., Li, Q., & Xia, J.-C. (2015). A phase I clinical trial utilizing autologous tumor-infiltrating lymphocytes in patients with primary hepatocellular carcinoma. *Oncotarget*, *6*(38), 41339–41349.

Jochmus, I., Schäfer, K., Faath, S., Müller, M., & Gissmann, L. (1999). Chimeric virus-like particles of the human papillomavirus type 16 (HPV 16) as a prophylactic and therapeutic vaccine. *Archives of Medical Research*, *30*(4), 269–274.

Kaltgrad, E., O'Reilly, M. K., Liao, L., Han, S., Paulson, J. C., & Finn, M. G. (2008). On-Virus Construction of Polyvalent Glycan Ligands for Cell-Surface Receptors. *Journal of the American Chemical Society*, *130*(14), 4578–4579.

Kaufmann, A. M., Nieland, J. D., Jochmus, I., Baur, S., Friese, K., Gabelsberger, J., Gieseking, F., Gissmann, L., Glasschröder, B., Grubert, T., Hillemanns, P., Höpfl, R., Ikenberg, H.,

Schwarz, J., Karrasch, M., Knoll, A., Küppers, V., Lechmann, M., Lelle, R. J., … Schneider, A. (2007). Vaccination trial with HPV16 L1E7 chimeric virus-like particles in women suffering from high grade cervical intraepithelial neoplasia (CIN 2/3). *International Journal of Cancer*, *121*(12), 2794–2800.

Kawamura, H., Li, X., Harper, S. J., Bates, D. O., & Claesson-Welsh, L. (2008). Vascular endothelial growth factor (VEGF)-A165b is a weak in vitro agonist for VEGF receptor-2 due to lack of coreceptor binding and deficient regulation of kinase activity. *Cancer Research*, *68*(12), 4683–4692.

Kershaw, M. H., Westwood, J. A., & Darcy, P. K. (2013). Gene-engineered T cells for cancer therapy. *Nature Reviews. Cancer*, *13*(8), 525–541. https://doi.org/10.1038/nrc3565

Khawar, I. A., Kim, J. H., & Kuh, H.-J. (2015). Improving drug delivery to solid tumors: Priming the tumor microenvironment. *Journal of Controlled Release*, *201*, 78–89.

Kieran, M. W., Kalluri, R., & Cho, Y.-J. (2012). The VEGF Pathway in Cancer and Disease: Responses, Resistance, and the Path Forward. *Cold Spring Harbor Perspectives in Medicine*, *2*(12).

Kikuchi, T. (2006). Genetically modified dendritic cells for therapeutic immunity. *The Tohoku Journal of Experimental Medicine*, *208*(1), 1–8.

Kim, H. J., Kim, S. Y., Lim, S. J., Kim, J. Y., Lee, S. J., & Kim, H.-J. (2010). One-step chromatographic purification of human papillomavirus type 16 L1 protein from Saccharomyces cerevisiae. *Protein Expression and Purification*, *70*(1), 68–74.

Kim, H.-J., & Cantor, H. (2014). CD4 T-cell subsets and tumor immunity: The helpful and the not-so-helpful. *Cancer Immunology Research*, *2*(2), 91–98.

Kim, J.-H., Kim, B. S., & Lee, S.-K. (2020). Regulatory T Cells in Tumor Microenvironment and Approach for Anticancer Immunotherapy. *Immune Network, 20*(1).

Kim, K.-H., Kwon, Y.-M., Lee, Y.-T., Kim, M.-C., Hwang, H. S., Ko, E.-J., Lee, Y., Choi, H.-J., & Kang, S.-M. (2018). Virus-Like Particles Are a Superior Platform for Presenting M2e Epitopes to Prime Humoral and Cellular Immunity against Influenza Virus. *Vaccines*, *6*(4).

Kingston, N. J., Kurtovic, L., Walsh, R., Joe, C., Lovrecz, G., Locarnini, S., Beeson, J. G., & Netter, H. J. (2019). Hepatitis B virus-like particles expressing Plasmodium falciparum epitopes induce complement-fixing antibodies against the circumsporozoite protein. *Vaccine*, *37*(12), 1674–1684.

Kirnbauer, R., Booy, F., Cheng, N., Lowy, D. R., & Schiller, J. T. (1992). Papillomavirus L1 major capsid protein self-assembles into virus-like particles that are highly immunogenic. *Proceedings of the National Academy of Sciences of the United States of America*, *89*(24), 12180–12184.

Klug, F., Prakash, H., Huber, P. E., Seibel, T., Bender, N., Halama, N., Pfirschke, C., Voss, R. H., Timke, C., Umansky, L., Klapproth, K., Schäkel, K., Garbi, N., Jäger, D., Weitz, J., Schmitz-Winnenthal, H., Hämmerling, G. J., & Beckhove, P. (2013). Low-Dose Irradiation Programs Macrophage Differentiation to an iNOS+/M1 Phenotype that Orchestrates Effective T Cell Immunotherapy. *Cancer Cell*, *24*(5), 589–602.

Koch, S., & Claesson-Welsh, L. (2012). Signal Transduction by Vascular Endothelial Growth Factor Receptors. *Cold Spring Harbor Perspectives in Medicine*, *2*(7).

Kondo, K., Ochi, H., Matsumoto, T., Yoshikawa, H., & Kanda, T. (2008). Modification of human papillomavirus-like particle vaccine by insertion of the cross-reactive L2-epitopes. *Journal of Medical Virology*, *80*(5), 841–846.

Koury, J., Lucero, M., Cato, C., Chang, L., Geiger, J., Henry, D., Hernandez, J., Hung, F., Kaur, P., Teskey, G., & Tran, A. (2018). Immunotherapies: Exploiting the Immune System for Cancer Treatment. *Journal of Immunology Research*, *2018*, e9585614.

Kowalczyk, D. W., Wysocki, P. J., & Mackiewicz, A. (2003). Cancer immunotherapy using cells modified with cytokine genes. *Acta Biochimica Polonica*, *50*(3), 613–624.

Labani-Motlagh, A., Ashja-Mahdavi, M., & Loskog, A. (2020). The Tumor Microenvironment: A Milieu Hindering and Obstructing Antitumor Immune Responses. *Frontiers in Immunology*, *11*.

Lanier, L. L. (2008). Evolutionary struggles between NK cells and viruses. *Nature Reviews. Immunology*, *8*(4), 259–268.

Leavitt, A. D., Roberts, T. M., & Garcea, R. L. (1985). Polyoma virus major capsid protein, VP1. Purification after high level expression in Escherichia coli. *The Journal of Biological Chemistry*, *260*(23), 12803–12809.

Leder, C., Kleinschmidt, J. A., Wiethe, C., & Müller, M. (2001). Enhancement of Capsid Gene Expression: Preparing the Human Papillomavirus Type 16 Major Structural Gene L1 for DNA Vaccination Purposes. *Journal of Virology*, *75*(19), 9201–9209.

Lee, H. L., Jang, J. W., Lee, S. W., Yoo, S. H., Kwon, J. H., Nam, S. W., Bae, S. H., Choi, J. Y., Han, N. I., & Yoon, S. K. (2019). Inflammatory cytokines and change of Th1/Th2 balance as prognostic indicators for hepatocellular carcinoma in patients treated with transarterial chemoembolization. *Scientific Reports*, *9*(1), Article 1.

Lee, S., & Margolin, K. (2012). Tumor-infiltrating lymphocytes in melanoma. *Current Oncology Reports*, *14*(5), 468–474.

Leitner, W. W., Ying, H., & Restifo, N. P. (1999). DNA and RNA-based vaccines: Principles, progress and prospects. *Vaccine*, *18*(9–10), 765–777.

Lenz, P., Lowy, D. R., & Schiller, J. T. (2005). Papillomavirus virus-like particles induce cytokines characteristic of innate immune responses in plasmacytoid dendritic cells. *European Journal of Immunology*, *35*(5), 1548–1556.

Li, M., Bharadwaj, U., Zhang, R., Zhang, S., Mu, H., Fisher, W. E., Brunicardi, F. C., Chen, C., & Yao, Q. (2008). Mesothelin is a malignant factor and therapeutic vaccine target for pancreatic cancer. *Molecular Cancer Therapeutics*, *7*(2), 286–296.

Lin, Y.-L., Hu, Y.-C., Liang, C.-C., Lin, S.-Y., Liang, Y.-C., Yuan, H.-P., & Chiang, B.-L. (2014). Enterovirus-71 Virus-Like Particles Induce the Activation and Maturation of Human Monocyte-Derived Dendritic Cells through TLR4 Signaling. *PLOS ONE*, *9*(10), e111496.

Lipson, E. J., & Drake, C. G. (2011). Ipilimumab: An Anti-CTLA-4 Antibody for Metastatic Melanoma. *Clinical Cancer Research : An Official Journal of the American Association for Cancer Research*, *17*(22), 6958–6962.

Liu, M. A., & Ulmer, J. B. (2000). Gene-Based Vaccines. *Molecular Therapy*, *1*(6), 497–500.

Liu, M., & Guo, F. (2018). Recent updates on cancer immunotherapy. *Precision Clinical Medicine*, *1*(2), 65–74.

Liu, W. J., Liu, X. S., Zhao, K. N., Leggatt, G. R., & Frazer, I. H. (2000). Papillomavirus Virus-like Particles for the Delivery of Multiple Cytotoxic T Cell Epitopes. *Virology*, *273*(2), 374–382.

Liu, Y., Chen, X., Han, W., & Zhang, Y. (2017). Tisagenlecleucel, an approved anti-CD19 chimeric antigen receptor T-cell therapy for the treatment of leukemia. *Drugs of Today (Barcelona, Spain: 1998)*, *53*(11), 597–608.

Liu, Y., & Zeng, G. (2012). Cancer and Innate Immune System Interactions: Translational Potentials for Cancer Immunotherapy. *Journal of Immunotherapy (Hagerstown, Md. : 1997)*, *35*(4), 299–308.

Lizotte, P. H., Wen, A. M., Sheen, M. R., Fields, J., Rojanasopondist, P., Steinmetz, N. F., & Fiering, S. (2016). In situ vaccination with cowpea mosaic virus nanoparticles suppresses metastatic cancer. *Nature Nanotechnology*, *11*(3), Article 3.

Locke, F. L., Miklos, D. B., Jacobson, C. A., Perales, M.-A., Kersten, M.-J., Oluwole, O. O., Ghobadi, A., Rapoport, A. P., McGuirk, J., Pagel, J. M., Muñoz, J., Farooq, U., van Meerten, T., Reagan, P. M., Sureda, A., Flinn, I. W., Vandenberghe, P., Song, K. W., Dickinson, M., … Westin, J. R. (2022). Axicabtagene Ciloleucel as Second-Line Therapy for Large B-Cell Lymphoma. *New England Journal of Medicine*, *386*(7), 640–654.

Lucocq, J. (2008). Quantification of structures and gold labeling in transmission electron microscopy. *Methods in Cell Biology*, *88*, 59–82.

Maher, J., & Davies, E. T. (2004). Targeting cytotoxic T lymphocytes for cancer immunotherapy. *British Journal of Cancer*, *91*(5), 817–821.

Mahmood, T., & Yang, P.-C. (2012). Western Blot: Technique, Theory, and Trouble Shooting. *North American Journal of Medical Sciences*, *4*(9), 429–434.

Maione, F., & Giraudo, E. (2015). Tumor Angiogenesis: Methods to Analyze Tumor Vasculature and Vessel Normalization in Mouse Models of Cancer. In R. Eferl & E. Casanova (Eds.), *Mouse Models of Cancer: Methods and Protocols* (pp. 349–365). Springer.

Markel, G., Cohen-Sinai, T., Besser, M. J., Oved, K., Itzhaki, O., Seidman, R., Treves, A. J., Fridman, E., Keisari, Y., Dotan, Z., Ramon, J., & Schachter, J. (2009). Preclinical Evaluation of Adoptive Cell Therapy for Patients with Metastatic Renal Cell Carcinoma. *Anticancer Research*, *29*(1), 145–154.

Martínez-Lostao, L., Anel, A., & Pardo, J. (2015). How Do Cytotoxic Lymphocytes Kill Cancer Cells? *Clinical Cancer Research*, *21*(22), 5047–5056.

Mathews, S. T., Plaisance, E. P., & Kim, T. (2009). Imaging systems for westerns: chemiluminescence vs. infrared detection. *Methods in molecular biology (Clifton, N.J.)*, *536*, 499–513.

Matić, S., Rinaldi, R., Masenga, V., & Noris, E. (2011). Efficient production of chimeric Human papillomavirus 16 L1 protein bearing the M2e influenza epitope in Nicotiana benthamiana plants. *BMC Biotechnology*, *11*(1), 106.

McAleer, W. J., Buynak, E. B., Maigetter, R. Z., Wampler, D. E., Miller, W. J., & Hilleman, M. R. (1984). Human hepatitis B vaccine from recombinant yeast. *Nature*, *307*(5947), 178–180.

McCarron, A., Donnelley, M., McIntyre, C., & Parsons, D. (2016). Challenges of up-scaling lentivirus production and processing. *Journal of Biotechnology*, *240*, 23–30.

McGrath, M., de Villiers, G. K., Shephard, E., Hitzeroth, I. I., & Rybicki, E. P. (2013). Development of human papillomavirus chimaeric L1/L2 candidate vaccines. *Archives of Virology*, *158*(10), 2079–2088.

Mena, J. A., Ramírez, O. T., & Palomares, L. A. (2007). Population kinetics during simultaneous infection of insect cells with two different recombinant baculoviruses for the production of rotavirus-like particles. *BMC Biotechnology*, *7*, 39.

Mishra, M., Tiwari, S., & Gomes, A. V. (2017). Protein purification and analysis: Next generation Western blotting techniques. *Expert Review of Proteomics*, *14*(11), 1037–1053.

Modesti, A., D'Orazi, G., Masuelli, L., Modica, A., Scarpa, S., Bosco, M. C., & Forni, G. (1993). Ultrastructural evidence of the mechanisms responsible for interleukin-4-activated rejection of a spontaneous murine adenocarcinoma. *International Journal of Cancer*, *53*(6), 988–993.

Mohsen, M. O., & Bachmann, M. F. (2022). Virus-like particle vaccinology, from bench to bedside. *Cellular & Molecular Immunology*, 1–19.

Mohsen, M. O., Heath, M. D., Cabral-Miranda, G., Lipp, C., Zeltins, A., Sande, M., Stein, J. V., Riether, C., Roesti, E., Zha, L., Engeroff, P., El-Turabi, A., Kundig, T. M., Vogel, M., Skinner, M. A., Speiser, D. E., Knuth, A., Kramer, M. F., & Bachmann, M. F. (2019). Vaccination with nanoparticles combined with micro-adjuvants protects against cancer. *Journal for ImmunoTherapy of Cancer*, *7*(1), 114.

Mohsen, M. O., Speiser, D. E., Knuth, A., & Bachmann, M. F. (2020). Virus-like particles for vaccination against cancer. *Wiley Interdisciplinary Reviews. Nanomedicine and Nanobiotechnology*, *12*(1).

Mohsen, M. O., Zha, L., Cabral-Miranda, G., & Bachmann, M. F. (2017). Major findings and recent advances in virus–like particle (VLP)-based vaccines. *Seminars in Immunology*, *34*, 123–132.

Monninger, M. K., Nguessan, C. A., Blancett, C. D., Kuehl, K. A., Rossi, C. A., Olschner, S. P., Williams, P. L., Goodman, S. L., & Sun, M. G. (2016). Preparation of viral samples

within biocontainment for ultrastructural analysis: Utilization of an innovative processing capsule for negative staining. *Journal of Virological Methods*, *238*, 70–76.

Morabito, A., Maio, E. D., Maio, M. D., Normanno, N., & Perrone, F. (2006). Tyrosine Kinase Inhibitors of Vascular Endothelial Growth Factor Receptors in Clinical Trials: Current Status and Future Directions. *The Oncologist*, *11*(7), 753–764.

Mossadegh, N., Gissmann, L., Müller, M., Zentgraf, H., Alonso, A., & Tomakidi, P. (2004). Codon optimization of the human papillomavirus 11 (HPV 11) L1 gene leads to increased gene expression and formation of virus-like particles in mammalian epithelial cells. *Virology*, *326*(1), 57–66.

Moynihan, K. D., & Irvine, D. J. (2017). Roles for innate immunity in combination immunotherapies. *Cancer Research*, *77*(19), 5215–5221.

Müller, M., Zhou, J., Reed, T. D., Rittmüller, C., Burger, A., Gabelsberger, J., Braspenning, J., & Gissmann, L. (1997). Chimeric Papillomavirus-like Particles. *Virology*, *234*(1), 93–111.

Munhoz, R. R., & Postow, M. A. (2016). Recent advances in understanding antitumor immunity. *F1000Research*, *5*.

Munshi, N. C., Anderson, L. D., Shah, N., Madduri, D., Berdeja, J., Lonial, S., Raje, N., Lin, Y., Siegel, D., Oriol, A., Moreau, P., Yakoub-Agha, I., Delforge, M., Cavo, M., Einsele, H., Goldschmidt, H., Weisel, K., Rambaldi, A., Reece, D., … San-Miguel, J. (2021). Idecabtagene Vicleucel in Relapsed and Refractory Multiple Myeloma. *The New England Journal of Medicine*, *384*(8), 705–716.

Musiani, P., Allione, A., Modica, A., Lollini, P. L., Giovarelli, M., Cavallo, F., Belardelli, F., Forni, G., & Modesti, A. (1996). Role of neutrophils and lymphocytes in inhibition of a mouse mammary adenocarcinoma engineered to release IL-2, IL-4, IL-7, IL-10, IFN-

alpha, IFN-gamma, and TNF-alpha. *Laboratory Investigation; a Journal of Technical Methods and Pathology*, *74*(1), 146–157.

Nafissi, N., Alqawlaq, S., Lee, E. A., Foldvari, M., Spagnuolo, P. A., & Slavcev, R. A. (2014). DNA Ministrings: Highly Safe and Effective Gene Delivery Vectors. *Molecular Therapy - Nucleic Acids*, *3*, e165.

Nafissi, N., & Slavcev, R. (2012). Construction and Characterization of an in-vivo Linear Covalently Closed DNA Vector Production System. *Microbial Cell Factories*, *11*, 154.

Najar, T. A., Khare, S., Pandey, R., Gupta, S. K., & Varadarajan, R. (2017). Mapping Protein Binding Sites and Conformational Epitopes Using Cysteine Labeling and Yeast Surface Display. *Structure*, *25*(3), 395–406.

Nakamura, T., & Matsumoto, K. (2005). Angiogenesis inhibitors: From laboratory to clinical application. *Biochemical and Biophysical Research Communications*, *333*(2), 289–291.

Naskalska, A., & Pyrć, K. (2015). Virus Like Particles as Immunogens and Universal Nanocarriers. *Polish Journal of Microbiology*, *64*(1), 3–13.

Nawrocki, S., Wysocki, P. J., & Mackiewicz, A. (2001). Genetically modified tumour vaccines: An obstacle race to break host tolerance to cancer. *Expert Opinion on Biological Therapy*, *1*(2), 193–204.

Nguyen, T. N. T., Sha, S., Hong, M. S., Maloney, A. J., Barone, P. W., Neufeld, C., Wolfrum, J., Springs, S. L., Sinskey, A. J., & Braatz, R. D. (2021). Mechanistic model for production of recombinant adeno-associated virus via triple transfection of HEK293 cells. *Molecular Therapy - Methods & Clinical Development*, *21*, 642–655.

Nicoli, F., Mantelli, B., Gallerani, E., Telatin, V., Bonazzi, I., Marconi, P., Gavioli, R., Gabrielli, L., Lazzarotto, T., Barzon, L., Palù, G., & Caputo, A. (2020). HPV-Specific Systemic

Antibody Responses and Memory B Cells are Independently Maintained up to 6 Years and in a Vaccine-Specific Manner Following Immunization with Cervarix and Gardasil in Adolescent and Young Adult Women in Vaccination Programs in Italy. *Vaccines*, *8*(1).

Nishida, N., Yano, H., Nishida, T., Kamura, T., & Kojiro, M. (2006). Angiogenesis in Cancer. *Vascular Health and Risk Management*, *2*(3), 213–219.

Nishimura, T., Iwakabe, K., Sekimoto, M., Ohmi, Y., Yahata, T., Nakui, M., Sato, T., Habu, S., Tashiro, H., Sato, M., & Ohta, A. (1999). Distinct Role of Antigen-Specific T Helper Type 1 (Th1) and Th2 Cells in Tumor Eradication in Vivo. *The Journal of Experimental Medicine*, *190*(5), 617–628.

Nooraei, S., Bahrulolum, H., Hoseini, Z. S., Katalani, C., Hajizade, A., Easton, A. J., & Ahmadian, G. (2021). Virus-like particles: Preparation, immunogenicity and their roles as nanovaccines and drug nanocarriers. *Journal of Nanobiotechnology*, *19*(1), 59.

Oaknin, A., Gilbert, L., Tinker, A. V., Brown, J., Mathews, C., Press, J., Sabatier, R., O'Malley, D. M., Samouelian, V., Boni, V., Duska, L., Ghamande, S., Ghatage, P., Kristeleit, R., Iii, C. L., Guo, W., Im, E., Zildjian, S., Han, X., … Pothuri, B. (2022). Safety and antitumor activity of dostarlimab in patients with advanced or recurrent DNA mismatch repair deficient/microsatellite instability-high (dMMR/MSI-H) or proficient/stable (MMRp/MSS) endometrial cancer: Interim results from GARNET—a phase I, single-arm study. *Journal for ImmunoTherapy of Cancer*, *10*(1), e003777.

Ohta, Y., Endo, Y., Tanaka, M., Shimizu, J., Oda, M., Hayashi, Y., Watanabe, Y., & Sasaki, T. (1996). Significance of vascular endothelial growth factor messenger RNA expression in primary lung cancer. *Clinical Cancer Research*, *2*(8), 1411–1416.

Okunade, K. S. (2020). Human papillomavirus and cervical cancer. *Journal of Obstetrics and Gynaecology*, *40*(5), 602–608.

Olave, M. C., & Graham, R. P. (2022). Mismatch repair deficiency: The what, how and why it is important. *Genes, Chromosomes & Cancer*, *61*(6), 314–321.

Olcese, V. A., Chen, Y., Schlegel, R., & Yuan, H. (2004). Characterization of HPV16 L1 loop domains in the formation of a type-specific, conformational epitope. *BMC Microbiology*, *4*, 29.

Ong, H. K., Tan, W. S., & Ho, K. L. (2017). Virus like particles as a platform for cancer vaccine development. *PeerJ*, *5*, e4053.

Palladini, A., Thrane, S., Janitzek, C. M., Pihl, J., Clemmensen, S. B., de Jongh, W. A., Clausen, T. M., Nicoletti, G., Landuzzi, L., Penichet, M. L., Balboni, T., Ianzano, M. L., Giusti, V., Theander, T. G., Nielsen, M. A., Salanti, A., Lollini, P.-L., Nanni, P., & Sander, A. F. (2018). Virus-like particle display of HER2 induces potent anti-cancer responses. *Oncoimmunology*, *7*(3), e1408749.

Palucha, A., Loniewska, A., Satheshkumar, S., Boguszewska-Chachulska, A. M., Umashankar, M., Milner, M., Haenni, A., & Savithri, H. S. (2005). Virus-Like Particles: Models for Assembly Studies and Foreign Epitope Carriers. *Progress in Nucleic Acid Research and Molecular Biology*, *80*, 135–168.

Pardoll, D. M. (2012). The blockade of immune checkpoints in cancer immunotherapy. *Nature Reviews. Cancer*, *12*(4), 252–264.

Park, M.-A., Kim, H. J., & Kim, H.-J. (2008). Optimum conditions for production and purification of human papillomavirus type 16 L1 protein from Saccharomyces cerevisiae. *Protein Expression and Purification*, *59*(1), 175–181.

Parker, M. W., Xu, P., Li, X., & Vander Kooi, C. W. (2012). Structural Basis for Selective Vascular Endothelial Growth Factor-A (VEGF-A) Binding to Neuropilin-1. *The Journal of Biological Chemistry*, *287*(14), 11082–11089.

Patel, M. C., Patkar, K. K., Basu, A., Mohandas, K. M., & Mukhopadhyaya, R. (2009). Production of immunogenic human papillomavirus-16 major capsid protein derived virus like particles. *The Indian Journal of Medical Research*, *130*(3), 213–218.

Pawson, T. (2002). Regulation and targets of receptor tyrosine kinases. *European Journal of Cancer*, *38*, S3–S10.

Peach, C. J., Mignone, V. W., Arruda, M. A., Alcobia, D. C., Hill, S. J., Kilpatrick, L. E., & Woolard, J. (2018). Molecular Pharmacology of VEGF-A Isoforms: Binding and Signalling at VEGFR2. *International Journal of Molecular Sciences*, *19*(4).

Pettersson, A., Nagy, J. A., Brown, L. F., Sundberg, C., Morgan, E., Jungles, S., Carter, R., Krieger, J. E., Manseau, E. J., Harvey, V. S., Eckelhoefer, I. A., Feng, D., Dvorak, A. M., Mulligan, R. C., & Dvorak, H. F. (2000). Heterogeneity of the Angiogenic Response Induced in Different Normal Adult Tissues by Vascular Permeability Factor/Vascular Endothelial Growth Factor. *Laboratory Investigation*, *80*(1), Article 1.

Pineo, C. B., Hitzeroth, I. I., & Rybicki, E. P. (2013). Immunogenic assessment of plant-produced human papillomavirus type 16 L1/L2 chimaeras. *Plant Biotechnology Journal*, *11*(8), 964–975.

Pinidis, P., Tsikouras, P., Iatrakis, G., Zervoudis, S., Koukouli, Z., Bothou, A., Galazios, G., & Vladareanu, S. (2016). Human Papilloma Virus' Life Cycle and Carcinogenesis. *Mædica*, *11*(1), 48–54.

Pinto, L. A., Edwards, J., Castle, P. E., Harro, C. D., Lowy, D. R., Schiller, J. T., Wallace, D., Kopp, W., Adelsberger, J. W., Baseler, M. W., Berzofsky, J. A., & Hildesheim, A. (2003). Cellular Immune Responses to Human Papillomavirus (HPV)-16 L1 in Healthy Volunteers Immunized with Recombinant HPV-16 L1 Virus-Like Particles. *The Journal of Infectious Diseases*, *188*(2), 327–338.

Pucci, C., Martinelli, C., & Ciofani, G. (2019). Innovative approaches for cancer treatment: Current perspectives and new challenges. *Ecancermedicalscience*, *13*, 961.

Pyeon, D., Vu, L., Giacobbi, N. S., & Westrich, J. A. (2020). The antiviral immune forces awaken in the cancer wars. *PLOS Pathogens*, *16*(9), e1008814.

Qin, Z., Schwartzkopff, J., Pradera, F., Kammertœns, T., Seliger, B., Pircher, H., & Blankenstein, T. (2003). A Critical Requirement of Interferon γ-mediated Angiostasis for Tumor Rejection by CD8+ T Cells. *Cancer Research*, *63*(14), 4095–4100.

Raghunandan, R. (2011). Virus-like particles: Innate immune stimulators. *Expert Review of Vaccines*, *10*(4), 409–411.

Rangel-Sosa, M. M., Aguilar-Córdova, E., & Rojas-Martínez, A. (2017). Immunotherapy and gene therapy as novel treatments for cancer. *Colombia medica (Cali, Colombia)*, *48*(3), 138–147.

Rao, N. H., Babu, P. B., Rajendra, L., Sriraman, R., Pang, Y.-Y. S., Schiller, J. T., & Srinivasan, V. A. (2011). Expression of codon optimized major capsid protein (L1) of human papillomavirus type 16 and 18 in Pichia pastoris; purification and characterization of the virus-like particles. *Vaccine*, *29*(43), 7326–7334.

Rayner, J. O., Kim, J. H., Roberts, R. W., Wood, R. R., Fouty, B., & Solodushko, V. (2021). Evaluation of DNA-Launched Virus-Like Particle Vaccines in an Immune Competent Mouse Model of Chikungunya Virus Infection. *Vaccines*, *9*(4), 345.

Release notice—Canadian Cancer Statistics 2019. (2019). *Health Promotion and Chronic Disease Prevention in Canada : Research, Policy and Practice*, *39*(8–9), 255.

Roden, R. B., Armstrong, A., Haderer, P., Christensen, N. D., Hubbert, N. L., Lowy, D. R., Schiller, J. T., & Kirnbauer, R. (1997). Characterization of a human papillomavirus type 16 variant-dependent neutralizing epitope. *Journal of Virology*, *71*(8), 6247–6252.

Roex, G., Timmers, M., Wouters, K., Campillo-Davo, D., Flumens, D., Schroyens, W., Chu, Y., Berneman, Z. N., Lion, E., Luo, F., & Anguille, S. (2020). Safety and clinical efficacy of BCMA CAR-T-cell therapy in multiple myeloma. *Journal of Hematology & Oncology*, *13*(1), 164.

Rohovie, M. J., Nagasawa, M., & Swartz, J. R. (2017). Virus-like particles: Next-generation nanoparticles for targeted therapeutic delivery. *Bioengineering & Translational Medicine*, *2*(1), 43–57.

Roldão, A., Mellado, M. C. M., Castilho, L. R., Carrondo, M. J. T., & Alves, P. M. (2010). Virus-like particles in vaccine development. *Expert Review of Vaccines*, *9*(10), 1149–1176.

Rolih, V., Caldeira, J., Bolli, E., Salameh, A., Conti, L., Barutello, G., Riccardo, F., Magri, J., Lamolinara, A., Parra, K., Valenzuela, P., Francia, G., Iezzi, M., Pericle, F., & Cavallo, F. (2020). Development of a VLP-Based Vaccine Displaying an xCT Extracellular Domain for the Treatment of Metastatic Breast Cancer. *Cancers*, *12*(6), 1492.

Rosca, E. V., Koskimaki, J. E., Rivera, C. G., Pandey, N. B., Tamiz, A. P., & Popel, A. S. (2011). Anti-angiogenic peptides for cancer therapeutics. *Current Pharmaceutical Biotechnology*, *12*(8), 1101–1116.

Rosenberg, S. A. (2014). IL-2: The First Effective Immunotherapy for Human Cancer. *Journal of Immunology (Baltimore, Md. : 1950)*, *192*(12), 5451–5458.

Rosenberg, S. A., Yang, J. C., Sherry, R. M., Kammula, U. S., Hughes, M. S., Phan, G. Q., Citrin, D. E., Restifo, N. P., Robbins, P. F., Wunderlich, J. R., Morton, K. E., Laurencot, C. M., Steinberg, S. M., White, D. E., & Dudley, M. E. (2011). Durable Complete Responses in Heavily Pretreated Patients with Metastatic Melanoma Using T Cell Transfer Immunotherapy. *Clinical Cancer Research : An Official Journal of the American Association for Cancer Research*, *17*(13), 4550–4557.

Roumenina, L. T., Daugan, M. V., Petitprez, F., Sautès-Fridman, C., & Fridman, W. H. (2019). Context-dependent roles of complement in cancer. *Nature Reviews Cancer*, *19*(12), Article 12.

Rout-Pitt, N., McCarron, A., McIntyre, C., Parsons, D., & Donnelley, M. (2018). Large-scale production of lentiviral vectors using multilayer cell factories. *Journal of Biological Methods*, *5*(2), e90.

RTS,S Clinical Trials Partnership, Agnandji, S. T., Lell, B., Fernandes, J. F., Abossolo, B. P., Methogo, B. G. N. O., Kabwende, A. L., Adegnika, A. A., Mordmüller, B., Issifou, S., Kremsner, P. G., Sacarlal, J., Aide, P., Lanaspa, M., Aponte, J. J., Machevo, S., Acacio, S., Bulo, H., Sigauque, B., … Vansadia, P. (2012). A phase 3 trial of RTS,S/AS01 malaria vaccine in African infants. *The New England Journal of Medicine*, *367*(24), 2284–2295.

Rump, A., Morikawa, Y., Tanaka, M., Minami, S., Umesaki, N., Takeuchi, M., & Miyajima, A. (2004). Binding of Ovarian Cancer Antigen CA125/MUC16 to Mesothelin Mediates Cell Adhesion*. *Journal of Biological Chemistry*, *279*(10), 9190–9198.

Sadremomtaz, A., Kobarfard, F., Mansouri, K., Mirzanejad, L., & Asghari, S. M. (2018). Suppression of migratory and metastatic pathways via blocking VEGFR1 and VEGFR2. *Journal of Receptor and Signal Transduction Research*, *38*(5–6), 432–441.

Sadremomtaz, A., Mansouri, K., Alemzadeh, G., Safa, M., Rastaghi, A. E., & Asghari, S. M. (2018). Dual blockade of VEGFR1 and VEGFR2 by a novel peptide abrogates VEGF-driven angiogenesis, tumor growth, and metastasis through PI3K/AKT and MAPK/ERK1/2 pathway. *Biochimica Et Biophysica Acta. General Subjects*, *1862*(12), 2688–2700.

Sakauchi, D., Sasaki, E. A. K., Anni, F. de O. B., Cianciarullo, A. M., Sakauchi, D., Sasaki, E. A. K., Anni, F. de O. B., & Cianciarullo, A. M. (2021). Production of HPV16 capsid proteins in suspension cultures of human epithelial cells. *World Journal of Advanced Research and Reviews*, *9*(3), Article 3.

Saladin, P. M., Zhang, B. D., & Reichert, J. M. (2009). Current trends in the clinical development of peptide therapeutics. *IDrugs: The Investigational Drugs Journal*, *12*(12), 779–784.

Sanchooli, A., Aghayipour, Kh., Naghlani, Sh. K., Samiee, Z., Kiasari, B. A., & Makvandi, M. (2020). Production of Human Papillomavirus Type-16 L1 VLP in Pichia pastoris. *Applied Biochemistry and Microbiology*, *56*(1), 51–57.

Sapp, M., Fligge, C., Petzak, I., Harris, J. R., & Streeck, R. E. (1998). Papillomavirus Assembly Requires Trimerization of the Major Capsid Protein by Disulfides between Two Highly Conserved Cysteines. *Journal of Virology*, *72*(7), 6186–6189.

Sarkar, S., Horn, G., Moulton, K., Oza, A., Byler, S., Kokolus, S., & Longacre, M. (2013). Cancer Development, Progression, and Therapy: An Epigenetic Overview. *International Journal of Molecular Sciences*, *14*(10), 21087–21113.

Schadendorf, D., Nghiem, P., Bhatia, S., Hauschild, A., Saiag, P., Mahnke, L., Hariharan, S., & Kaufman, H. L. (2017). Immune evasion mechanisms and immune checkpoint inhibition in advanced merkel cell carcinoma. *Oncoimmunology*, *6*(10).

Schädlich, L., Senger, T., Gerlach, B., Mücke, N., Klein, C., Bravo, I. G., Müller, M., & Gissmann, L. (2009). Analysis of modified human papillomavirus type 16 L1 capsomeres: the ability to assemble into larger particles correlates with higher immunogenicity. *Journal of virology*, *83*(15), 7690–7705.

Schädlich, L., Senger, T., Kirschning, C. J., Müller, M., & Gissmann, L. (2009). Refining HPV 16 L1 purification from E. coli: Reducing endotoxin contaminations and their impact on immunogenicity. *Vaccine*, *27*(10), 1511–1522.

Schäfer, K., Müller, M., Faath, S., Henn, A., Osen, W., Zentgraf, H., Benner, A., Gissmann, L., & Jochmus, I. (1999). Immune response to human papillomavirus 16 L1E7 chimeric virus-like particles: Induction of cytotoxic T cells and specific tumor protection. *International Journal of Cancer*, *81*(6), 881–888.

Schellenbacher, C., Huber, B., Skoll, M., Shafti-Keramat, S., Roden, R. B. S., & Kirnbauer, R. (2019). Incorporation of RG1 epitope into HPV16L1-VLP does not compromise L1-specific immunity. *Vaccine*, *37*(27), 3529–3534.

Schellenbacher, C., Roden, R., & Kirnbauer, R. (2009). Chimeric L1-L2 Virus-Like Particles as Potential Broad-Spectrum Human Papillomavirus Vaccines. *Journal of Virology*, *83*(19), 10085–10095.

Scheller, E. L., & Krebsbach, P. H. (2009). Gene Therapy. *Journal of Dental Research*, *88*(7), 585–596.

Schiller, J. T., & Lowy, D. R. (2012). Understanding and learning from the success of prophylactic human papillomavirus vaccines. *Nature Reviews Microbiology*, *10*(10), Article 10.

Schwarz, K., Meijerink, E., Speiser, D. E., Tissot, A. C., Cielens, I., Renhof, R., Dishlers, A., Pumpens, P., & Bachmann, M. F. (2005). Efficient homologous prime-boost strategies for T cell vaccination based on virus-like particles. *European Journal of Immunology*, *35*(3), 816–821.

Segura, M., Garnier, A., Durocher, Y., Coelho, H., & Kamen, A. (2007). Production of lentiviral vectors by large-scale transient transfection of suspension cultures and affinity chromatography purification. *Biotechnology and Bioengineering*, *98*, 789–799.

Sela, M., & Hilleman, M. R. (2004). Therapeutic vaccines: Realities of today and hopes for tomorrow. *Proceedings of the National Academy of Sciences of the United States of America*, *101*(Suppl 2), 14559.

Senger, T., Schädlich, L., Gissmann, L., & Müller, M. (2009). Enhanced papillomavirus-like particle production in insect cells. *Virology*, *388*(2), 344–353.

Seto, T., Higashiyama, M., Funai, H., Imamura, F., Uematsu, K., Seki, N., Eguchi, K., Yamanaka, T., & Ichinose, Y. (2006). Prognostic value of expression of vascular

endothelial growth factor and its flt-1 and KDR receptors in stage I non-small-cell lung cancer. *Lung Cancer (Amsterdam, Netherlands)*, *53*(1), 91–96.

Sharma, P., Kanapuru, B., George, B., Lin, X., Xu, Z., Bryan, W. W., Pazdur, R., & Theoret, M. R. (2022). FDA Approval Summary: Idecabtagene Vicleucel for Relapsed or Refractory Multiple Myeloma. *Clinical Cancer Research*, *28*(9), 1759–1764.

Shibuya, M. (2011). Vascular Endothelial Growth Factor (VEGF) and Its Receptor (VEGFR) Signaling in Angiogenesis: A Crucial Target for Anti- and Pro-Angiogenic Therapies. *Genes & Cancer*, *2*(12), 1097–1105.

Shirbaghaee, Z., & Bolhassani, A. (2016). Different applications of virus-like particles in biology and medicine: Vaccination and delivery systems. *Biopolymers*, *105*(3), 113–132.

Singh, M., Khong, H., Dai, Z., Huang, X.-F., Wargo, J. A., Cooper, Z. A., Vasilakos, J. P., Hwu, P., & Overwijk, W. W. (2014). Effective innate and adaptive anti-melanoma immunity through localized TLR-7/8 activation. *Journal of Immunology (Baltimore, Md. : 1950)*, *193*(9), 4722–4731.

Singh, S., Hassan, D., Aldawsari, H. M., Molugulu, N., Shukla, R., & Kesharwani, P. (2020). Immune checkpoint inhibitors: A promising anticancer therapy. *Drug Discovery Today*, *25*(1), 223–229.

Slupetzky, K., Shafti-Keramat, S., Lenz, P., Brandt, S., Grassauer, A., Sara, M., & Kirnbauer, R. (2001). Chimeric papillomavirus-like particles expressing a foreign epitope on capsid surface loops. *The Journal of General Virology*, *82*(0 11), 2799–2804.

Speiser, D. E., Schwarz, K., Baumgaertner, P., Manolova, V., Devevre, E., Sterry, W., Walden, P., Zippelius, A., Conzett, K. B., Senti, G., Voelter, V., Cerottini, J.-P., Guggisberg, D., Willers, J., Geldhof, C., Romero, P., Kündig, T., Knuth, A., Dummer, R., … Bachmann,

M. F. (2010). Memory and effector CD8 T-cell responses after nanoparticle vaccination of melanoma patients. *Journal of Immunotherapy (Hagerstown, Md.: 1997)*, *33*(8), 848–858.

Spurrell, E. L., & Lockley, M. (2014). Adaptive immunity in cancer immunology and therapeutics. *Ecancermedicalscience*, *8*. https://doi.org/10.3332/ecancer.2014.441

Stanley, M., Pinto, L. A., & Trimble, C. (2012). Human papillomavirus vaccines—Immune responses. *Vaccine*, *30 Suppl 5*, F83-87.

Stepanenko, A. A., & Dmitrenko, V. V. (2015). HEK293 in cell biology and cancer research: Phenotype, karyotype, tumorigenicity, and stress-induced genome-phenotype evolution. *Gene*, *569*(2), 182–190.

Steppert, P., Burgstaller, D., Klausberger, M., Tover, A., Berger, E., & Jungbauer, A. (2017). Quantification and characterization of virus-like particles by size-exclusion chromatography and nanoparticle tracking analysis. *Journal of chromatography. A*, *1487*, 89–99.

Sterner, R. C., & Sterner, R. M. (2021). CAR-T cell therapy: Current limitations and potential strategies. *Blood Cancer Journal*, *11*(4), Article 4.

Stewart, P. L. (2017). Cryo-electron microscopy and cryo-electron tomography of nanoparticles. *Wiley Interdisciplinary Reviews. Nanomedicine and Nanobiotechnology*, *9*(2).

Strober W. (2015). Trypan Blue Exclusion Test of Cell Viability. *Current protocols in immunology*, *111*, A3.B.1–A3.B.3.

Sun, B., Hyun, H., Li, L., & Wang, A. Z. (2020). Harnessing nanomedicine to overcome the immunosuppressive tumor microenvironment. *Acta Pharmacologica Sinica*, *41*(7), Article 7.

Suzich, J. A., Ghim, S. J., Palmer-Hill, F. J., White, W. I., Tamura, J. K., Bell, J. A., Newsome, J. A., Jenson, A. B., & Schlegel, R. (1995). Systemic immunization with papillomavirus L1 protein completely prevents the development of viral mucosal papillomas. *Proceedings of the National Academy of Sciences of the United States of America*, *92*(25), 11553–11557.

Szécsi, J., Gabriel, G., Edfeldt, G., Michelet, M., Klenk, H. D., & Cosset, F.-L. (2009). DNA Vaccination with a Single-Plasmid Construct Coding for Viruslike Particles Protects Mice against Infection with a Highly Pathogenic Avian Influenza A Virus. *The Journal of Infectious Diseases*, *200*(2), 181–190.

Takahashi, S. (2011). Vascular endothelial growth factor (VEGF), VEGF receptors and their inhibitors for antiangiogenic tumor therapy. *Biological & Pharmaceutical Bulletin*, *34*(12), 1785–1788.

Tan, E., Chin, C. S. H., Lim, Z. F. S., & Ng, S. K. (2021). HEK293 Cell Line as a Platform to Produce Recombinant Proteins and Viral Vectors. *Frontiers in Bioengineering and Biotechnology*, *9*, 796991.

Tan, S., Li, D., & Zhu, X. (2020). Cancer immunotherapy: Pros, cons and beyond. *Biomedicine & Pharmacotherapy = Biomedecine & Pharmacotherapie*, *124*, 109821.

Tang, H., Qiao, J., & Fu, Y.-X. (2016). Immunotherapy and tumor microenvironment. *Cancer Letters*, *370*(1), 85–90.

Tariq, H., Batool, S., Asif, S., Ali, M., & Abbasi, B. H. (2022). Virus-Like Particles: Revolutionary Platforms for Developing Vaccines Against Emerging Infectious Diseases. *Frontiers in Microbiology*, *12*.

Taube, S., Kurth, A., & Schreier, E. (2005). Generation of recombinant Norovirus-like particles (VLP) in the human endothelial kidney cell line 293T. *Archives of Virology*, *150*(7), 1425–1431.

Thakur, A., & Lum, L. G. (2010). Cancer therapy with bispecific antibodies: Clinical experience. *Current Opinion in Molecular Therapeutics*, *12*(3), 340–349.

Thomas, P., & Smart, T. G. (2005). HEK293 cell line: A vehicle for the expression of recombinant proteins. *Journal of Pharmacological and Toxicological Methods*, *51*(3), 187–200.

Tiash, S., & Chowdhury, E. (2015). Growth factor receptors: Promising drug targets in cancer. *Journal of Cancer Metastasis and Treatment*, *1*(3), 190.

Timmers, M., Roex, G., Wang, Y., Campillo-Davo, D., Van Tendeloo, V. F. I., Chu, Y., Berneman, Z. N., Luo, F., Van Acker, H. H., & Anguille, S. (2019). Chimeric Antigen Receptor-Modified T Cell Therapy in Multiple Myeloma: Beyond B Cell Maturation Antigen. *Frontiers in Immunology*, *10*, 1613.

Toh, Z. Q., Licciardi, P. V., Fong, J., Garland, S. M., Tabrizi, S. N., Russell, F. M., & Mulholland, E. K. (2015). Reduced dose human papillomavirus vaccination: An update of the current state-of-the-art. *Vaccine*, *33*(39), 5042–5050.

Tornesello, A. L., Tagliamonte, M., Buonaguro, F. M., Tornesello, M. L., & Buonaguro, L. (2022). Virus-like Particles as Preventive and Therapeutic Cancer Vaccines. *Vaccines*, *10*(2), 227.

Tosolini, M., Kirilovsky, A., Mlecnik, B., Fredriksen, T., Mauger, S., Bindea, G., Berger, A., Bruneval, P., Fridman, W.-H., Pagès, F., & Galon, J. (2011). Clinical impact of different

classes of infiltrating T cytotoxic and helper cells (Th1, th2, treg, th17) in patients with colorectal cancer. *Cancer Research*, *71*(4), 1263–1271.

Touze, A., El Mehdaoui, S., Sizaret, P. Y., Mougin, C., Muñoz, N., & Coursaget, P. (1998). The L1 major capsid protein of human papillomavirus type 16 variants affects yield of virus-like particles produced in an insect cell expression system. *Journal of clinical microbiology*, *36*(7), 2046–2051.

Tran, E., Robbins, P. F., Lu, Y.-C., Prickett, T. D., Gartner, J. J., Jia, L., Pasetto, A., Zheng, Z., Ray, S., Groh, E. M., Kriley, I. R., & Rosenberg, S. A. (2016). T-Cell Transfer Therapy Targeting Mutant KRAS in Cancer. *The New England Journal of Medicine*, *375*(23), 2255–2262.

Tumban, E. (2019). A Current Update on Human Papillomavirus-Associated Head and Neck Cancers. *Viruses*, *11*(10).

Uddin, M. N., Henry, B., Carter, K. D., Roni, M. A., & Kouzi, S. S. (2019). A Novel Formulation Strategy to Deliver Combined DNA and VLP Based HPV Vaccine. *Journal of Pharmacy & Pharmaceutical Sciences: A Publication of the Canadian Society for Pharmaceutical Sciences, Societe Canadienne Des Sciences Pharmaceutiques*, *22*(1), 536–547.

Vähä-Koskela, M. J. V., Heikkilä, J. E., & Hinkkanen, A. E. (2007). Oncolytic viruses in cancer therapy. *Cancer Letters*, *254*(2), 178–216.

Valero-Pacheco, N., Pérez-Toledo, M., Villasís-Keever, M. Á., Núñez-Valencia, A., Boscó-Gárate, I., Lozano-Dubernard, B., Lara-Puente, H., Espitia, C., Alpuche-Aranda, C., Bonifaz, L. C., Arriaga-Pizano, L., Pastelin-Palacios, R., Isibasi, A., & López-Macías, C.

(2016). Antibody Persistence in Adults Two Years after Vaccination with an H1N1 2009 Pandemic Influenza Virus-Like Particle Vaccine. *PLoS ONE*, *11*(2).

Van den Bergh, J. M. J., Guerti, K., Willemen, Y., Lion, E., Cools, N., Goossens, H., Vorsters, A., Van Tendeloo, V. F. I., Anguille, S., Van Damme, P., & Smits, E. L. J. M. (2014). HPV vaccine stimulates cytotoxic activity of killer dendritic cells and natural killer cells against HPV-positive tumour cells. *Journal of Cellular and Molecular Medicine*, *18*(7), 1372–1380.

Varsani, A., Williamson, A.-L., de Villiers, D., Becker, I., Christensen, N. D., & Rybicki, E. P. (2003). Chimeric Human Papillomavirus Type 16 (HPV-16) L1 Particles Presenting the Common Neutralizing Epitope for the L2 Minor Capsid Protein of HPV-6 and HPV-16. *Journal of Virology*, *77*(15), 8386–8393.

Varsani, A., Williamson, A.-L., Jaffer, M. A., & Rybicki, E. P. (2006). A deletion and point mutation study of the human papillomavirus type 16 major capsid gene. *Virus Research*, *122*(1–2), 154–163.

Vicente, T., Roldão, A., Peixoto, C., Carrondo, M. J. T., & Alves, P. M. (2011). Large-scale production and purification of VLP-based vaccines. *Journal of Invertebrate Pathology*, *107*, S42–S48.

Villa, L. L., Costa, R. L. R., Petta, C. A., Andrade, R. P., Paavonen, J., Iversen, O.-E., Olsson, S.-E., Høye, J., Steinwall, M., Riis-Johannessen, G., Andersson-Ellstrom, A., Elfgren, K., Krogh, G. von, Lehtinen, M., Malm, C., Tamms, G. M., Giacoletti, K., Lupinacci, L., Railkar, R., … Barr, E. (2006). High sustained efficacy of a prophylactic quadrivalent human papillomavirus types 6/11/16/18 L1 virus-like particle vaccine through 5 years of follow-up. *British Journal of Cancer*, *95*(11), 1459–1466.

Voskoboinik, I., Whisstock, J. C., & Trapani, J. A. (2015). Perforin and granzymes: Function, dysfunction and human pathology. *Nature Reviews. Immunology*, *15*(6), 388–400.

Waldman, A. D., Fritz, J. M., & Lenardo, M. J. (2020). A guide to cancer immunotherapy: From T cell basic science to clinical practice. *Nature Reviews Immunology*, *20*(11), Article 11.

Wang, D., Liu, X., Wei, M., Qian, C., Song, S., Chen, J., Wang, Z., Xu, Q., Yang, Y., He, M., Chi, X., Huang, S., Li, T., Kong, Z., Zheng, Q., Yu, H., Wang, Y., Zhao, Q., Zhang, J., … Li, S. (2020). Rational design of a multi-valent human papillomavirus vaccine by capsomere-hybrid co-assembly of virus-like particles. *Nature Communications*, *11*, 2841.

Wang, H., Yu, J., Lu, X., & He, X. (2016). Nanoparticle systems reduce systemic toxicity in cancer treatment. *Nanomedicine (London, England)*, *11*(2), 103–106.

Wang, J. W., & Roden, R. B. S. (2013). Virus-like particles for the prevention of human papillomavirus-associated malignancies. *Expert Review of Vaccines*, *12*(2).

Wang, R., Yang, L., Zhang, C., Wang, R., Zhang, Z., He, Q., Chen, X., Zhang, B., Qin, Z., Wang, L., & Zhang, Y. (2018). Th17 cell-derived IL-17A promoted tumor progression via STAT3/NF-κB/Notch1 signaling in non-small cell lung cancer. *OncoImmunology*, *7*(11), e1461303.

Weigelin, B., den Boer, A. T., Wagena, E., Broen, K., Dolstra, H., de Boer, R. J., Figdor, C. G., Textor, J., & Friedl, P. (2021). Cytotoxic T cells are able to efficiently eliminate cancer cells by additive cytotoxicity. *Nature Communications*, *12*(1), Article 1.

Weiskopf, K., & Weissman, I. L. (2015). Macrophages are critical effectors of antibody therapies for cancer. *MAbs*, *7*(2), 303–310.

Wherry, E. J., & Kurachi, M. (2015). Molecular and cellular insights into T cell exhaustion. *Nature Reviews. Immunology*, *15*(8), 486–499.

White, W. I., Wilson, S. D., Palmer-Hill, F. J., Woods, R. M., Ghim, S., Hewitt, L. A., Goldman, D. M., Burke, S. J., Jenson, A. B., Koenig, S., & Suzich, J. A. (1999). Characterization of a Major Neutralizing Epitope on Human Papillomavirus Type 16 L1. *Journal of Virology*, *73*(6), 4882–4889.

Whiteside, T. L. (2008). The tumor microenvironment and its role in promoting tumor growth. *Oncogene*, *27*(45), 5904–5912.

Witsch, E., Sela, M., & Yarden, Y. (2010). Roles for Growth Factors in Cancer Progression. *Physiology (Bethesda, Md.)*, *25*(2), 85–101.

Wolchok, J. D., Kluger, H., Callahan, M. K., Postow, M. A., Rizvi, N. A., Lesokhin, A. M., Segal, N. H., Ariyan, C. E., Gordon, R.-A., Reed, K., Burke, M. M., Caldwell, A., Kronenberg, S. A., Agunwamba, B. U., Zhang, X., Lowy, I., Inzunza, H. D., Feely, W., Horak, C. E., … Sznol, M. (2013). Nivolumab plus ipilimumab in advanced melanoma. *The New England Journal of Medicine*, *369*(2), 122–133.

Wolff, J. A., Malone, R. W., Williams, P., Chong, W., Acsadi, G., Jani, A., & Felgner, P. L. (1990). Direct gene transfer into mouse muscle in vivo. *Science (New York, N.Y.)*, *247*(4949 Pt 1), 1465–1468.

Woo, M.-K., An, J.-M., Kim, J.-D., Park, S.-N., & Kim, H.-J. (2008). Expression and purification of human papillomavirus 18 L1 virus-like particle from Saccharomyces cerevisiae. *Archives of Pharmacal Research*, *31*(2), 205–209.

Woo, S.-R., Corrales, L., & Gajewski, T. F. (2015). Innate immune recognition of cancer. *Annual Review of Immunology*, *33*, 445–474.

Woolard, J., Wang, W.-Y., Bevan, H. S., Qiu, Y., Morbidelli, L., Pritchard-Jones, R. O., Cui, T.-G., Sugiono, M., Waine, E., Perrin, R., Foster, R., Digby-Bell, J., Shields, J. D., Whittles,

C. E., Mushens, R. E., Gillatt, D. A., Ziche, M., Harper, S. J., & Bates, D. O. (2004). VEGF165b, an Inhibitory Vascular Endothelial Growth Factor Splice Variant: Mechanism of Action, In vivo Effect On Angiogenesis and Endogenous Protein Expression. *Cancer Research*, *64*(21), 7822–7835.

Wu, C., Kajitani, N., & Schwartz, S. (2017). Splicing and Polyadenylation of Human Papillomavirus Type 16 mRNAs. *International Journal of Molecular Sciences*, *18*(2), 366.

Xia, W., Bringmann, P., McClary, J., Jones, P. P., Manzana, W., Zhu, Y., Wang, S., Liu, Y., Harvey, S., Madlansacay, M. R., McLean, K., Rosser, M. P., MacRobbie, J., Olsen, C. L., & Cobb, R. R. (2006). High levels of protein expression using different mammalian CMV promoters in several cell lines. *Protein Expression and Purification*, *45*(1), 115–124.

Xing, H. R., & Zhang, Q. (2012). Real-time visualization and characterization of tumor angiogenesis and vascular response to anticancer therapies. *Methods in Molecular Biology (Clifton, N.J.)*, *872*, 115–127.

Yadav, R., Zhai, L., & Tumban, E. (2019). Virus-like Particle-Based L2 Vaccines against HPVs: Where Are We Today? *Viruses*, *12*(1).

Yamaoka, T., Kusumoto, S., Ando, K., Ohba, M., & Ohmori, T. (2018). Receptor Tyrosine Kinase-Targeted Cancer Therapy. *International Journal of Molecular Sciences*, *19*(11).

Yang, B., Jeang, J., Yang, A., Wu, T. C., & Hung, C.-F. (2015). DNA vaccine for cancer immunotherapy. *Human Vaccines & Immunotherapeutics*, *10*(11), 3153–3164.

Yang, J. C., & Rosenberg, S. A. (2016). Adoptive T-Cell Therapy for Cancer. *Advances in Immunology*, *130*, 279–294.

Young, K. R., Smith, J. M., & Ross, T. M. (2004). Characterization of a DNA vaccine expressing a human immunodeficiency virus-like particle. *Virology*, *327*(2), 262–272.

Yuan, J., Xu, W. W., Jiang, S., Yu, H., & Poon, H. F. (2018). The Scattered Twelve Tribes of HEK293. *Biomedical and Pharmacology Journal*, *11*(2), 621–623.

Zaczek, A., Brandt, B., & Bielawski, K. P. (2005). The diverse signaling network of EGFR, HER2, HER3 and HER4 tyrosine kinase receptors and the consequences for therapeutic approaches. *Histology and Histopathology*, *20*(3), 1005–1015.

Zahavi, D., & Weiner, L. (2020). Monoclonal Antibodies in Cancer Therapy. *Antibodies*, *9*(3).

Zahin, M., Joh, J., Khanal, S., Husk, A., Mason, H., Warzecha, H., Ghim, S., Miller, D. M., Matoba, N., & Jenson, A. B. (2016). Scalable Production of HPV16 L1 Protein and VLPs from Tobacco Leaves. *PLOS ONE*, *11*(8), e0160995.

Zepeda-Cervantes, J., Ramírez-Jarquín, J. O., & Vaca, L. (2020). Interaction Between Virus-Like Particles (VLPs) and Pattern Recognition Receptors (PRRs) From Dendritic Cells (DCs): Toward Better Engineering of VLPs. *Frontiers in Immunology*, *11*.

Zhang, J., Yun, J., Shang, Z., Zhang, X., & Pan, B. (2009). Design and optimization of a linker for fusion protein construction. *Progress in Natural Science*, *19*(10), 1197–1200.

Zhang, S., Yong, L.-K., Li, D., Cubas, R., Chen, C., & Yao, Q. (2013). Mesothelin Virus-Like Particle Immunization Controls Pancreatic Cancer Growth through CD8+ T Cell Induction and Reduction in the Frequency of CD4+foxp3+ICOS− Regulatory T Cells. *PLOS ONE*, *8*(7), e68303.

Zhao, Q., Potter, C. S., Carragher, B., Lander, G., Sworen, J., Towne, V., Abraham, D., Duncan, P., Washabaugh, M. W., & Sitrin, R. D. (2014). Characterization of virus-like particles in

GARDASIL® by cryo transmission electron microscopy. *Human Vaccines & Immunotherapeutics*, *10*(3), 734–739.

Zhu, J. (2012). Mammalian cell protein expression for biopharmaceutical production. *Biotechnology Advances*, *30*(5), 1158–1170.

Zirlik, K., & Duyster, J. (2018). Anti-Angiogenics: Current Situation and Future Perspectives. *Oncology Research and Treatment*, *41*(4), 166–171.

Appendices

Appendix A

HPV L1 DNA-VLP sequences

atgagcctgtggctgcccagcgaggccaccgtgtacctgccccccgtgcccgtgagcaaggtggtgagcaccgacgagtacgtggcca
gaaccaacatctactaccacgccggcaccagcagactgctggccgtgggccacccctacttccccatcaagaagcccaacaacaacaag
atcctggtgcccaaggtgagcggcctgcagtacagagtgttcagaatccacctgcccgaccccaacaagttcggcttccccgacaccagct
tctacaaccccgacacccagagactggtgtgggcctgcgtgggcgtggaggtgggcagaggccagcccctgggcgtgggcatcagcg
gccacccccctgctgaacaagctggacgacaccgagaacgccagcgcctacgccgccaacgccggcgtggacaacagagagtgcatca
gcatggactacaagcagacccagctgtgcctgatcggctgcaagcccccccatcggcgagcactggggcaagggcagcccctgcaccaa
cgtggccgtgaaccccggcgactgcccccccctggagctgatcaacaccgtgatccaggacggcgacatggtggacaccggcttcggc
gccatggacttcaccaccctgcaggccaacaagagcgaggtgcccctggacatctgcaccagcatctgcaagtaccccgactacatcaag
atggtgagcgagccctacggcgacagcctgttcttctacctgagaagagagcagatgttcgtgagacacctgttcaacagagccggcgcc
gtgggcgagaacgtgcccgacgacctgtacatcaagggcagcggcagcaccgccaacctggccagcagcaactacttccccacccccca
gcggcagcatggtgaccagcgacgcccagatcttcaacaagccctactggctgcagagagcccagggccacaacaacggcatctgctg
gggcaaccagctgttcgtgaccgtggtggacaccaccagaagcaccaacatgagcctgtgcgccgccatcagcaccagcgagaccacc
tacaagaacaccaacttcaaggagtacctgagacacggcgaggagtacgacctgcagttcatcttccagctgtgcaagatcaccctgaccg
ccgacgtgatgacctacatccacagcatgaacagcaccatcctggaggactggaacttcggcctgcagccccccccccggcggcaccctg
gaggacacctacagattcgtgaccagccaggccatcgcctgccagaagcacacccccccccgcccccaaggaggacccccctgaagaagt
acaccttctgggaggtgaacctgaaggagaagttcagcgccgacctggaccagttccccctgggcagaaagttcctgctgcaggccggc
ctgaaggccaagcccaagttcaccctgggcaagagaaaggccacccccaccaccagcagcaccagcaccaccgccaagagaaagaa
gagaaagctgtga

Figure A.1 HPV16 L1 human codon optimized capsid sequence

atgagcctgtggctgcccagcgaggccaccgtgtacctgccccccgtgcccgtgagcaaggtggtgagcaccgacgagtacgtggcca
gaaccaacatctactaccacgccggcaccagcagactgctggccgtgggccacccctacttccccatcaagaagcccaacaacaacaag
atcctggtgcccaaggtgagcggcctgcagtacagagtgttcagaatccacctgcccgaccccaacaagttcggcttccccgacaccagct
tctacaaccccgacacccagagactggtgtgggcctgcgtgggcgtggaggtgggcagaggccagcccctgggcgtgggcatcagcg
gccacccccctgctgaacaagctggacgacaccgagaacgccagcgcctacgccggctgcatcaagccccaccagggccagcacatctg
caacgacgaggggccaacgccggcgtggacaacagagagtgcatcagcatggactacaagcagacccagctgtgcctgatcggctgc
aagccccccatcggcgagcactggggcaagggcagcccctgcaccaacgtggccgtgaaccccggcgactgccccccccctggagctg
atcaacaccgtgatccaggacggcgacatggtggacaccggcttcggcgccatggacttcaccaccctgcaggccaacaagagcgaggt
gcccctggacatctgcaccagcatctgcaagtaccccgactacatcaagatggtgagcgagccctacggcgacagcctgttcttctacctg
agaagagagcagatgttcgtgagacacctgttcaacagagccggcgccgtgggcgagaacgtgcccgacgacctgtacatcaagggca
gcggcagcaccgccaacctggccagcagcaactacttccccacccccagcggcagcatggtgaccagcgacgcccagatcttcaacaa
gccctactggctgcagagagcccagggccacaacaacggcatctgctggggcaaccagctgttcgtgaccgtggtggacaccaccaga
agcaccaacatgagcctgtgcgccgccatcagcaccagcgagaccacctacaagaacaccaacttcaaggagtacctgagacacggcg
aggagtacgacctgcagttcatcttccagctgtgcaagatcaccctgaccgccgacgtgatgacctacatccacagcatgaacagcaccat
cctggaggactggaacttcggcctgcagccccccccggcggcaccctggaggacacctacagattcgtgaccagccaggccatcgcct
gccagaagcacaccccccccgcccccaaggaggacccccctgaagaagtacaccttctgggaggtgaacctgaaggagaagttcagcgc
cgacctggaccagttccccctgggcagaaagttcctgctgcaggccggcctgaaggccaagcccaagttcaccctgggcaagagaaag
gccacccccaccaccagcagcaccagcaccaccgccaagagaaagaagagaaagctgtga

Figure A.2 HPV16 L1 human codon optimized capsid sequence with the VGB sequence inserted into the DE loop region. The highlighted region indicates the inserted VGB sequence. The GGC bases that are coloured in red are linker sequences placed before and after the inserted VGB sequence.

atgagcctgtggctgcccagcgaggccaccgtgtacctgccccccgtgcccgtgagcaaggtggtgagcaccgacgagtacgtggcca
gaaccaacatctactaccacgccggcaccagcagactgctggccgtgggccacccctacttccccatcaagaagcccaacaacaacaag
atcctggtgcccaaggtgagcggcctgcagtacagagtgttcagaatccacctgcccgaccccaacaagttcggcttccccgacaccagct
tctacaaccccgacacccagagactggtgtgggcctgcgtgggcgtggaggtgggcagaggccagcccctgggcgtgggcatcagcg
gccacccccctgctgaacaagctggacgacaccgagaacgccagcgcctacgccgccaacgccggcgtggacaacagagagtgcatca
gcatggactacaagcagacccagctgtgcctgatcggctgcaagcccccccatcggcgagcactggggcaagggcagcccctgcaccaa
cgtggccgtgaaccccggcgactgcccccccctggagctgatcaacaccgtgatccaggacggcgacatggtggacaccggcttcggc
gccatggacttcaccaccctgcaggccaacaagagcgaggtgcccctggacatctgcaccagcatctgcaagtaccccgactacatcaag
atggtgagcgagccctacggcgacagcctgttcttctacctgagaagagagcagatgttcgtgagacacctgttcaacagagccggcgcc
gtgggcgagaacgtgcccgacgacctgtacatcaagggcagcggcagcaccgccaacctggccagcagcaactacttccccacccccca
gcggcagcatggtgaccagcgacgcccagatcttcaacaagccctactggctgcagagagcccagggccacaacaacggcatctgctg
gggcaaccagctgttcgtgaccgtggtggacaccaccagaagcaccaacatgagcctgtgcgccgccatcagcaccagcgagaccacc
tacaagaacaccaacttcaaggagtacctgagacacggcgaggagtacgacctgcagttcatcttccagctgtgcaagatcaccctgaccg
ccgacgtgatgacctacatccacagcatgaacagcaccatcctggaggactggaacttcggcctgcagccccccccggcggcaccctg
gaggacacctacagattcgtgaccagccaggccatcgcctgccagaaggctgcatcaagccccaccagggccagcacatctgcaacg
acgagggccccccgcccccaaggaggacccccctgaagaagtacaccttctgggaggtgaacctgaaggagaagttcagcgccgacct
ggaccagttccccctgggcagaaagttcctgctgcaggccggcctgaaggccaagcccaagttcaccctgggcaagagaaaggccacc
cccaccaccagcagcaccagcaccaccgccaagagaaagaagagaaagctgtga

Figure A.3 HPV16 L1 human codon optimized capsid sequence with the VGB sequence inserted into the H4 helix region. The highlighted region indicates the inserted VGB sequence. The GGC bases that are coloured in red are linker sequences placed before and after the inserted VGB sequence.

Appendix B

Media and buffer compositions

Table B.1 Composition of media and buffers used for experiments

Media/Buffer Name	Composition
LB Broth	12.5 g of LB (containing tryptone, yeast extract, and NaCl) in 500 mL of MilliQ water
LB Agar	12.5 g of LB (containing tryptone, yeast extract, and NaCl), 6.5 g of agar in 500 mL of MilliQ water
DMEM + 10% FBS	6.7 g of DMEM powder and 50 mL of FBS, in 500 mL of MilliQ water
1X Wash Buffer (TBS-T)	20 mM Tris HCl (pH = 7.4), 150 mM NaCl, and 0.1% (w/v) Tween 20 in 1L of MilliQ water
1X Wash Buffer (PBS-T)	137 mM NaCl, 2.7 mM KCl, 10mM Na_2HPO_4, 1.8 mM KH_2PO_4, and 0.1% (w/v) Tween 20 in 1L of MilliQ water
Blocking Buffer (5% skim milk)	5 g of skim milk in 100 mL of TBS-T or PBS-T
10X Running Buffer	30 g Tris base, 144 g glycine, and 10 g SDS in 1L of MilliQ water
10X Running Buffer (non-denaturing)	30 g Tris base and 155 g glycine in 1L of MilliQ water
RIPA Buffer	25 mM Tris HCl pH 7.6, 150 mM NaCl, and 1% NP-50 in 100 mL of MilliQ water

DMEM: Dulbecco's Modified Eagle Medium; FBS: fetal bovine serum; LB: Luria Burtani; PBS-T: phosphate-buffered saline/tween; SDS: sodium dodecyl sulfate; TBS-T: tris-buffered saline/tween

Appendix C

Comparative study for VLP selection

Table C.1 Comparative study for VLP selection with scoring rubric

Virus	Ease of Characterization/ Production	Immunogenicity	Peptide Fusion Tolerance	Final Score
HPV	-non-enveloped - easier to characterize, produce and purify (Buonaguro et al., 2011; Naskalska & Pyrć, 2015) (+2) -single protein (L1 capsid protein) required for VLP assembly (+2) -well characterized VLP (Deschuyteneer et al., 2010; Zhao et al., 2014) (+1) -generally, HPV L1 proteins don't assemble into VLPs in bacterial cells (Bang et al., 2016) (-1) -in mammalian cells high concentration of L1 is required for VLP production (Mossadegh et al., 2004) (-1)	-induces high humoral and cellular immune responses (Bellone et al., 2009; D. M. Harper et al., 2006; Toh et al., 2015; Villa et al., 2006) (+1) -HPV VLP vaccines extensively studied for immunogenicity and safety in patients (Buonaguro et al., 2011) (+1) -some pre-existing neutralizing Abs against HPV in humans (J. W. Wang & Roden, 2013) (-1)	-L1 protein can be easily fused to peptides for VLP display (Huber et al., 2017; Varsani et al., 2003; Yadav et al., 2019) (+1)	
Score	***+ 3***	***+ 1***	***+1***	***+5***
AAV	-non-enveloped - easier to characterize, produce and purify (Backovic et al., 2012; Naskalska & Pyrć, 2015) (+2) -stable and can form over a variety of pH and temperatures (Nieto et al., 2012; Xie et al., 2002) (+1) -requires co-expression with an associated protein (encoded within a different frame of the right ORF) for VLP production and expression without the associated protein resulted in less efficient production (Le et al., 2019) (-1) -VP3 alone can form VLPs but requires a nuclear localization	-requires high doses to stimulate a potent immune response (-1) -wide pre-existing immunity in humans (-1) -strong Ab response induction and enhances Ab response against display peptides (Manzano-Szalai et al., 2014) (+1)	-successful VLP display using the VP3 protein have been shown (Manzano-Szalai et al., 2014; Nieto et al., 2012) (+1) -peptide insertions at aa position 587 and 588 of AAV2 has been well studied (Boucas et al., 2009;	

	signal fusion (Hoque et al., 1999) (-1)		Manzano-Szalai et al., 2014)	
Score	***+1***	***-1***	***+1***	***+1***
HBV	-non enveloped – easier to characterize, produce and purify (Naskalska & Pyrć, 2015; Spice et al., 2020) (+2) -single protein required for VLP production (HBV core antigen) (Miyanohara et al., 1986) or the HBV surface antigen (Bayer et al., 1968) (+2) -HBV surface antigen VLP licensed however HBV core-based vaccine has not been licensed (Buonaguro et al., 2011) (+1) -HBV core VLPs can be produced in a variety of expression systems including *Escherichia coli (E. coli)* (Pumpens & Grens, 2001; Zeltins, 2013) (+1) - concerns regarding particle instability (Lu et al., 2015) (-2) -HBV core not used to existing without encompassing nucleic acid which could explain its instability (Lu et al., 2015) (-2)	-HBV core protein can increase the immunogenicity against display peptides (Geldmacher et al., 2004; J. Guo et al., 2019) (+1) -HBV surface antigen less immunogenic compared to core protein (J. Guo et al., 2019) (-1) -commercially available HBV vaccines based on the surface antigen show induction of potent immune responses (Buonaguro et al., 2011; West & Calandra, 1996) (+1)	-effective peptide display within the major immunodomi-nant region and c-terminal of the core protein (Aston-Deaville et al., 2020) (+1)	
Score	***+2***	***+1***	***+1***	***+4***
IV	-enveloped – harder to characterize and produce, and contains host membrane proteins (Buonaguro et al., 2011; Dai et al., 2018; Naskalska & Pyrć, 2015) (-2) -can be produced using one protein (D'Aoust et al., 2010) (+2), however, most use a combination of more than one protein (McCraw et al., 2018) (-1)	-wide pre-existing immunity in humans due to infection and previous vaccination (M.-C. Kim et al., 2014) (-1) -demonstrates protective effects, cross reactive responses, and high serum Ab levels (Bright et al., 2007; Buonaguro et al., 2011; Quan et al., 2007) (+1)	-presence of host membrane proteins in enveloped VLPs can influence display of fusion peptides (Buonaguro et al., 2011; Dai et al., 2018; Naskalska & Pyrć, 2015) (-1)	

Score	***-1***	***0***	***-1***	***-2***
CoV	-enveloped – harder to characterize and produce, and contains host membrane proteins (Buonaguro et al., 2011; Dai et al., 2018; Naskalska & Pyrć, 2015) (-2) -more than one protein required for VLP assembly (varied combinations of the spike, membrane, envelope and nuclear proteins) in previous studies (Siu et al., 2008) (-2)	-coronavirus strains show oncolytic activity and can induce anti-tumour immune responses (Verheije et al., 2006; Würdinger et al., 2003; Würdinger et al., 2005) (+1)	-presence of host membrane proteins in enveloped VLPs can influence display of fusion peptides (Buonaguro et al., 2011; Dai et al., 2018; Naskalska & Pyrć, 2015) (-1)	
Score	***-4***	***+1***	***-1***	***-4***
CPMV	-non enveloped – easier to characterize, produce and purify (Naskalska & Pyrć, 2015; Spice et al., 2020) (+2) -CPMV VLPs cannot be produced in *E. coli* or yeast. Only insect or plant cells can be used (Rohovie et al., 2017; Saunders et al., 2009; Steinmetz et al., 2011) -coat proteins cannot be obtained in sufficient quantities (Rohovie et al., 2017; Saunders et al., 2009; Steinmetz et al., 2011) (-1) -complex requirements for VLP formation – efficient production of VLP only when L and S proteins are released from RNA-2 polyproteins or VP60 (Saunders et al., 2009) (-2)	-can stimulate anti-tumour immunity that promotes oncolysis (Albakri et al., 2020; Lizotte et al., 2016; Shukla et al., 2020) (+1) -plant-based virus makes it safe for human application (Steinmetz et al., 2011) (+1)	-successful display of ligands on its surface (Rohovie et al., 2017) (+1)	
Score	***-2***	***+2***	***+1***	***+1***
HIV	-enveloped – harder to characterize and produce, and contains host membrane proteins (Buonaguro et al., 2011; Dai et al., 2018; Naskalska & Pyrć, 2015) (-2)	-HIV gag matrix protein could trigger nonspecific immune responses and cause unwanted side effects (Nika et al., 2019) (-1)	-successful peptide/protein display (Nika et al., 2017, 2019) (+1)	

	-single protein required for VLP assembly (gag matrix protein, pr55 gag protein) (Deml et al., 2005; Nika et al., 2017, 2019) (+2)	-able to induce maturation of DCs and macrophages, and increase production of cytokines and activated T and B-cells (Sailaja et al., 2007) (+1)		
Score	***0***	***0***	***+1***	***+1***

aa: amino acid; AAV: adeno-associated virus; CPMV: cowpea mosaic virus; CoV: coronavirus; DC: dendritic cell; HBV: hepatitis B virus; HIV: human immunodeficiency virus; HPV: human papillomavirus; IV: influenza virus; ORF: open reading frame; VLP: virus-like particle

[1] The scores ((+) = positive attribute; (-) = negative attribute) indicate the level of the major features (ease of characterization/production, immunogenicity, and peptide fusion tolerance) that are characteristic of each VLP listed based on their benefits and limitations outlined in previous studies.

Appendix D

Cloning data for DNA-VLP plasmid construction

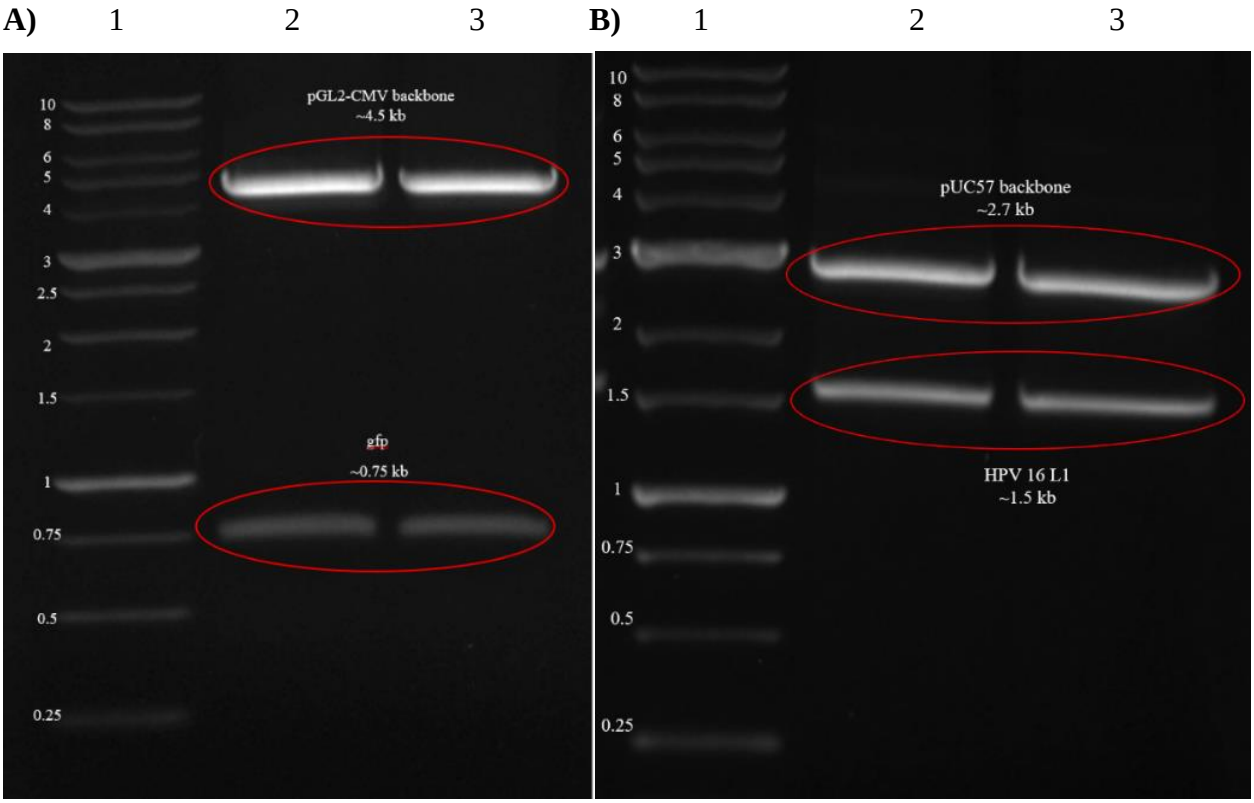

Figure D.1. Agarose gel of restriction enzyme digestion reactions. The pGL2-CMV-gfp and pUC57-L1 plasmids were digested with NotI HF and PmeI and subsequently run on a 0.8% gel for 1 h and 30 min at 88 V. **A)** Agarose gel of the digested pGL2-CMV-gfp plasmid. Lane 1: 1kb DNA FroggoBio (Concord, CA) Ladder (Catalogue No. DM010-R500). The size of the DNA ladder bands is indicated on the left side of the image in kb; Lanes 2 and 3: pGL2-CMV-gfp restriction digest reactions. **B)** Agarose gel of the digested pUC57 L1 plasmid. Lane 1: 1kb Plus DNA FroggoBio (Concord, CA) Plus Ladder (Catalogue No. DM015-R500). The size of the DNA ladder bands is indicated on the left side of the image in kb; Lanes 2 and 3: pUC57 L1 restriction digest reactions.

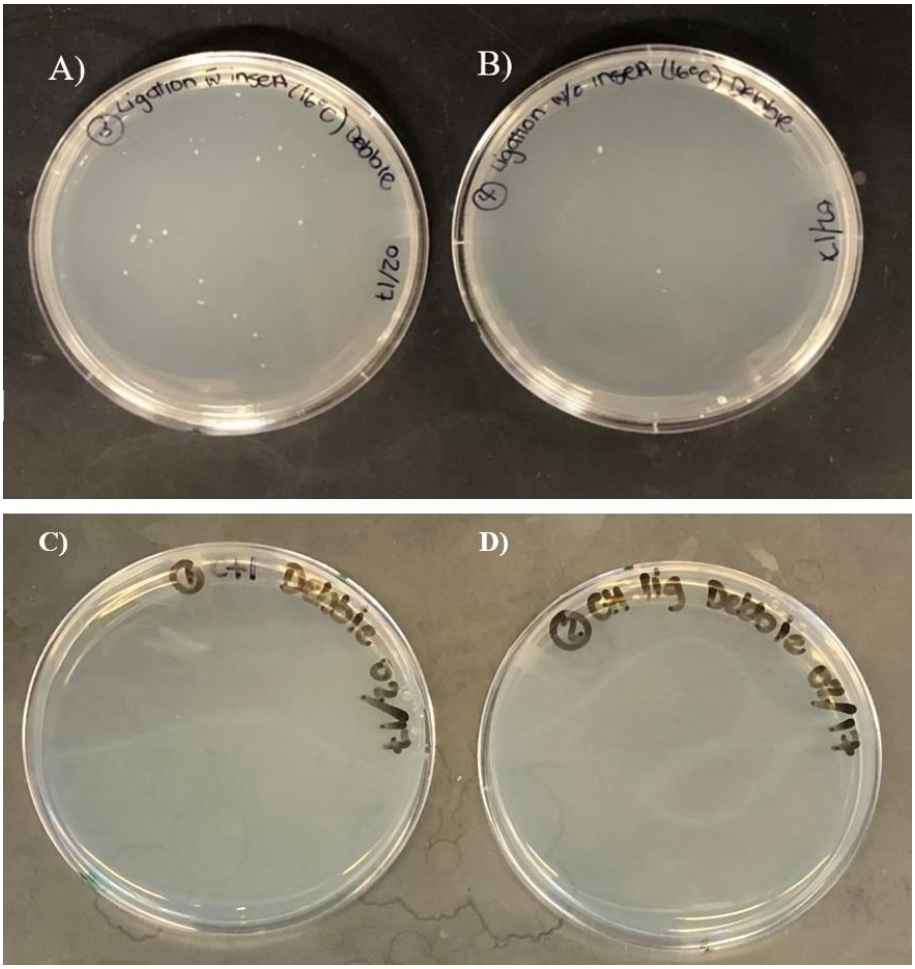

Figure D.2. Transformation of competent JM109 *E. coli* cells with ligation reactions. A) LB + Amp agar plate of transformed competent JM109 cells with a ligation reaction containing the backbone vector (pGL2-CMV) and insert (L1); **B)** LB + Amp agar plate of transformed competent JM109 cells with a ligation reaction of the cut backbone vector (pGL2-CMV); C) LB + Amp agar plate of competent JM109 cells; D) LB + Amp agar plate of transformed competent JM109 cells with a ligation reaction containing no DNA.

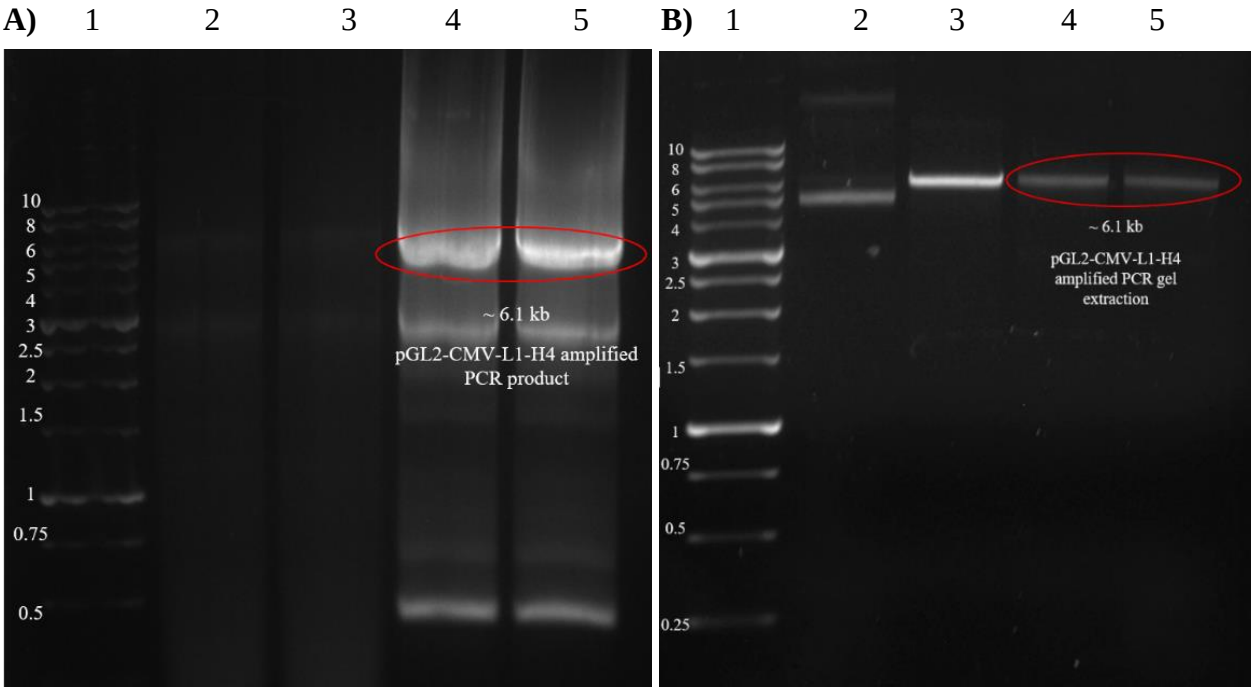

Figure D.3. Agarose gels of pGL2-CMV-L1 PCR amplification with VGB primers. The PCR reactions and gel extractions were run on a 0.8% gel for ~ 1 h and 30 min at 88 V. **A)** pGL2-CMV-L1 PCR amplification reaction with VGB H4 forward and reverse primers (Table 5). Lane 1: 1kb FroggoBio (Concord, CA) DNA ladder (Catalogue No. DM010-R500). The size of the DNA ladder bands is indicated on the left side of the image in kb; Lanes 2 and 3: PCR reaction containing no plasmid DNA; Lanes 4 and 5: PCR reaction of pGL2-CMV-L1 plasmid amplified with VGB H4 forward and reverse primers. **B)** Gel extraction of pGL2-CMV-L1 PCR amplification with VGB H4 forward and reverse primers. Lane 1: 1kb FroggoBio (Concord, CA) DNA ladder (Catalogue No. DM010-R500). The size of the DNA ladder bands is indicated on the left side of the image in kb; Lane 2: pGL2-CMV-L1 plasmid; Lane 3: pGL2-CMV-L1 digested with NotI HF (linearized); Lanes 4 and 5: Gel extracted pGL2-CMV-L1 PCR product amplified with VGB H4 forward and reverse primers.